Click chemistry modification of surface-bound peptides towards applications in printable electronics

Zur Erlangung des akademischen Grades eines

DOKTORS DER NATURWISSENSCHAFTEN

(Dr. rer. nat.)

Fakultät für Chemie und Biowissenschaften

Karlsruher Institut für Technologie (KIT) – Universitätsbereich

genehmigte

DISSERTATION

von

Martin Schlageter

aus

Karlsruhe

Dekan: Prof. Dr. Peter Roesky

Referent: Prof. Dr. Annie Powell

Korreferent: Prof. Dr. Burkhard Luy

Tag der mündlichen Prüfung: 17.07.2015

This thesis was completed in the period from October 2011 to June 2015 in the Institute for Nanotechnology (INT) of the Karlsruhe Institute of Technology KIT under the supervision of Prof. Dr. Annie K. Powell

Index

1 Introduction

1.1 Peptide synthesis

The International Union of Pure and Applied Chemistry IUPAC defined peptides in the following way:

(Peptides are) “Amides derived from two or more amino carboxylic acid molecules (the same or different) by formation of a covalent bond from the carbonyl carbon of one to the nitrogen atom of another with formal loss of water.”[1]

Amino acids are molecules that contain both an amine and a carboxylic acid function, typically but not exclusively on neighbouring carbon atoms. Peptides are an important class of compound that consists of amino acids that are connected via a peptide bond (Figure 1).

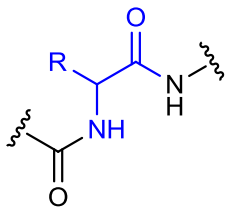

Figure 1 amino acid (blue) in a peptide sequence, R = side chain.

Because amino acids are bifunctional monomers that carry both functional groups that form a peptide bond, the synthesis of artificial peptides requires sophisticated synthetic strategies to prevent unwanted reactions. The carboxylic acid function has to be activated in order to form a peptide bond with a free amine. This activation can be achieved by the direct use of coupling agents like dicyclohexyl carbodiimide (DCC) or diisopropyl carbodiimide (DIC), or by the pre-formation of so-called active esters with reagents like n-hydroxycuccinimid (HOSu) or pentafluorophenol. (HOPfp) (Figure 2).

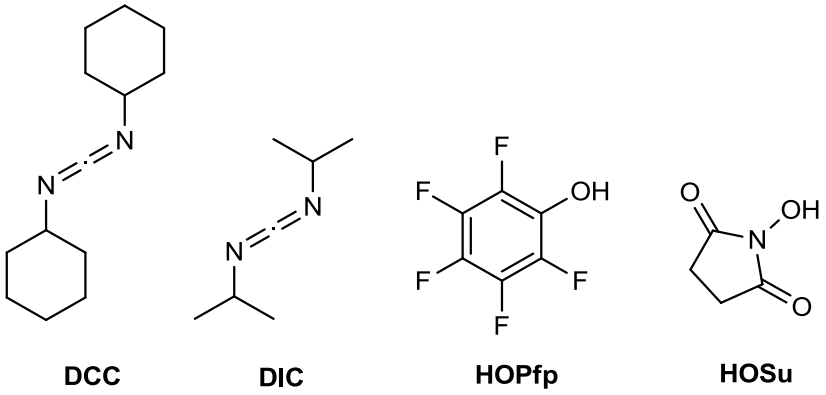

Figure 2 activation reagents for the carboxylic acids.

In order to avoid polymerisation of the bifunctional amino acids, it is necessary to protect the amine function first. This protection is done on the N terminus in form of so-called carbamates that can be cleaved under mild conditions. Figure 3 shows two of the most common protecting groups.

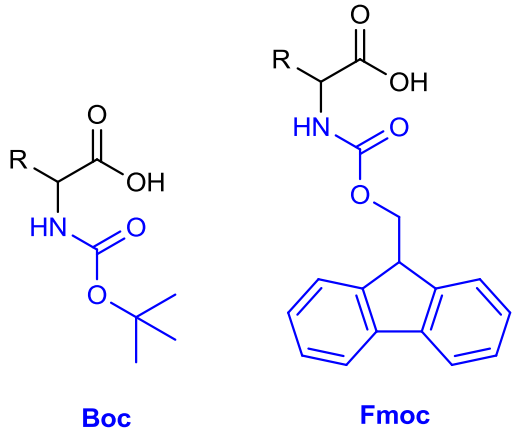

Figure 3 Boc and Fmoc protecting groups.

Tert-butoxycarbonyl (Boc) is introduced via its anhydride and is cleaved with acid, whereas 9-fluorenylmethoxycarbonyl (Fmoc) is introduced as OSu active ester and cleaved in basic media.

Early peptide synthesis was conducted in solution phase, but with its increasing popularity, practical problems occurred. As Robert Bruce Merrifield pointed out,[2] problems with solubility and purification of the synthesis products grow immensely with increasing chain length. To overcome these shortcomings, Merrifield developed a method for the synthesis of peptides in solid phase, for which he received the 1984 Nobel Prize for Chemistry. His idea was to grow the

peptide chain on a modified polymer that carries a linker. The first amino acid is bound to a linker on the polymer as an ester. The peptide chain growth is done one amino acid at a time, with three steps for each amino acid added (Figure 4).

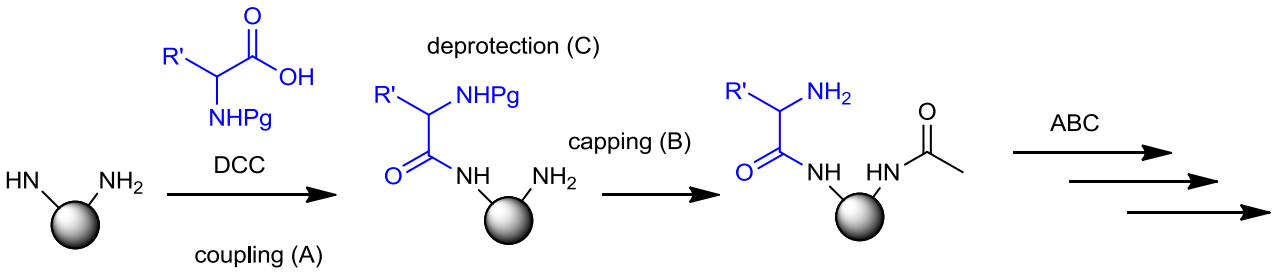

Figure 4 working principle of solid phase peptide synthesis.

An amino acid is coupled to an active amino terminus on the polymer (step A) using any of the above mentioned activation methods. Capping (step B) of unreacted amine function with acetic acid ensures growth of only the desired peptide. Next, the protecting group Pg from the newly coupled amino acid is removed (step C) and the steps repeat. Finally, the peptide is cleaved from the surface. This method has been combined with other technologies to be used in combinatorial chemistry, like bead-based combinatorial peptide synthesis or peptide laser printing.[3]

1.2 Particle-based peptide synthesis

Using classical Merrifield synthesis, only few different peptide sequences can be obtained at a given time. In 2008, Breitling et al. reported a method for the particle-based synthesis that is based on a laser printer.[4] The working principle is depicted in Figure 5.

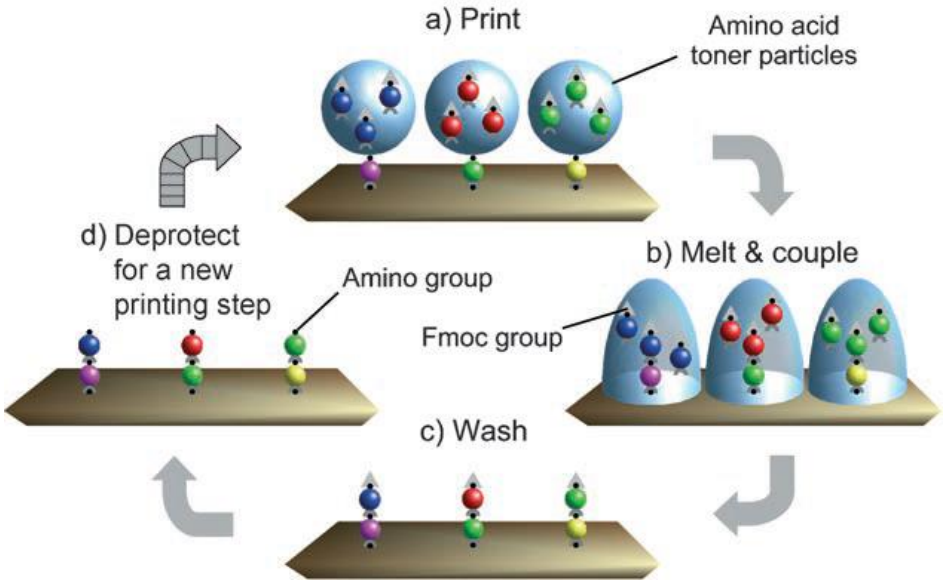

Figure 5 Working principle of particle-based peptide synthesis by Breitling et al., courtesy of Wiley-VCH, Weinheim.

Amino acid building blocks are being dissolved with a resin as matrix material and various auxiliary compounds and the solvent removed by spray-drying to obtain amino acid toner particles. These particles are then printed to a glass slide covered with a polymer thin film with a β-alanine already coupled to the polymer (step a). The polymer surface can be either polyethyleneglycol methacrylate (pegma) or a copolymer of 10% ethyleneglycol methacrylate and 90% methylmethacrylate (pmma) (pegma 10/90).

The peptide coupling proceeds when the glass slide is heated and the matrix resin melts, acting as solvent for the reaction (step b). After completion, the resin is washed away, the unreacted N-termini of the previous amino acid are capped with acetic anhydride (step c) and the fmoc protecting group removed to receive the next building block (step d). In this way, a large variety of amino acid sequences can be generated quickly on a relatively small surface. This method is suited much better for screening experiments than the classical approach and is now provided commercially by the PepPerPrint GmbH.[5]

1.3 Copper-catalyzed azide alkyne cycloaddition CuAAC

Huisgen discovered that, under rather harsh conditions, alkynes and azides react in a 1,3 dipolar cycloaddition reaction to give triazoles.

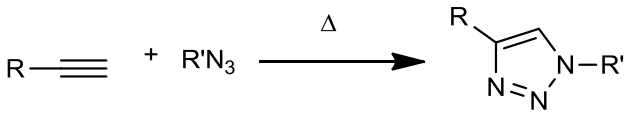

It was not until 2002 that Sharpless and Meldal independently discovered that Cu(I) is capable of catalysing this reaction.[6] Not only could the cycloaddition be performed at room temperature in hours instead of days, it was also found to give selectively the 1,4-substituted triazoles. This reaction is the most famous representative for the concept of click chemistry.[7] It has therefore been coined Cu catalysed azide alkyne click reaction, or short CuAAC. Figure 6 shows the mechanism of the CuAAC reaction as proposed by Himo et al.[8]

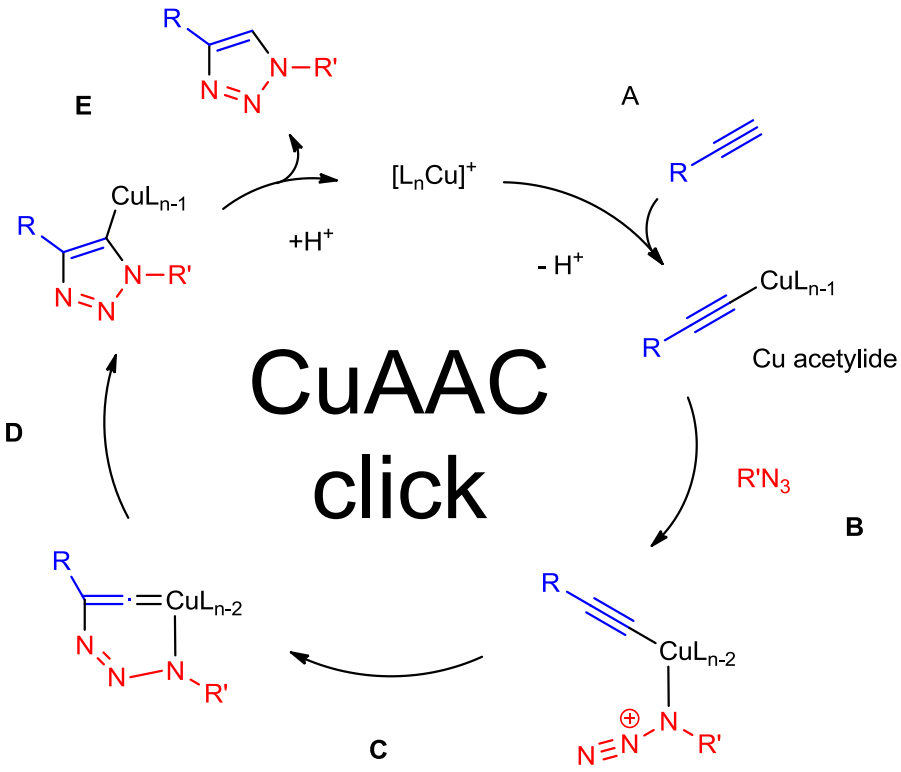

Figure 6 Mechanism of the CuAAC click reaction as proposed by Himo et al.

The catalytic cycle begins with the formation of a Cu acetylide (step A). In the next step, azide coordniates to Cu (B) and forms a metallacycle by an attack of the terminal nitrogen on the C-2

carbon atom in the alkyne (step C). The cycle finally contracts (step D) and releases the catalyst to form the 1,4-substituted triazole. Because of its high tolerance for functional groups, reliability and versatility, CuAAC has gained much attention in the past decade.

1.4 Peptide-based diodes

In Nature, light harvesting is performed by so-called photosystems, big arrangements of many antennae and one reaction center. When irradiated with proper light, chromophores in the antennae generate electron-hole pairs that are able to migrate (so-called excitons). Those diffuse to the reaction center, where charges are separated. This is achieved via directional electron tunneling. There exist several theoretical models to describe electron tunneling between a donor and an acceptor, mainly differing in the level of detail considered. As Noy et al. pointed out,[9] only two principle parameters are necessary to understand the natural engineering of single electron transfer, namely the tunneling distances and driving forces.

The EU project "PepDiode"[10] is an attempt to build up a screening and search for well performing peptide-based diodes that can be used for charge separation in novel solar cells. (Figure 4) shows how directional electron tunnelling could be achieved in a peptide.

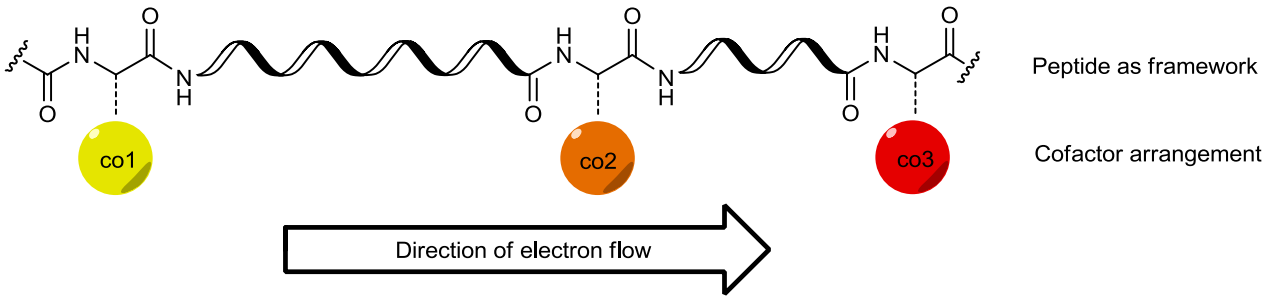

Figure 7 Directional electron tunnelling along peptides with redox cofactors (co) with different distances and redox potentials (colours of the spheres; potential gets more negative from left to right).

A series of so-called redox cofactors, redox active molecules that are stable in their relevant oxidation states, is arranged using peptides as framework. Distance and potential gradients generate a preferred direction of electron flow through the arrangement. Aside from different technical challenges, an important part is to provide a variety of redox cofactors.

1.5 Ferrocene

In 1951, Kealy and Pauson tried to synthesize fulvalene by reducing a cyclopentadienyl Grignard with Iron (III)-chloride (Figure 8). But instead of the desired product they observed the formation of an orange, crystalline solid which turned out to be ferrocene **Fc**.

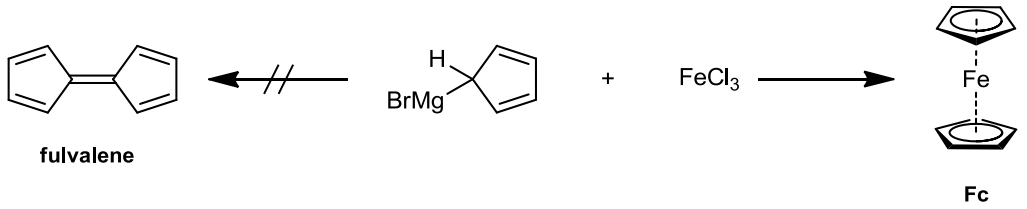

Figure 8 Discovery of Ferrocene by Kealy and Pauson in 1951, intended reaction (left) and actual reaction (right).

Ferrocene combines a redox-centre with two rich aromatic cycles. Its remarkable stability against moisture and air combined with the largely solvent-independent potential led to the use of ferrocene / ferrocenium as reference for redox potentials, mainly applied in cyclic voltammetry. These properties qualify ferrocene as a promising redox cofactor, while at the same time providing certain difficulties concerning its functionalization. In many modern organic syntheses, metal catalysts are used. Applying those to ferrocene may cause unwanted redox reactions and prevent conversion.

2 Aim of the present work

The aim of the first part of the project was to investigate methods for grafting redox cofactors onto peptides. In order to function with particle-based peptide synthesis, the amino acids need to be protected with a fluorenylmethoxycarbonyl protecting group (Fmoc) and the C-terminus has to be activated as pentafluorophenyl (OPfp) active ester. The cofactor has to withstand the conditions of peptide synthesis, including global deprotection with 50% aqueous trifluoroacetic acid. Moreover, the synthesis of cofactor amino acids needs to be affordable and feasible in at least 10 g scale, since this is the minimum amount that can be processed into toner particles. All of these features present a significant challenge in terms of finding robust systems.

A number of redox cofactors based on simple molecules should be synthesised. Ferrocene derivatives should be obtained and their robustness and electrochemical properties be determined.

The possibility of using coordination clusters as redox cofactors should be investigated. To achieve this, modified ligands suitable for grafting should be synthesized. Next, coordination clusters should be synthesized and characterized, and a way should be found to verify the grafting reaction. The suitability of the clusters for grafting in terms of robustness should be investigated.

3 Results and discussion

3.1 Ferrocene peptide conjugates from literature

Because of its chemical stability and well-known reactivity, ferrocene was chosen as a model compound to find a suitable method for grafting redox cofactors onto peptides. Various synthetic pathways to ferrocene peptide conjugates can be found in literature. In order to see if they can be adopted for other redox active moieties, their reliability should be investigated. The reproduction of literature syntheses[11] for two ferrocene peptide conjugates was attempted. The first example was L-ferrocenylalanine **1** (Figure 9).

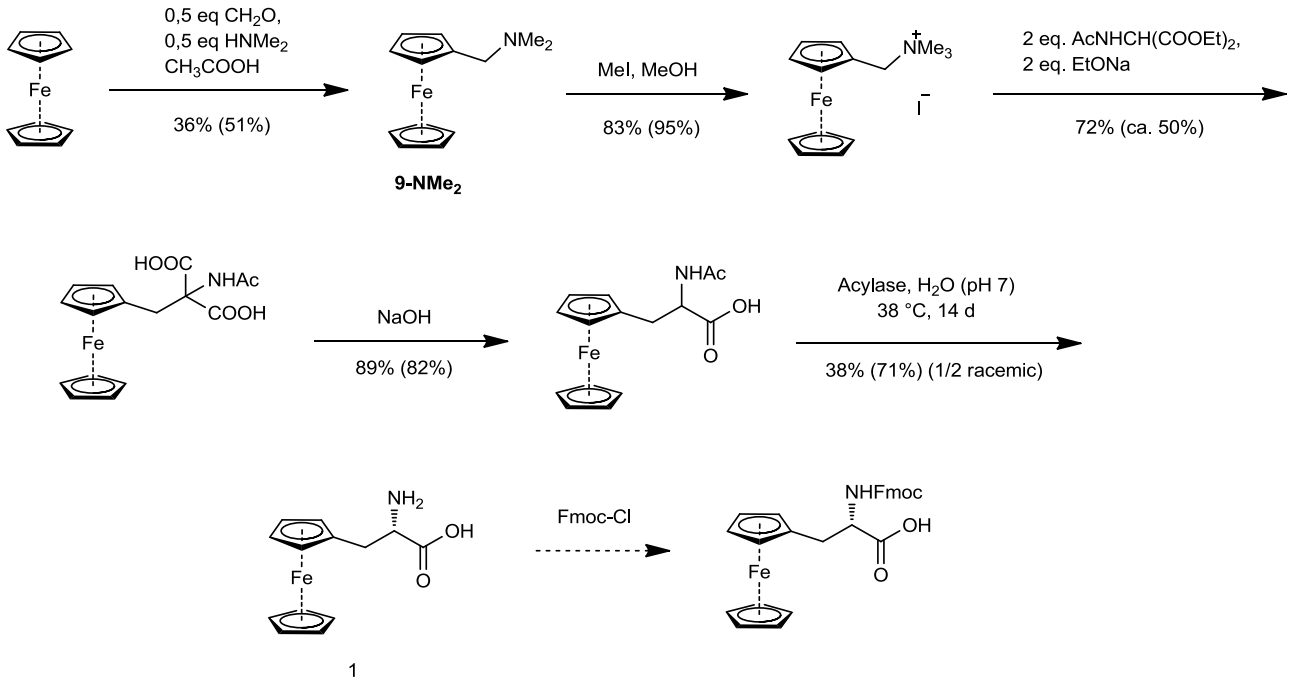

Figure 9 Reproduction of literature synthesis for L-ferrocenyl alanine (numbers in brackets are literature values).

The combined literature yield from ferrocene to the enantiomer **L-1** is 7.3%. Assuming the reaction scales up with the same efficiency and fmoc protection proceeds with quantitative yield, more than 100 g of ferrocene have to be used in the first step. A large contribution to that is the racemic resolution at a late stage of synthesis. Literature research gave an interesting

molecule that is achiral and where the ferrocene moiety is not located at the side chain, but is itself part of the peptide (Figure 10).

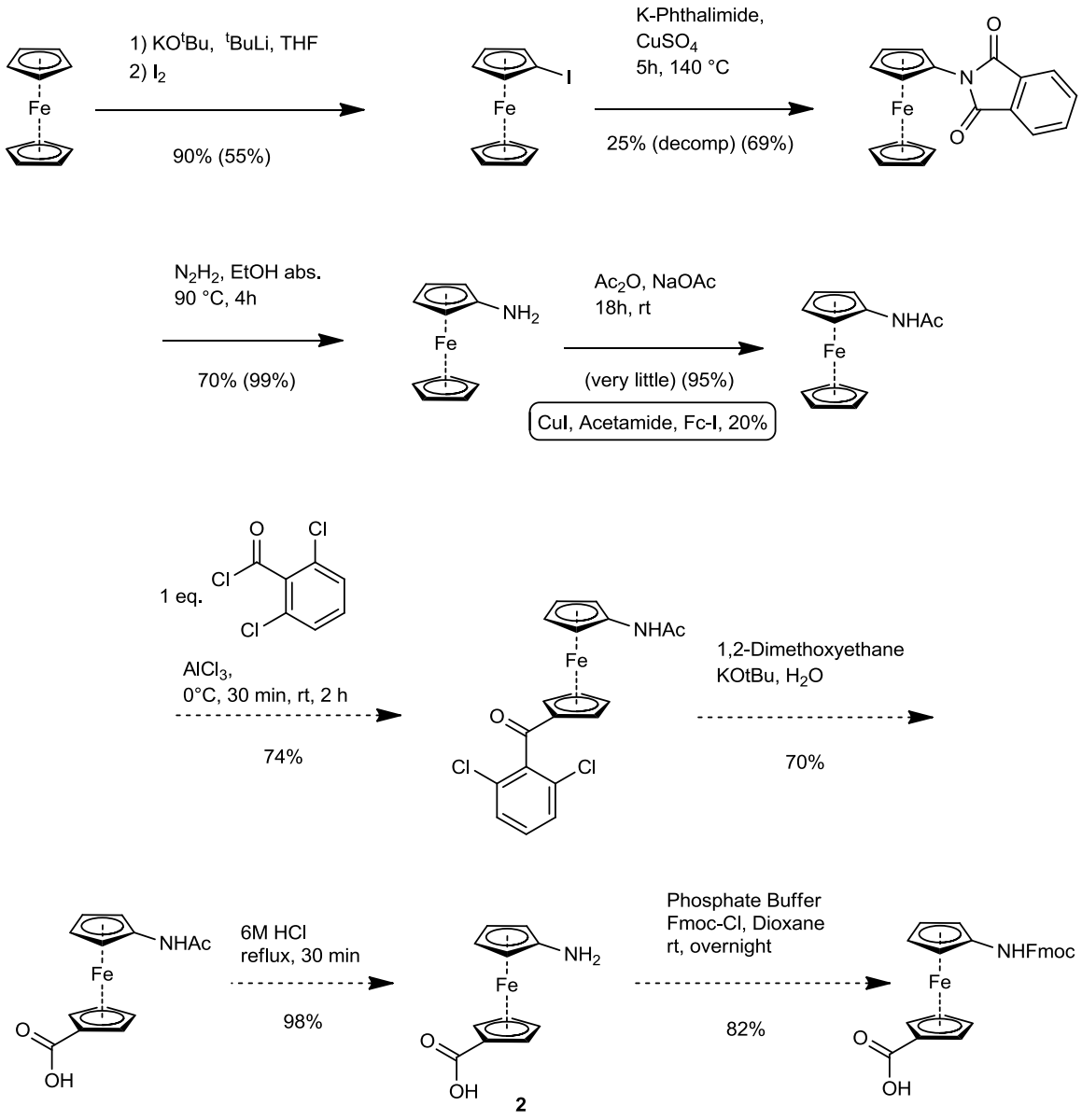

Figure 10 Reproduction of literature procedure for 1-Amino-1'-carboxyferrocene 2.

Typical for syntheses of ferrocene peptide conjugates found in literature are high number of synthetic steps and moderate yields. Although these methods are appropriate for producing the final product in the 100 mg scale, considering the requirement of 10 g of each amino acid it was not reasonable to adopt these methods for the functionalization of new cofactors. At this point it was decided that this approach is not preferable and other options had to be found.

3.2 Friedel-Crafts acylation on Ferrocene as model reaction for cofactor functionalization

Ferrocene and many other redox active molecules share an aromatic system as a common motif. Literature research produced a method for the one-step preparation of L-2-amino-4-oxo-4-phenylbutanoic acid hydrochloride from benzene and aspartic anhydride hydrochloride (Figure 11). [12]

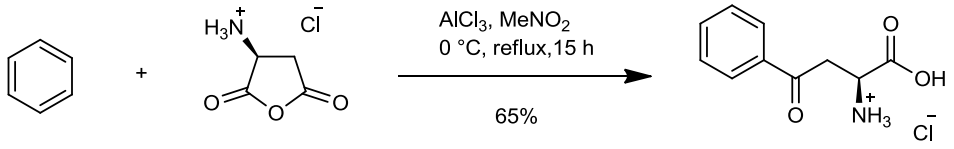

Figure 11 One-step enantioselective friedel-crafts acylation of Benzene with aspartic anhydride hydrochloride.

All reactants are inexpensive and readily available. These features are highly desirable for the functionalization of redox-active compounds. Reactions of various carboxylic anhydrides with ferrocene are well known in literature and the conditions are comparable. Figure 13 shows an example of such a reaction with a very similar anhydride that gives the product in a moderate yield.[13]

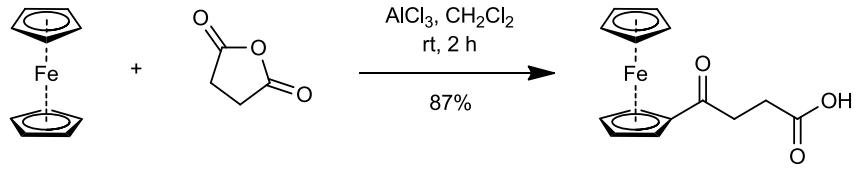

Figure 12 Literature example for a Friedel-Crafts acylation of Ferrocene with Succinic Anhydride.

Since both cp groups of ferrocene are significantly more activated for electrophilic aromatic substitutions than benzene, it was expected that this reaction would run smoothly. A variety of reaction conditions for the synthesis of **3** (Figure 13) was tested.

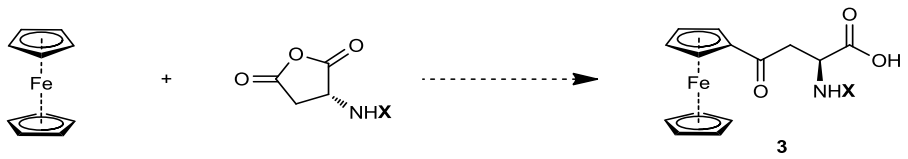

Figure 13 General reaction equation for Friedel-Crafts acylation of Ferrocene with aspartic anhydrides.

Table 1 Original reaction conditions by Jiang et al. applied to ferrocene.

#	Solvent	Catalyst	X	reaction Conditions	Oxidation	Observations
1	$MeNO_2$	$AlCl_3$	H · HCl	rt, 48 h	immediate	no conversion
2	$PhNO_2$	$AlCl_3$	H · HCl	120 °C, 48 h	immediate	formation of insoluble brown substance
3	$PhNO_2$	-	H · HCl	120 °C, 48 h	-	no conversion

First, the reaction was conducted under the original conditions used by Jiang et al., using nitromethane and $AlCl_3$ (Table 1, entry 1). The reaction mixture was partitioned between H_2O and CH_2Cl_2 and the aqueous phases were treated with ascorbic acid. The reduced species were extracted and identified via TLC, which turned out to be exclusively ferrocene.

It follows that ferrocene immediately got oxidized and the reaction did not yield any product. With nitrobenzene (entry 2) the formation of an insoluble brown, tar-like substance was observed. Without $AlCl_3$, no oxidation occurred (entry 3). As Bauer and Foucault[14] found, mixtures of $AlCl_3$ and nitromethane generate NO^+ that could, in combination with the strong Lewis acid, oxidize ferrocene. Typically, in Friedel-Crafts reactions with ferrocene the acylation agent is formed prior to addition of the reactant. The above mentioned experiments were repeated with a modified procedure where $AlCl_3$ and the anhydride were stirred at 0 °C for 1 h before adding ferrocene; however the results remained the same. Further experiments were conducted in the same fashion. In addition, nitrobenzene is suspected to be carcinogenic and should therefore be replaced whenever possible. Thus, it was necessary to apply other solvents

to the reaction. In Table 2, an overview of a series of experiments with different solvents is given.

Table 2 Variation of solvent and N substituent X.

#	Solvent	Catalyst	X	Reaction Conditions	Oxidation	Observations
1	CH_2Cl_2	$AlCl_3$	H · HCl	Reflux, 33 h	slow	no conversion
2	Dioxane	$AlCl_3$	H · HCl	Reflux, 48 h	-	no conversion
3	$PhNO_2$	$AlCl_3$	$COCH_3$	120 °C, 16 h	immediate	Insoluble brown precipitate
4	CH_2Cl_2	$AlCl_3$	$COCH_3$	reflux, 16 h	slow	no conversion
5	Pyridine	$AlCl_3$	$COCH_3$	rt, 16 h	-	brown solution
6	Pyridine	$AlCl_3$	$COCH_3$	rt, 72 h	-	brown solution
7	DMF	$AlCl_3$	$COCH_3$	rt, 72 h	-	brown solution
8	DMSO	$AlCl_3$	$COCH_3$	rt, 72 h	-	Yellow solution, white precipitate
9	THF	$AlCl_3$	$COCH_3$	rt, 72 h	slow	no conversion
10	CS_2	$AlCl_3$	$COCH_3$	rt, 16 h	immediate	no conversion
11	$MeNO_2$	$AlCl_3$	Fmoc	rt, 16 h	immediate	no conversion
12	CH_2Cl_2	$AlCl_3$	Fmoc	rt, 16 h	slow	no conversion
13	CH_2Cl_2	$AlCl_3$	$COCF_3$	rt, 16 h	slow	violet solution

With the use of the hydrochloride of aspartic anhydride and CH_2Cl_2 or dioxane (Table 2, entries 2 and 3) as solvents, no reaction could be observed, but oxidation did not occur either. It was concluded that the very low solubility, due to the ionic nature of the hydrochloride, prevented the formation of the acylation agent. In order to improve the solubility, further experiments were conducted using N-acetylated aspartic anhydride. It was expected that this neutral anhydride shows an improved solubility and would form the acylation agent with $AlCl_3$. With pyridine and dmf as solvents (entries 5, 6, 7), the mixture turned brown over the course of the

reaction. After the reaction H_2O, $NaHCO_3$ and fmoc-Cl were added to protect expectedly formed free amino acids that could then be extracted into CH_2Cl_2. NMR spectra from the isolated material could not identify the desired product. The application of fmoc-aspartic anhydride was expected to further improve the solubility of the anhydride. In experiments with $AlCl_3$ (entries 11 and 12) no conversion was achieved. As is known in the literature, $AlCl_3$ can decompose the fmoc protecting group[15], which is probably the cause of this result.

An interesting outcome was observed with trifluoroacetamide protected anhydride (entry 19). Directly after addition of the anhydride / $AlCl_3$ mixture, a colour change from yellow to violet occurred. This is typically associated with the formation of the acylium ion. After aqueous workup, only one product was found in the organic phase. The aqueous phase was nearly colourless, indicating little oxidation during the reaction. Mass spectroscopy showed a very small amount of the desired product, whereas NMR analysis revealed the almost exclusive formation of trifluoroacetyl ferrocene (Figure 14).

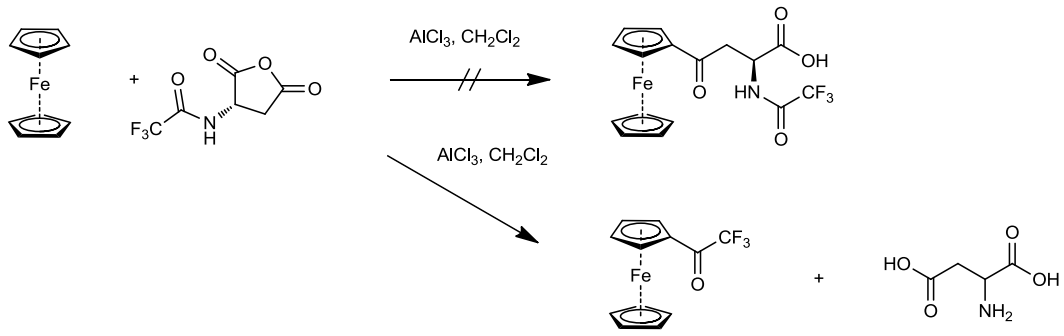

Figure 14 Reaction of Ferrocene with Trifluoroacetyl protected aspartic anhydride.

Although there are numerous examples of successful acylation using N-trifluoroacetyl aspartic anhydride on both electron rich and poor aromatic systems have been published (e.g. [16]) no report of a trifluoroacetyl transfer could be found. Since the anhydride was thoroughly dried before use, contamination with trifluoroacetic anhydride is unlikely, particularly given the high yield of the reaction. Interestingly, the reaction under the same conditions with $SnCl_4$ as catalyst resulted in oxidation of Fc. This leads to the assumption that $AlCl_3$ is capable of deprotecting trifluoroacetamides, which is in contrast to what is stated in literature.[15]

Friedel-Crafts acylation can be catalysed by Lewis acids other than $AlCl_3$ and even strong Brønsted acids. Additional experiments were performed using triflic acid, which has been shown to be an effective catalyst with anhydrides and tin tetrachloride, which is a liquid and could therefore, in contrast to $AlCl_3$, mix well with the solvent and enable the formation of an acylation agent. The results are shown in Table 3.

Table 3 Friedel-crafts experiments with triflic acid and tin tetrachloride.

#	Solvent	Catalyst	X	Reaction Conditions	Oxidation	Observations
17	$MeNO_2$	TfOH	Fmoc	rt, 0.5 h	immediate	no conversion
17	CH_2Cl_2	TfOH	Fmoc	rt, 0.5 h	immediate	no conversion
18	CH_2Cl_2	$SnCl_4$	$COCH_3$	rt, 16 h	immediate	no conversion
19	CH_2Cl_2	$SnCl_4$	$COCF_3$	Reflux, 16 h	immediate	no conversion
20	CS_2	$SnCl_4$	$COCH_3$	rt, 16 h	immediate	no conversion

In summary, no reaction conditions could be found to convert ferrocene into an amino acid in one step using Friedel-Crafts acylation. Not only did the reaction fail to produce the desired product, but it also became clear that a thorough optimization procedure would be necessary for the synthesis of each individual redox cofactor amino acid conjugate.

3.3 Grafting cofactors onto peptides using click chemistry

3.3.1 Preparation of clickable amino acids

In order to avoid the synthetic and practical problems described in the previous section, it was decided to apply copper-catalysed azide alkyne click chemistry (CuAAC) that allows for the post-synthetic grafting of redox cofactors onto peptides. The principle of this approach is shown in Figure 15.

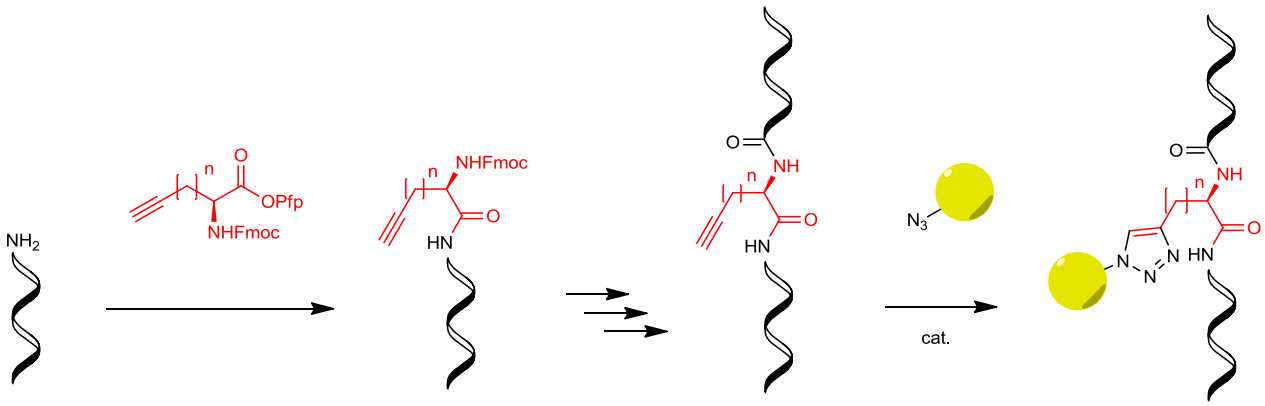

Figure 15 Principle of post-synthetic grafting via click chemistry, yellow sphere represents redox cofactor.

In the first step, an artificial amino acid carrying a clickable functional group like an alkyne is placed at a specific point in the peptide. After peptide synthesis is completed and global deprotection was performed, the cofactor is finally attached.

This method provides a series of advantages over the direct incorporation of cofactors into an amino acid. First, only one amino acid has to be produced in 10 g amount and turned into an amino acid toner. This way, the cofactors only need to be produced in small amounts in order to be applied. It is expected that some cofactors, particularly coordination clusters, are sensitive to the reaction conditions employed in peptide synthesis. By post-synthetically attaching them, this problem is avoided. Furthermore, a plethora of accordingly functionalized redox-active molecules that have also been proven to undergo CuAAC click reactions can be found in the literature.

The first step was to synthesize an amino acid to introduce a clickable function into a peptide. The alkyne was chosen to be at the peptide because unlike the azide it can be modified for consecutive click reactions. Although fmoc is a base-labile protecting group, few reports for successful nucleophilic substitution reactions on such protected amino acids involving strong bases can be found in the literature (e.g. [17]). In an effort to get the least number of synthetic steps to produce an fmoc protected alkyne-containing amino acid, an O-alkylation of Fmoc-serine with propargyl bromide (Figure 16) was tested.

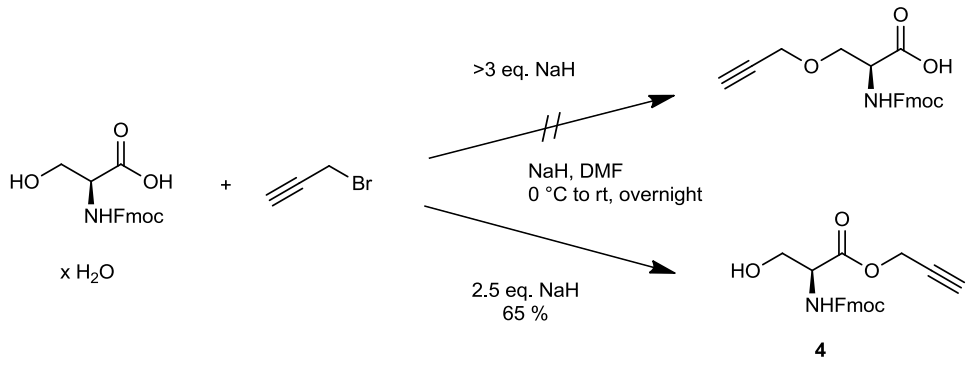

Figure 16 Test for O-Alkylation of Fmoc-serine with Propargyl Bromide and Sodium hydride as base.

When using more than 3 eq. of the base, the fmoc protecting group was cleaved, while 2.5 eq. yielded the propargyl ester **4** in 65% yield. A variety of reaction conditions was employed, but the desired product could not be obtained with this method. As a consequence, a very similar procedure to that in the literature[18] using boc protected serine was reproduced in moderate yield (Figure 17).

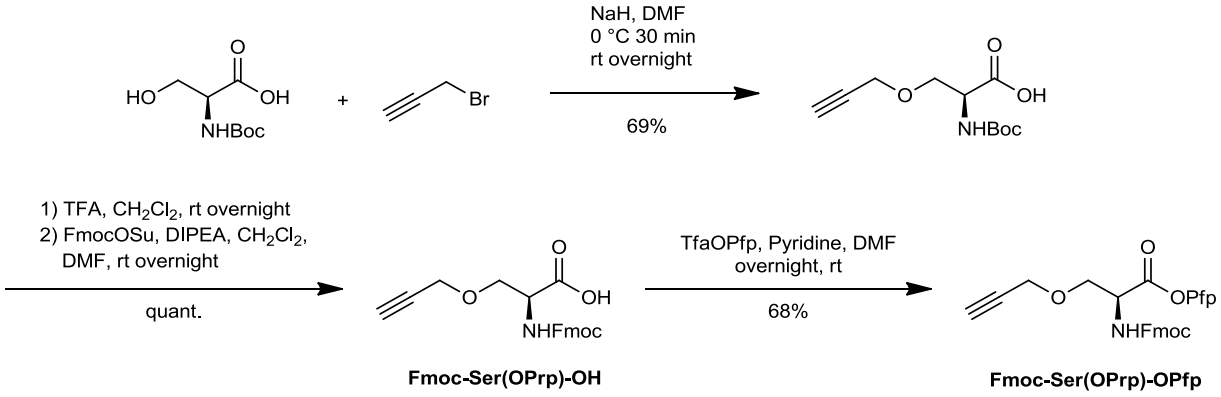

Figure 17 O-alkylation of boc-serine with propargyl bromide and subsequent exchange of the protecting group.

Cleavage of the *tert*-butyl carbamate and protection of the amine function with fmoc succinimide was achieved in quantitative yield. Subsequently, the carboxylic acid function was converted to a pentafluorophenyl (Pfp) ester with pentafluorophenyl trifluoroacetate (TfaOPfp) according to a procedure developed by Green et al.[19] in moderate yield.

The position of the cofactor along the peptide backbone is determined by the sequence of the peptides, whereas the distance from the backbone is given by the linker (Figure 18).

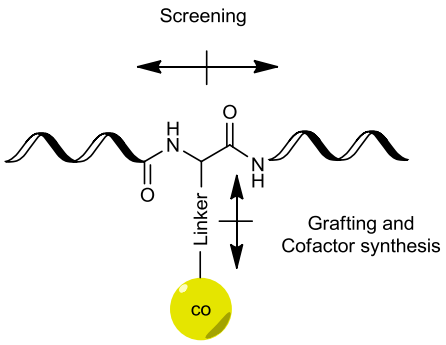

Figure 18 Influences on the position of a cofactor co and ways to tune them.

The amino acid sequence can be optimized by screening while the linker between the backbone and the cofactor is determined by synthesis of the amino acid and cofactors. The size and rigidity of this linker between a redox active species and the backbone of the peptide is likely to have an influence on the mobility of the cofactor and therefore on its relative position towards other cofactors in the molecule. It is also expected that it could have an effect on the efficiency of the click reaction in larger peptides with side chains of neighbouring amino acids as steric constraints. In order to provide a second option for the size of the linker, another alkyne containing amino acid should be synthesized. Therefore, commercially available fmoc-L-propargyl glycine (**Fmoc-Pra**) was converted into Fmoc-Pra-OPfp in a 200 mg scale experiment with quantitative yield (Figure 19)

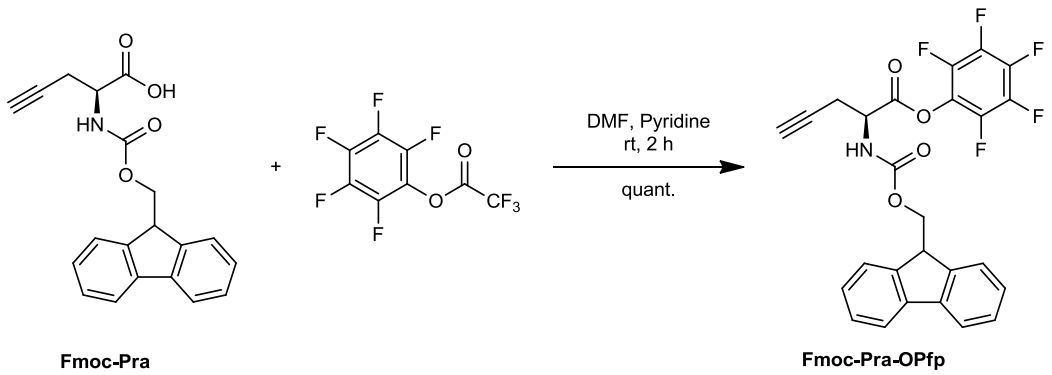

Figure 19 Pfp-activation of Fmoc-Propargylglycine.

This synthesis was successfully upscaled to 5 g experiments, where the yield decreased to 90 %. Both **Fmoc-Pra-OPfp** and **Fmoc-Ser(OPrg)-OPfp** were exposed to air and moisture at room temperature over several days to see if any degradation occurred. Neither of them showed any changes in reactivity or appearance.

3.3.2 Investigation of click reaction on a glass slide surface by fluorescent imaging

Fluorescent imaging is widely used in biological applications, where a fluorescent dye is linked to a specific binder that binds a target. A sample can be stained with such a dye and investigated towards the existence and distribution of its target. In order to visualize a successful click reaction on the glass slide surface, this principle should be applied. Because such fluorophores are commercially available but very expensive, the first step was to synthesize a suitable fluorophore that can be used with the available GenePix scanner. The group of Balaban provided a series of styrylpyridinium dyes that contain an amine function and work with the wavelengths required for this purpose. They were subjected to a diazo transfer reaction with imidazole-1-sulfonyl azide hydrochloride **5** to yield the corresponding azides (Figure 20).

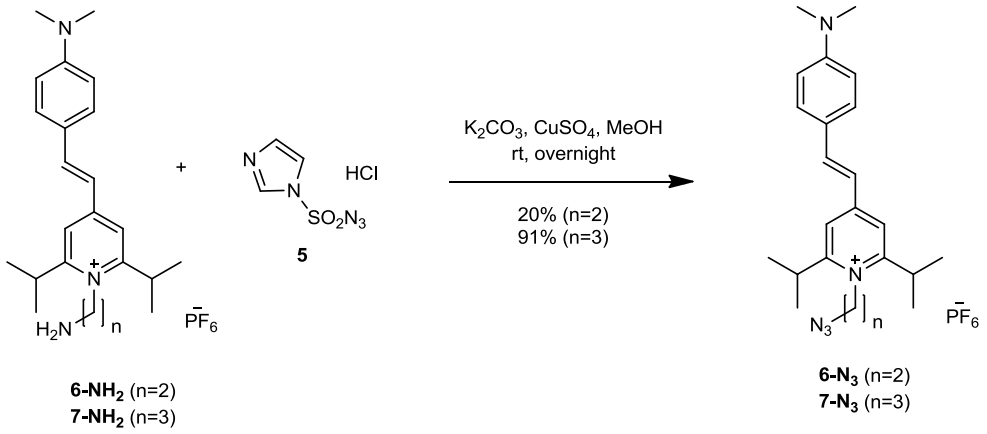

Figure 20 Diazo transfer reaction on Styrylpyridinium fluorophores.

The first experiment with **6-NH_2** yielded only 20% of the desired product, which is not satisfactory taking into account the multi-step nature of the fluorophore synthesis.[20] It was concluded that due to the isopropyl groups close to the amine function, the steric hindrance is responsible for the low yield. An experiment with **7-NH_2**, in which the amino group is separated from the fluorophore by an additional CH_2 unit, confirmed this assumption with a substantially larger yield. The polarity of the product was considerably lower than of the reactants and could therefore easily be separated by passing it through a short plug of silica using acetonitrile as eluent. This modified fluorophore was now used as a marker to demonstrate successful click reactions on the previously prepared, structured glass slide.

3.3.3 Fluorophore of structured glass slide surface

Following a procedure by Breitling et al.[21], **Fmoc-Pra-OPfp** was coupled to a glass slide surface in form of a pattern. The complete slide was brought into reaction with **6-N_3** using $CuSO_4$ / ascorbic acid in DMF for 1 h and after washing and drying, scanned using a GenePix fluorescence scanner. A detail of the fluorescence scan is shown in Figure 21.

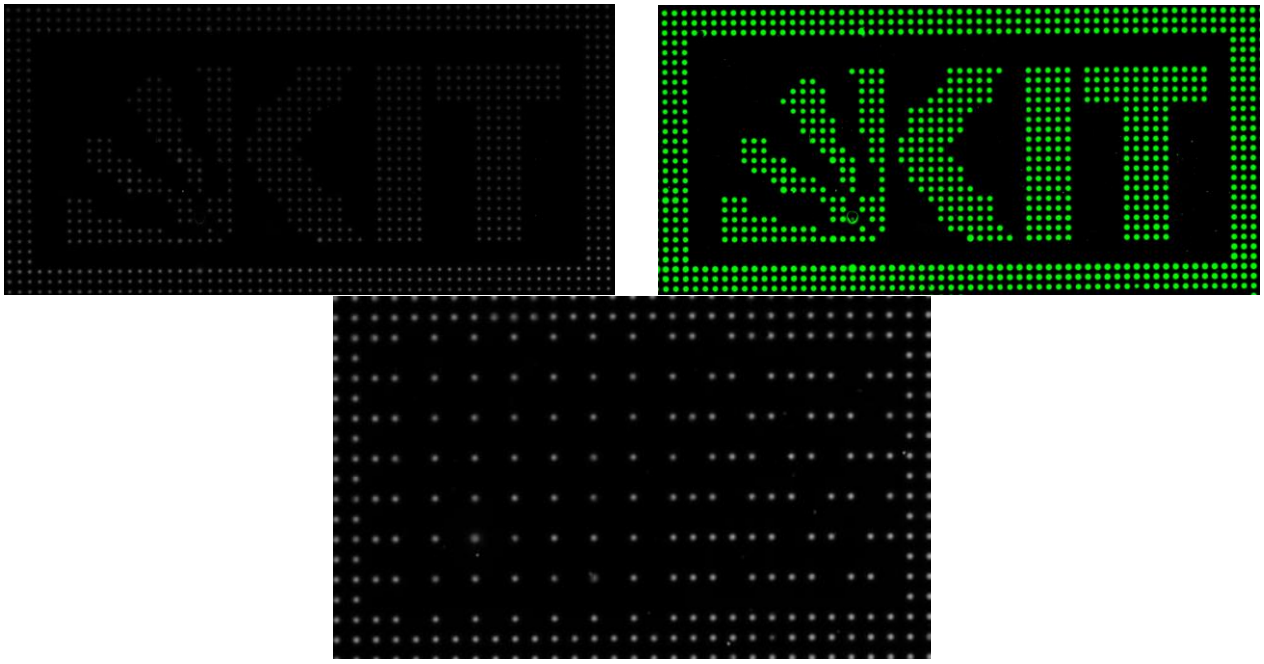

Figure 21 Detail of the structured slide. Pitch (point-to-point distance) = 250 µm. Top left: normal image; top right: picture with intensity threshold; bottom: different region of slide, larger zoom.

As can be seen in the images, the shape of the amino acid spots is well defined, the separation is good and the background is very low. This result allows some important conclusions to be drawn. The reaction is very selective and produces few artefacts, the structuring process does not harm the alkyne function in **Pra** and the reaction time of one hour is sufficient. Neither the activated amino acid nor the fluorophore show any unspecific binding to the surface. These findings confirm the feasibility of CuAAC as a grafting method onto peptides on glass slide surfaces.

3.3.4 Investigation with X-ray photoelectron spectroscopy (XPS)

It is known that click reactions on polymers can leave traces of copper in the product material.[22] Since this would constitute a redox active impurity that could lead to misinterpretations of electrochemical data of the final peptide, it was necessary to investigate the product with regard to copper. Another important piece of information to obtain was the amount of substance that was clicked onto the surface. Thus, a quantitative method had to be used. From the available methods, only energy dispersive x-ray scattering (EDX) and x-ray photoelectron spectroscopy (XPS) qualified for such investigations.

Pegma 10/90 glass slide surfaces for peptide synthesis are already functionalized with fmoc-β-alanine. It follows that the surface already contains considerable amounts of carbon, nitrogen and oxygen, both from the polymer and the amino acid. It is also certain that the click reaction will not dramatically change the content of these elements on the surface. From these considerations, it was concluded that the best way to investigate click chemistry with EDX or XPS was to introduce a heteroatom. Since the concept of a chemical marker proved to be useful, it should be applied again, this time with azidomethyl ferrocene **9-N_3**, which has been shown to undergo click reactions.[23]

Since click grafting should later be applied to coordination clusters, which can be sensitive to hydrolysis with large amounts of H_2O, it was necessary to carry out the reactions in organic solvents. A series of five glass slide samples was prepared to be measured via X-ray photoelectron spectroscopy. One slide was left blank as a reference sample for the background. Two samples were subjected to click reaction conditions with azidomethylferrocene and $CuSO_4$ / ascorbic acid and $Cu(CH_3CN)_4BF_4$ respectively. For each of these, a control sample was generated by first exposing them to **9-N_3** for the duration of the click reaction, then washing and in a second step applying the catalyst, again for the same duration. With these conditions, the click reaction should not proceed. Nevertheless all reaction conditions were applied to the control samples. It should be noted that the samples that were exposed to ascorbic acid were washed additionally with H_2O to remove the crystalline solid that formed on the slide surface. The XPS results are shown in Figure 22

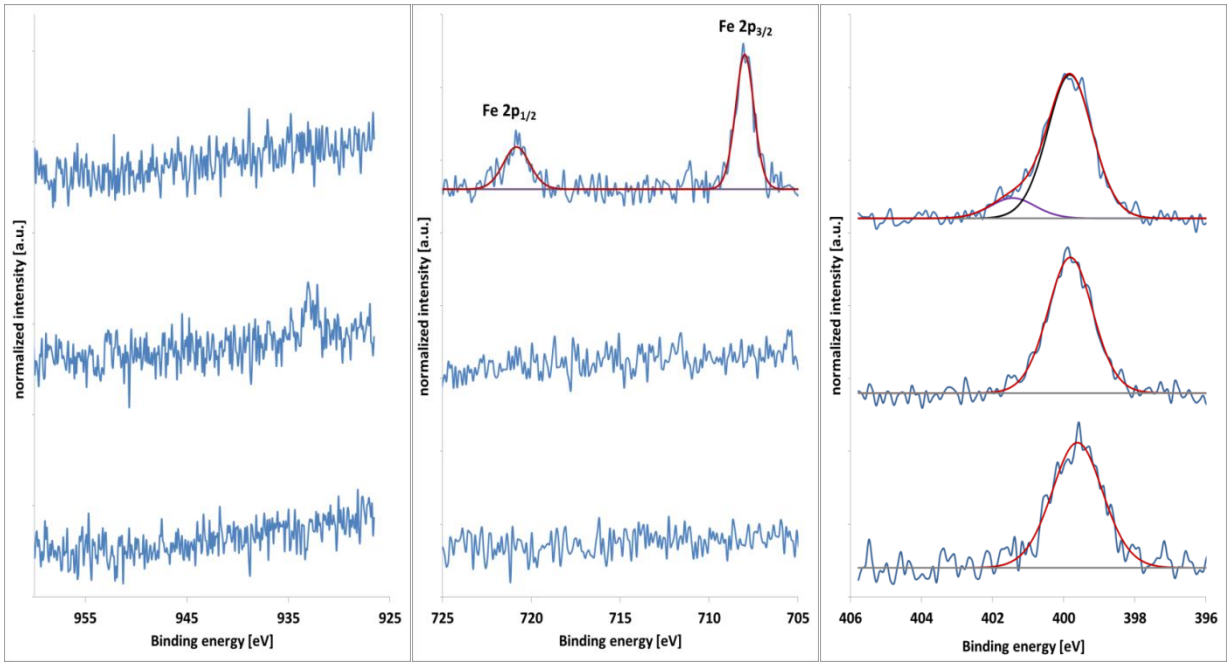

Figure 22 XPS results for $FcCH_2N_3$ clicked on glass slide, left Cu 2p, centre Fe 2p, right N 1s, top click reaction centre control sample, bottom blank sample.

In both the $CuSO_4$ / ascorbic acid and $[Cu(CH_3CN)_4]BF_4$ catalyzed click reaction, the Fe 2p scan shows an Fe $2p_{1/2}$ line at 707.9 eV and an Fe $2p_{3/2}$ line at ca. 719 eV, which both correspond to the ferrocene moiety, according to Weidner et al.[24] N 1s scans show no remaining azide, Cu 2p scans no remaining Cu. Table 4 shows the parameters for the parameters for the Fe $2p_{1/2}$ lines of the samples.

Table 4 Parameters for Fe 2p scans of clicked glass slides, BE = binding energy.

	BE (eV)	atomic %
blank slide	-	-
$CuSO_4$ / ascorbic acid catalysis	708	0.2
control	-	-
$Cu(CH_3CN)_4BF_4$ catalysis	707.9	0.2
control	710.3	0.2
	712.4	0.1

The control sample of the $[Cu(CH_3CN)_4]BF_4$ catalysed reaction showed two lines of 0.2 $\%_{atom}$ at 710.3 and 712.4 eV, which both were significantly broader compared to those of Fe(II) in Fc. The line with the lower energy corresponds to a ferrocenium (fc^+) species.[25] It is not known what caused the oxidation to ferrocenium in only one of the samples. A reasonable explanation for it being on the pegma thin film is that due to the increased polarity of the ionic fc^+ it shows stronger adhesion to the strongly polar polyethylene glycol polymer.

Although the results are close to the detection limit of 0.1 Atom%, they allow for some important conclusions to be drawn. Over the course of 12 h, both applied catalysts give comparable results. Copper is not accumulated in the polymer, or its amount is neglectible. Mainly, the feasibility of CuAAC using Propargylglycine on pegma 10/90 thin films could be demonstrated.

3.4 Synthesis of modified alkyne amino acids for consecutive click reactions

In the previous section, the feasibility of single step CuAAC click reactions on pegma 10/90 glass slide surfaces could be shown. The next step was to increase the scope of post-synthetic click grafting to consecutive click reactions.

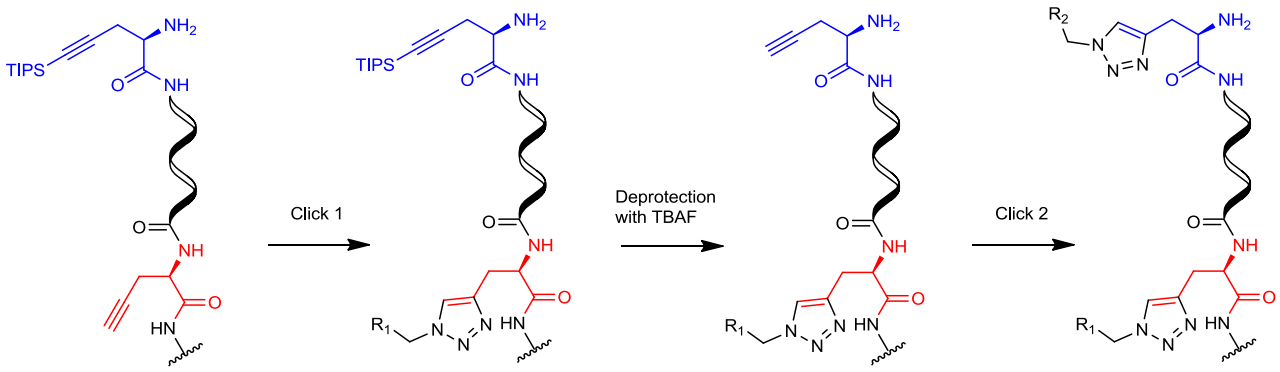

Figure 23: General procedure of consecutive click reactions with deprotection.

A crucial step in the mechanism of CuAAC is the formation of a copper acetylide. In general, copper catalysis works exclusively with terminal alkynes. Literature research showed that with replacing the terminal proton on an alkyne with an easily cleavable trialkylsilyl protecting group, a two-step consecutive sequence is achieved.[26] Peptide synthesis in which this chemistry should be included involves the use of strong acids and bases such as piperidine and trifluoroacetic acid (TFA). The triisopropylsilyl (TIPS) group is sterically demanding and a comparatively stable protecting group for alkynes. It has been shown to be one of only a few silyl groups to withstand treatment with TFA and pyridine.[ref] It is also the one with the best yield for the protection of the alkyne, and is therefore the group of choice.

The first step towards consecutive click reactions was to synthesize an accordingly modified amino acid. The first conversion was done with N-boc protected DL-propargylglycine which was prepared from commercially available DL-propargylglycine in one step using standard protecting group chemistry. **Boc-Pra-OH** was then converted to **Boc-Pra(TIPS)-OH** by a nucleophilic substitution on triisopropylsilyl chloride (Figure 24).

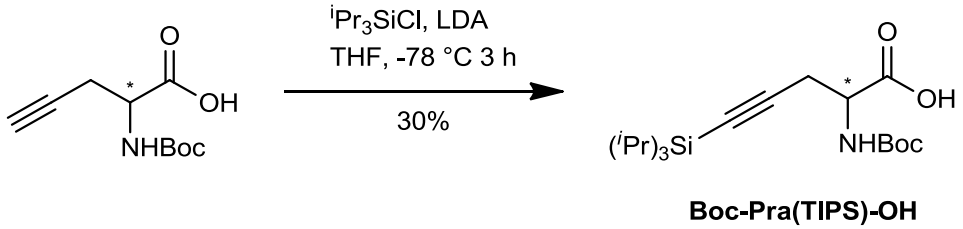

Figure 24 one-step protection of boc-propargylglycine with TIPS.

Conversions involving a triisopropyl group are known to have low yields because of its high steric demand. Considering the high price for **Pra** derivatives, it was desired to find a route that applies different reactants. Recently Maier et al. published a method for the synthesis of a triethylsilyl protected propargylglycine derivative. [27] Because this method relies on far less expensive reactants, it was adopted to synthesize **Boc-Pra(TIPS)-OH**. The methyl ester from the original procedure was replaced with *tert*-butyl, because deprotection of the carboxylic and amino group can then be performed in one step. *Tert*-butyl 2-((tert-butoxycarbonyl)amino)-3-iodopropanoate **8** was brought into reaction with zinc and subsequently with CuCN and LiCl to generate a Knochel cuprate **9**. After this umpolung, (bromoethynyl)triisopropylsilane was added to form the desired TIPS protected propargylglycine *tert*-butyl ester **10** in only 17% yield (Figure 25).

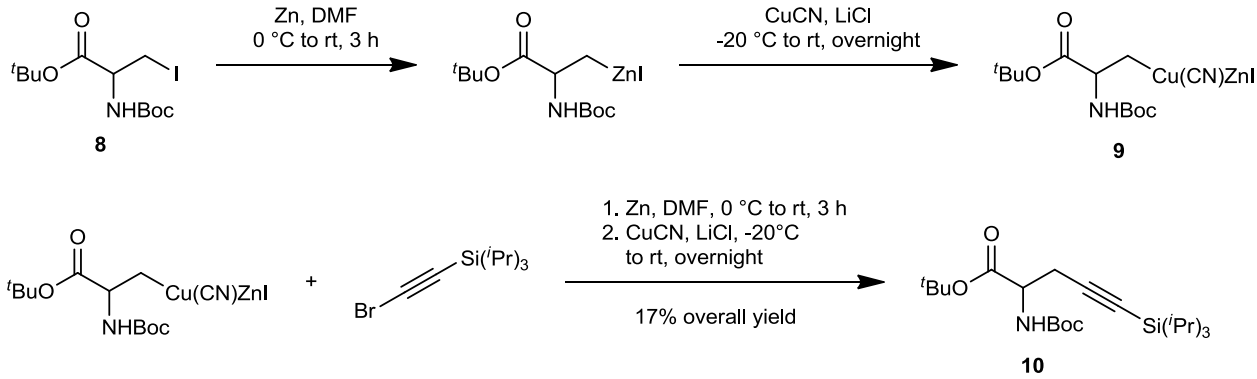

Figure 25 Conversion of 8 into knochel-cuprate 9 and subsequent substitution reaction to 10.

In TIPS-bromoacetylene the reaction site is even closer to TIPS as in the propargyl analogue, which is probably the cause for the low overall yield. High-yield conversions involving the TIPS

moiety are typically done under reflux for days. The yield of the conversion could be improved by heating, although this increases the danger of β-elimination.

The deprotection and saponification step was conducted with a mixture of trifluoroacetic acid in CH_2Cl_2 (1:2) until thin layer chromatography showed no more reactant, which took about 1 h. The free amine was then protected with fmoc-OSu and after aqueous workup purified via column chromatography. Two fractions were recovered from the column and were identified as the desired fmoc protected amino acid in 35% yield and the corresponding *tert*-butyl ester (Figure 26).

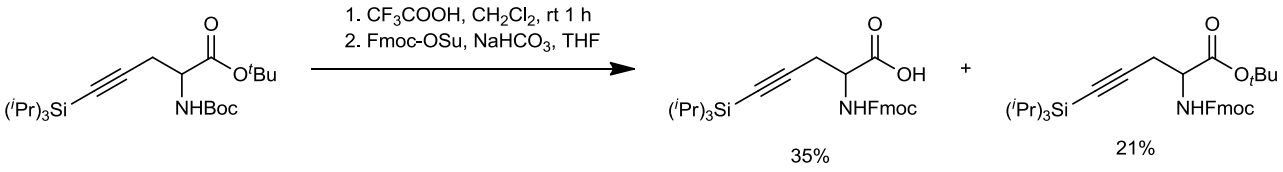

Figure 26 deprotection, saponification and fmoc protection of 10.

From this result it follows that the TIPS protecting group is stable towards TFA as expected. It also shows that the saponification of the *tert*-butyl ester needs either more time or heating to complete the reaction. Nevertheless, the reaction gave enough material that was successfully converted to the active ester and used to prepare glass slides containing both the protected and unprotected amino acid. These experiments are presented in section 3.5.2.

In order to produce two complete sets of amino acids to choose from, a protected version of **Ser(OPrp)-OH** should be synthesized as well. The first attempt was to bring a modified propargyl bromide into reaction with boc-serine in the same fashion as for the unmodified version (Figure 27).

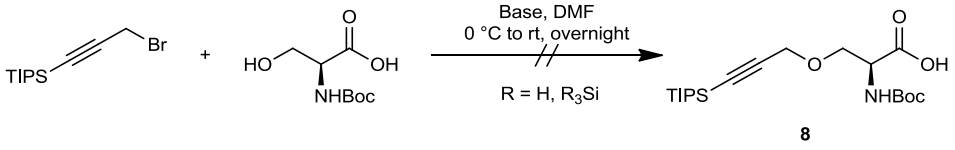

Figure 27: Attempted nucleophilic substitution reaction to synthesize 8.

No conversion was achieved using this synthetic route. This probably results from the high steric demand of the TIPS protecting group and the close proximity of it to the carbon atom to be substituted. In an effort to take the reaction site further away from TIPS, boc-serine was converted to the corresponding iodide and reacted with TIPS-propargyl alcohol. The conversion was tested with strong (NaH, KO^tBu) and moderate (diisopropylethylamine) bases, which resulted in quantitative elimination to **9** (Figure 28)

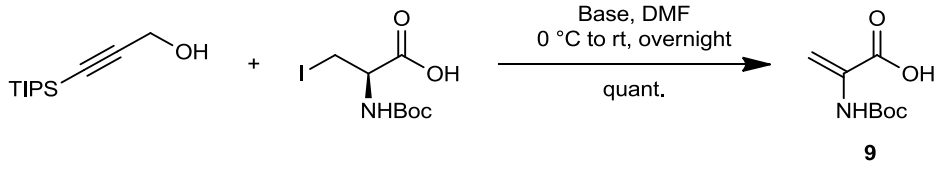

Figure 28: Unwanted elimination reaction instead of nucleophilic substitution.

These findings can be rationalized as resulting from the high steric demand of the TIPS group and from iodine being a good leaving group. At this point it was decided to first perform experiments to confirm the feasibility of consecutive click reactions on glass slide surfaces and eventually continue optimization of the synthetic procedure.

3.5 Verification of consecutive click reactions

3.5.1 Verification by fluorescence scanning

A method had to be found to verify the planned click reaction sequence. The first approach was to find two fluorophores that show different excitation and emission maxima and could therefore be distinguished via fluorescence scanning. Three different fluorophores from the group of Balaban were converted to the corresponding azides and applied to a blank glass slide in form of a dilute solution. After evaporation of the solvents, the slide was scanned using both wavelength settings of the scanner. The resulting scans are shown in Figure 29.

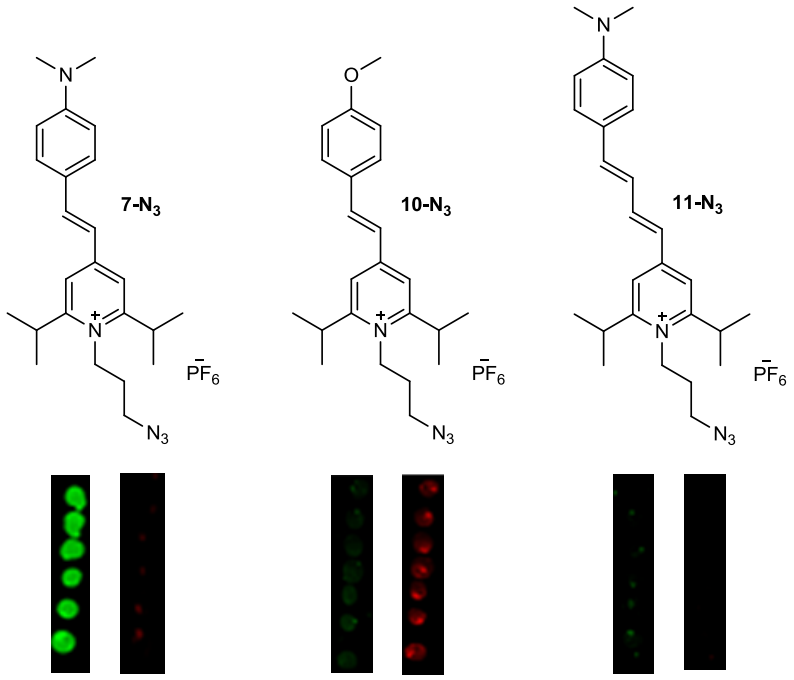

Figure 29 Scans of the different fluorophores using the 635 nm (red) and 532 nm channel (green).

7-N_3 is clearly visible in the 532 nm scan and almost invisible in the 635 nm scan and is therefore a good candidate for the experiment. **10-N_3** is slightly visible in both scans and **11-N_3** cannot be detected at all. The 635 nm channel is designed to work with cyanin 5 dyes which are commercially available in clickable form. Because of the very high price (1 mg = 100€) of the dye and the fact that a simple fluorescence scan does not give a quantitative measure to compare the reactions, it was decided to use a different method for the investigation of consecutive click reactions. If a scanner were available that is more flexible in terms of excitation and emission

wavelength, and that gives quantitative data about the scans, this approach would nevertheless be favourable over other methods because of its simplicity and speed.

3.5.2 Verification via XPS

The concept of using a metallocene as marker for XPS is described in section 3.3.4. It was extended to investigate consecutive click reactions using azidomethyl ruthenocene **12-N_3**, the synthesis of which is shown in section 3.6.1, as a second independent marker.

Reactions on the glass slide surface were performed following procedures developed by Christopher Schirwitz.[28] As a basis for the experiments pegma 10/90 coated glass slides with N-fmoc-β-alanine already coupled to the surface, so-called synthesis slides, were used. One such slide was deprotected with piperidine and reacted with **fmoc-Pra(TIPS)-OPfp** in DMF. After washing, another deprotection step with piperidine was conducted. Next, **fmoc-Pra-OPfp** was coupled onto the peptide. This slide was then cut into small sections (1x1 cm) and used for a series of experiments. An example is shown in Figure 30

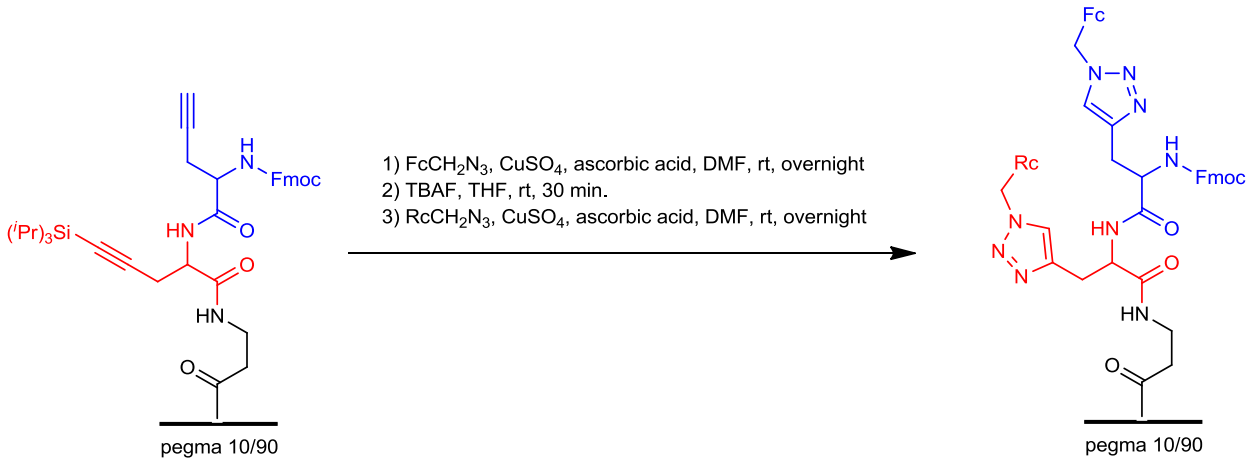

Figure 30 consecutive click reaction on surface-bound peptide.

The resulting glass slide surfaces were characterized by XPS, the results are shown in Figure 31.

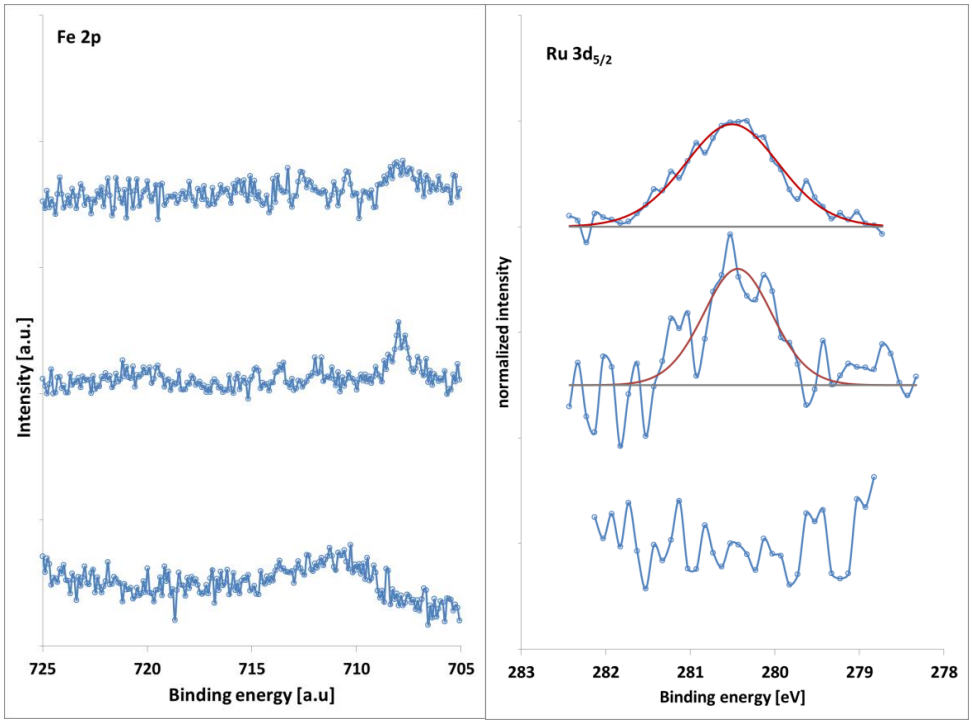

Figure 31 XPS scans of Ru $3d_{5/2}$ and Fe $2p_{3/2}$ for consecutively clicked ferrocene and ruthenocene derivatives.

In the experiment represented by the scans at the top, the ferrocene derivative was clicked in the first step and the ruthenocene derivative in the second step, in the scan in the middle vice versa. The scans on the bottom show the control sample. In neither of the samples, fluorine from the TBAF deprotection could be found. However, the lines for Fe ($2p_{3/2}$, 707 eV) and Ru ($3d_{5/2}$, 280.4 eV) in these experiments were much smaller than expected (comp. with Figure 22).

Samples were prepared with only the protected amino acid to test if the deprotection worked. As can be seen in Table 5, the results show that both the deprotection and subsequent click reaction give comparable results to the unprotected alkyne.

Table 5 Parameters for the xps measurements for click reactions with $FcCH_2N_3$ on Fmoc-Pra(TIPS) at pegma 10/90.

	line	BE [eV]	Atomic %
TFA deprotected	Fe $2p_{3/2}$	708,2	0,1
control (no catalyst)	Fe $2p_{3/2}$	711,0	0,2
TIPS protected	Fe $2p_{3/2}$	-	-

The click reaction did not proceed without prior deprotection of the alkyne. The control sample for the Fc click reaction again contains $Fe^{(III)}$ (see Table 4 for comparison). This line was not present when Ferrocene was clicked to the surface, although the washing steps were the same. This phenomenon should be investigated further. Figure 32 shows the Ru 3d scans for $RcCH_2N_3$ clicked on Fmoc-Pra (top), deprotected Fmoc-Pra(TIPS) (middle) and a blank sample (bottom).

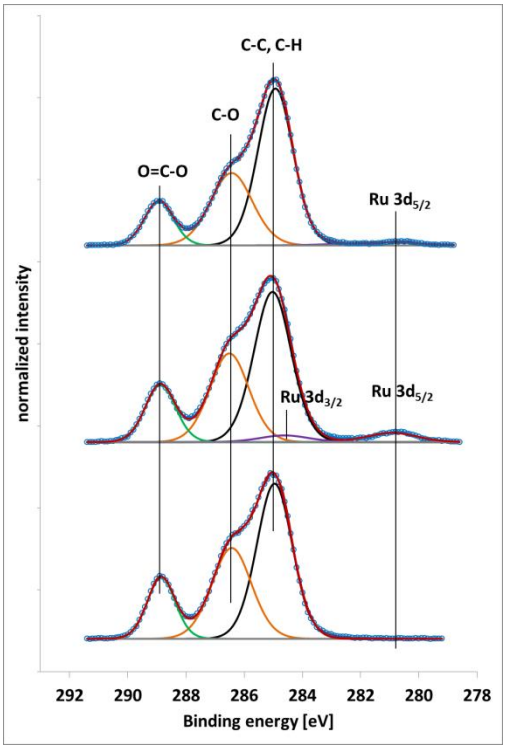

Figure 32 XPS scans for Ru 3d for $RcCH_2N_3$ clicked on Fmoc-Pra (top), Fmoc-Pra(TIPS) after TBAF deprotection (middle) and a blank sample with Fmoc-Pra at pegma 10/90, C 1s lines belong to pegma / pmma copolymer.

Table 6 shows that the click reactions of $RcCH_2N_3$ and $FcCH_2N_3$ give comparable results.

Table 6 Parameters for the xps measurements in Figure 32.

	line	BE [eV]	atomic %
Fmoc-Pra, unprotected	Ru $3d_{5/2}$	280,5	0,1
Fmoc-Pra (TIPS), deprotected	Ru $3d_{5/2}$	280,5	0,1
blank sample	-	-	-

To this point, some very important information could be collected. The individual steps of the consecutive click sequence work very well and reliable, but are considerably less effective when

both reactions are done on the same peptide in close proximity. The TIPS protecting group withstands the treatment with TFA, as shown in the saponification step (see Figure 26). The coupling steps onto the glass slide and the results from XPS measurements showed that TIPS is stable towards piperidine treatment. In Section 3.3.3 could be shown that the structuring does not corrupt the function of the alkyne amino acid. From this follows that the method is feasible and suited for consecutive click grafting.

It is necessary to explore the limits of this approach, particularly the constraints of how close the alkyne functions can be to still get good results. This should be the subject of a new research project.

3.5.3 Synthesis of a thioalkyl conjugated amino acid for iridium-catalyzed click reactions

Early in 2014, Ding et al.[29] published a new variety of azide alkyne click chemistry that utilizes thioalkynes and iridium catalysis and is claimed to be insensitive to air and moisture. Moreover, the reaction is orthogonal to CuAAC. In order to further extend the scope of post-synthetic click grafting, this reaction should be added to the reaction sequence. Figure 33 shows how a three-step consecutive click reaction could be applied to post synthetic grafting on a peptide, where the optimum order should be tested.

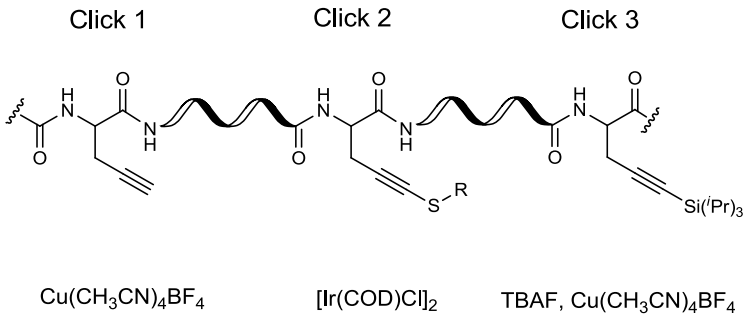

Figure 33 Example of a peptide for three consecutive click reactions.

A simple experiment was devised to test if IrAAC works with redox active moieties like ferrocene. For testing, a modified propargyl alcohol should be used as thioalkyne. Following the synthetic protocol by Ding et al., propargyl alcohol was brought into reaction with butyllithium and methyl disulphide. Instead of the expected thioalkyne, a dithioalkene was received (Figure 34).

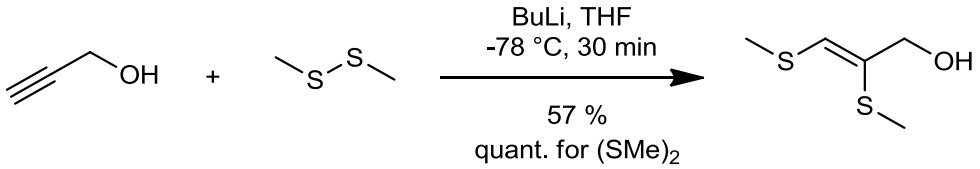

Figure 34 Reaction of propargyl alcohol with butyllithium and methyl disulphide.

This can be explained by the formation of the desired thioalkyne in a first step and the subsequent nucleophilic addition of methyl thiolate which occurred as a by-product of the nucleophilic attack on the disulphide (Figure 35).

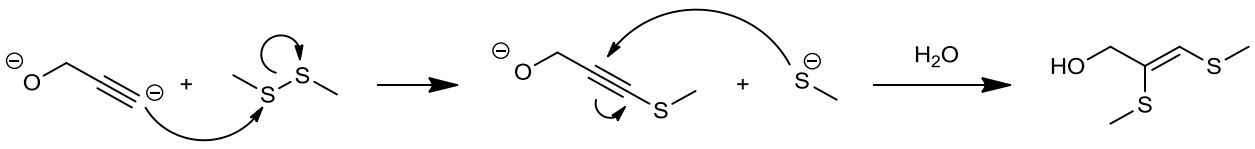

Figure 35 Possible pathway of dithioalkene synthesis.

In fact, a reaction under similar conditions can be found in literature that is claimed to proceed in this way.[30] The desired product was then successfully synthesized according to a different procedure by Heaps et al.[31], using methylthiocyanate as electrophilic thiolating agent (Figure 36).

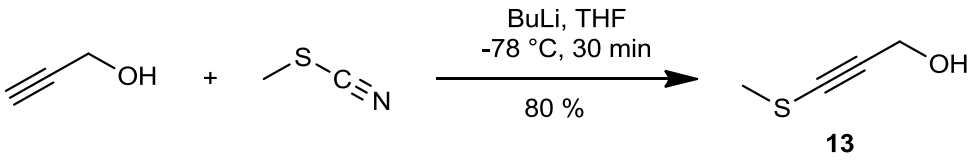

Figure 36 Synthesis of 3-(methylthio)prop-2-yn-1-ol 13 according to Heaps et al.

With the reactants now available, the IrAAC click reaction between **13** and **12-N_3** was conducted successfully (Figure 37).

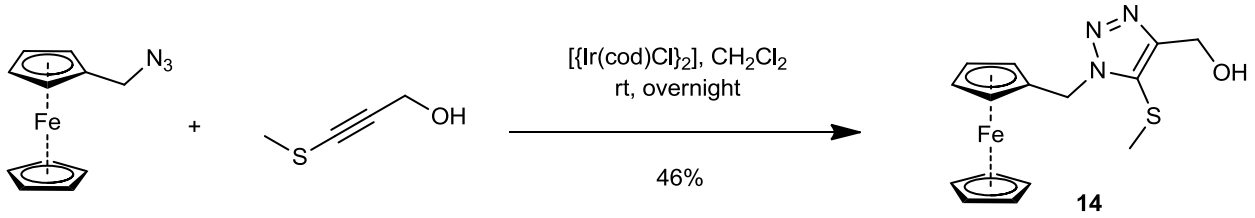

Figure 37 Iridium catalyzed click reaction between 13 and 12-N_3.

The yield was only 46% after purification, but no optimization of the reaction conditions was undertaken. From the purified product, large orange crystals could be grown that were characterized via X-Ray single crystal diffraction. The crystal structure of 14 is shown in Figure 38.

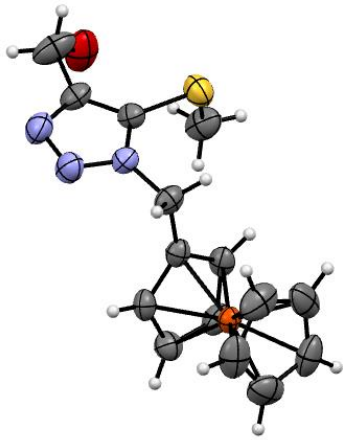

Figure 38 crystal structure of 14.

A very important piece of information from this structure is that the measured crystal contains only one of the two possible regioisomers. The entire solid product was then subjected to powder x-ray diffractometry for comparison. Figure 39 shows the resulting powder pattern in comparison with the theoretical pattern that was calculated from the single crystal data.

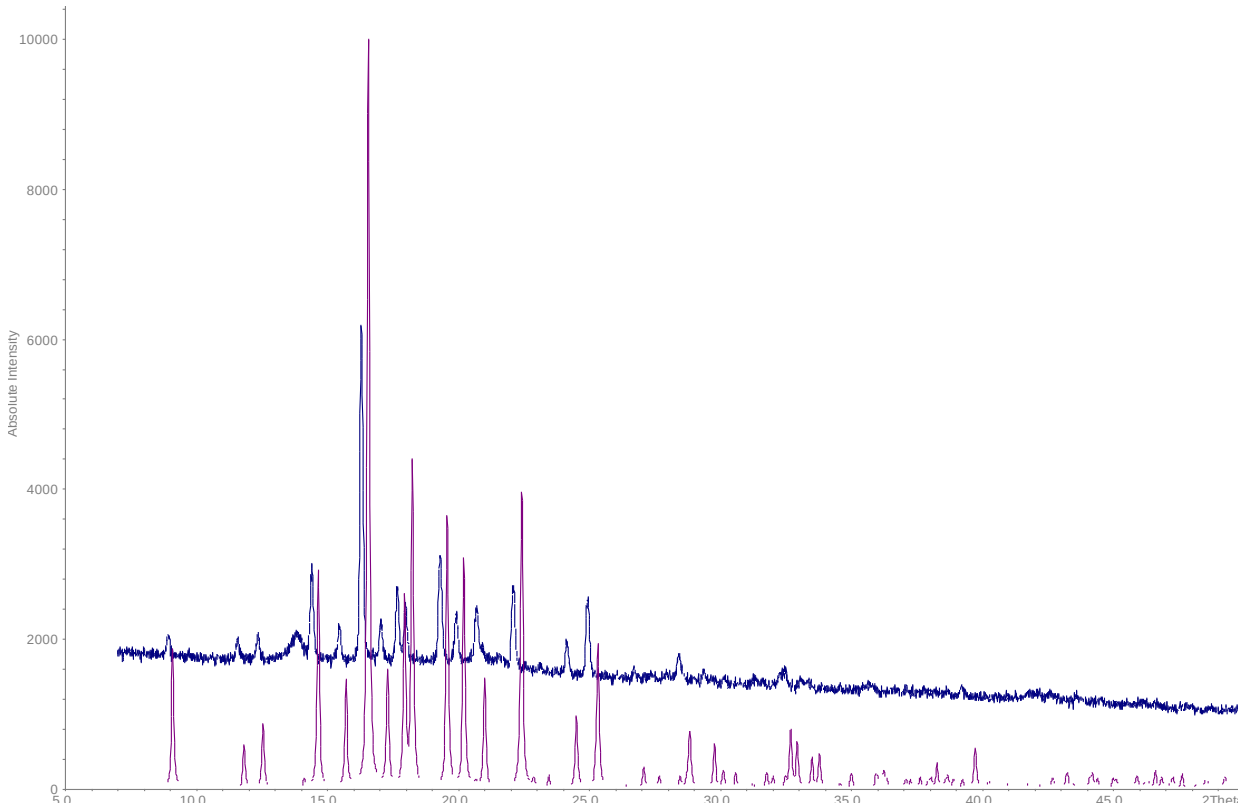

Figure 39 measured (upper) and calculated (lower) powder diffraction pattern for 14.

The broad and noisy signal at 14° belongs to the sticky tape that was used to contain the powder sample. The slight shift of the signals results from the fact that the powder measurement was done at room temperature and the single crystal measurement at 150 K, where the elemental cell is smaller due to less thermal vibration. Aside from this shift the patterns are in good agreement. From this follows that the entire isolated substance consists of a single regioisomer. Although the 46% yield leads to the suspicion that the other regioisomer was formed in equal amounts but not isolated. However, it is expected that the antimer has similar chemical properties, including polarity. Therefore, it should show a similar retention factor on a TLC plate, however nothing even remotely similar could be found in the crude product of the reaction.

In order to test for the orthogonality of the CuAAC and IrAAC reactions, the same experiment was conducted with $CuSO_4$ and ascorbic acid instead of $[Ir(COD)Cl]_2$. Even after leaving the reaction mixture overnight at room temperature, no change was observed via TLC. This confirms that CuAAC and IrAAC qualify for the implementation in a consecutive click reaction sequence. On the basis of this very promising preliminary result, it was planned to include IrAAC in the consecutive click reaction sequence. Therefore, it was necessary to synthesize an accordingly modified amino acid.

Since the thiomethyl group is far less sterically demanding than TIPS, the reaction with an activated serine derivative was more likely to succeed. However, no substitution was achieved, but exclusively elimination (Figure 40).

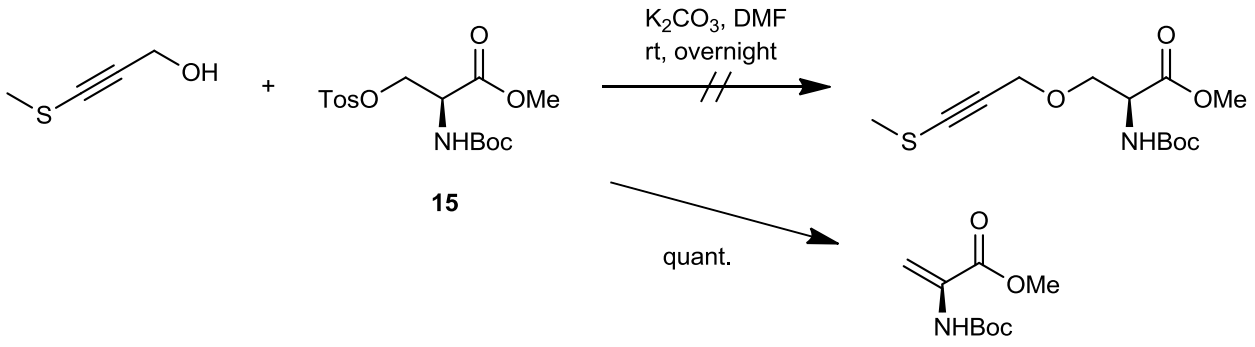

Figure 40 Reaction of tosylate 15 with 13.

In parallel to the first experiments with propargyl alcohol and disulphide, similar conditions were applied to propargylglycine (Figure 41). 3

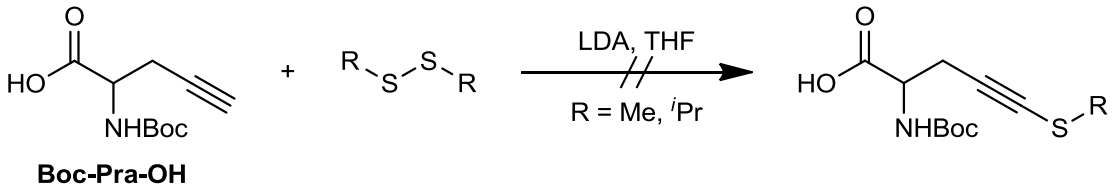

Figure 41 failed conversion of Boc-Pra-OH to thioalkyne.

The desired product could not be obtained. In 1992, Kabanyane and MaGee[32] reported the issue of sulphide attacking the thioalkyne. They successfully conducted the reaction by adding methyl iodide as scavenger. Changing the reaction protocol accordingly did not lead to the desired product. Since it was effective for the modification of propargyl alcohol, methyl thiocyanate was applied to boc-propargylglycine with *n*-butyllithium as base (Figure 42).

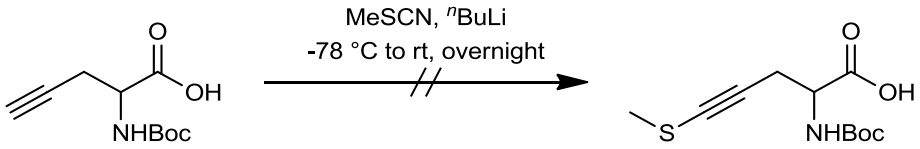

Figure 42 attempted reaction of Boc-Pra with MeSCN and BuLi.

Only a small amount of propargylglycine could be recovered from the reaction mixture. The desired product could not be obtained with this strategy. Bieber et al. reported in 2004 a "short and efficient preparation of alkynyl selenides, sulphides and tellurides" based on a reaction of the alkyne, a bis-chalcogenide and copper iodide in DMSO with a plethora of substrates.[33] Their procedure provides moderate to good yields under mild reaction conditions, which is precisely what is needed for the functionalization of propargyl glycine. A series of experiments was conducted with boc- and fmoc-protected propargyl glycine, methyl- and isopropyl disulphide.

In the cases of boc-pra, no conversion could be observed at room temperature. The reactions were monitored via TLC, performing a miniature workup. A small sample of the reaction solution was dissolved in a little water, acidified with HCl and the product extracted with CH_2Cl_2. Monitoring these reactions with TLC is particularly difficult because of DMSO being hard to remove. Additionally, boc-pra does not show uv absorption and therefore had to be stained

using $KMnO_4$. The results from this monitoring were inconclusive and workup showed that no product was formed. In order to screen for appropriate reaction conditions, fmoc-pra was applied since it absorbs UV radiation well and additionally its deprotection can easily be detected. In addition to the sparingly soluble CuI, $Cu(CH_3CN)_4BF_4$ was applied to catalyse the reaction, with the expectation of improving reactivity with a higher catalyst concentration. In any case, the fmoc group was slowly cleaved while no thiolation was observed. Conducting the reaction at 80 °C only led to quicker deprotection. Through time constraints it was not possible to perform further reactions on this part of the project.

An alternative to IrAAC could be Ruthenium catalysed azide alkyne click (RuAAC) chemistry, which works with internal as well as terminal alkynes. The disadvantages of using RuAAC are that catalysis is less regiospecific and produces 1,5- instead of 1,4-substituted triazoles as main product and needs inert atmosphere and dry solvents. The synthesis of an accordingly modified amino acid was performed via O-alkylation of boc-serine with 1-bromopent-2-yne (Figure 43).

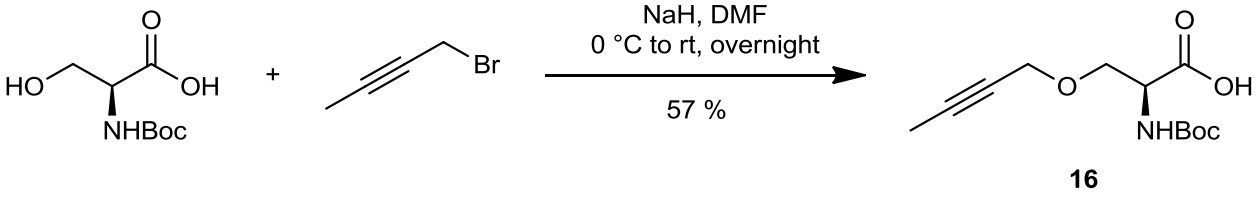

Figure 43 Synthesis of amino acid 16 containing an internal alkyne for RuAAC.

3.6 Structurally simple redox cofactors

3.6.1 Azide functionalization of redox active compounds

A requirement for click grafting is the availability of a method to functionalize the redox active molecules with an azide function. Several methods are known to introduce an azide into molecules. One is the previously mentioned diazo transfer reaction to an amine using imidazolesulfonyl azide. Other methods include the use of sodium azide to substitute a halide and, in combination with acetic acid, to substitute an alcohol.

The first molecule targeted was azidomethylferrocene. Few examples are given in the literature where dimethylaminomethyl ferrocene **9-NMe$_2$** is activated by methylation and then substituted with azide. Since **9-NMe$_2$** is expensive to purchase and the synthesis (see section 3.1) did not give good yields, this approach was not favoured. Most literature procedures however suggest treating hydroxymethylferrocene with sodium azide and glacial acetic acid with heating[34], which is dangerous for producing larger amounts of substance. Therefore it was desirable to test an alternative route, applying the diazo transfer reaction (Figure 44).

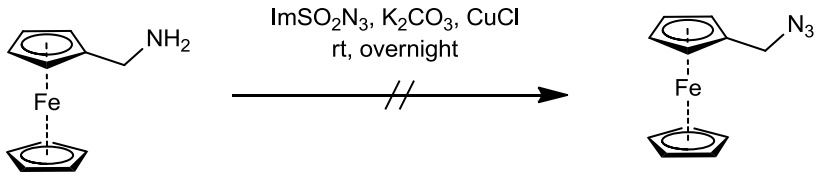

Figure 44 Tested diazotransfer on aminomethylferrocene with Imidazolesulfonyl azide.

The reaction did not proceed as expected, but instead azidomethyl ferrocene **9-OH** was oxidized, probably by the diazo transfer reagent. It follows that this method does not qualify for the functionalization of oxidation sensitive molecules. **9-N$_3$** was then synthesized following a literature method described by Hardy et al.[35] (Figure 45) with a minor change to the procedure.

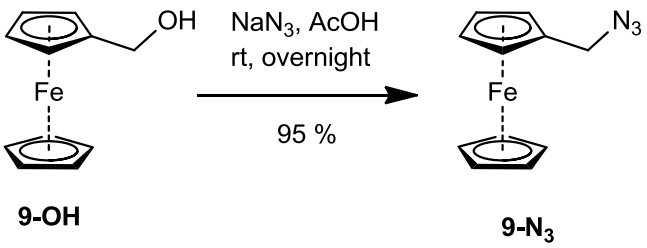

Figure 45 Nucleophilic substitution on hydroxymethyl ferrocene.

During the reaction of NaN_3 with glacial acetic acid, hydrazoic acid is liberated. Although only produced in small amounts, heating HN_3 seemed to be too dangerous, particularly considering the unreliable temperature adjustment of the used equipment. Therefore, the reaction was carried out at room temperature overnight, instead of 3.5h at 50°C, which gave comparable results.

Changing the metal in the metallocene will have a large impact on its redox properties. Ruthenocene is known to typically show two-electron oxidation. The product of this reaction is unstable, which is why it is irreversible.[36] Azidomethyl ruthenocene **12-N_3** was synthesized in three steps from ruthenocene. First, a literature procedure[37] was employed to produce ruthenocene carboxaldehyde, that was subsequently reduced to hydroxymethyl ruthenocene with $NaBH_4$, similar to the corresponding Fc derivative (vide supra). The hydroxyl group was then replaced by azide in a nucleophilic substitution with NaN_3 and acetic acid (Figure 46).

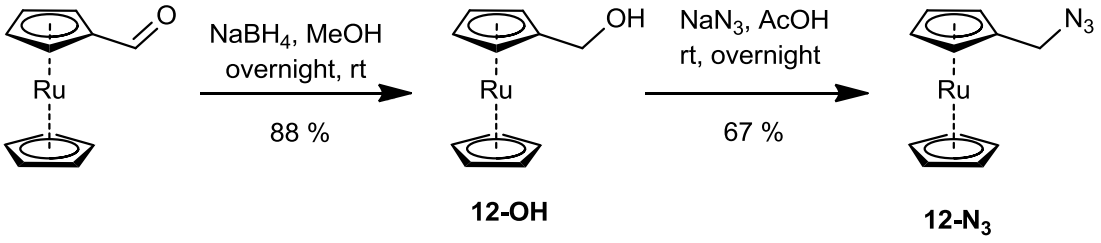

Figure 46 Synthesis of azidomethyl ruthenocene from ruthenocene carboxaldehyde.

In their publication from 2011, Patra and Metzler-Nolte reported that the reaction of **12-OH** with NaN_3 in acetic acid at elevated temperatures did yield trace amounts of **12-N_3**, but gave mostly the aldehyde.[38] For the same reasons as described for the synthesis of the ferrocene analogue, the nucleophilic substitution was carried out at room temperature. It was found that the reaction proceeded as expected, with only minor oxidation to the aldehyde.

The redox potential of ferrocene is influenced by the substituents on the Cp rings. An electron withdrawing group will increase its redox potential whereas an electron donating group will decrease it. In order to broaden the spectrum of available cofactors, ferrocene and acetyl ferrocene were brought into reaction with 2-bromoacetyl chloride and $AlCl_3$ in a Friedel-Crafts acylation, producing bromoacetyl ferrocene **17-Br** and 1-acetyl-1'-bromoacetyl ferrocene **18-Br** respectively. Nucleophilic substitution of bromine with azide gave the corresponding azides (Figure 47).

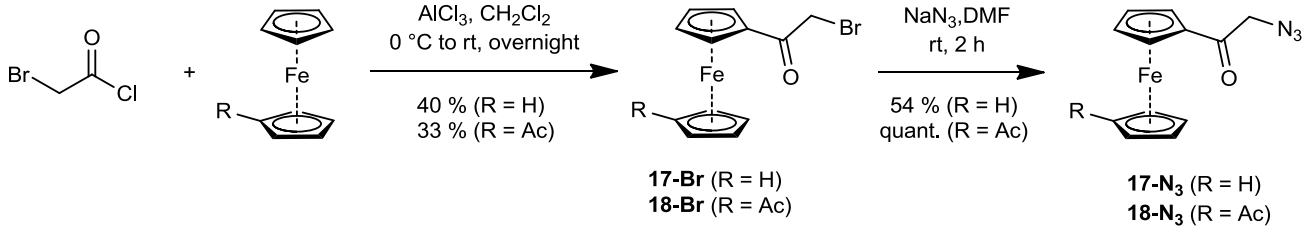

Figure 47 Two-step synthesis of azidoacetyl ferrocene 17-N_3 and 1-acetyl-1'-azidoacetyl ferrocene 18-N_3.

It was found that the reaction time in the nucleophilic substitution step is important since longer exposure of the reactants to the reaction conditions led to the formation of an insoluble brown substance. The same behaviour was observed in the NMR samples of **17-N_3** and **18-N_3** in $CDCl_3$, as well as for prolonged time in DMF solution, because of which the samples and reaction solutions were prepared shortly prior to use. The neat material appears to be stable when stored in a fridge.

The same approach was tested with 3-chloropropionyl chloride as reagent, in order to provide additional options for the chain length between peptide and cofactor. The corresponding 2-chloropropionyl ferrocene and 1-acetyl-1'-(2-chloropropionyl) ferrocene were subjected to NaN_3 and DMF and the progress of the reaction monitored via TLC. Instead of nucleophilic substitution, only the previously described decomposition could be observed. This is probably due to chloride being a less good leaving group compared to bromide.

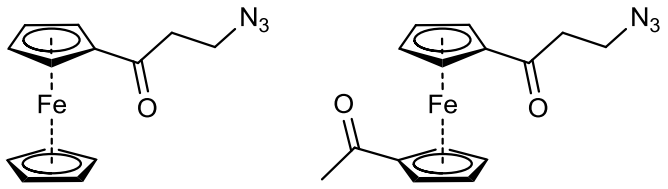

Figure 48 aspired acylferrocene derivatives.

In order to further increase the redox potential, the same synthesis was tested with trifluoroacetyl ferrocene as reactant (Figure 49).

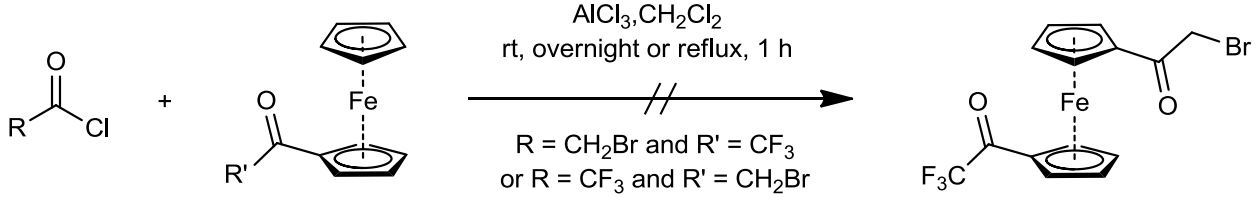

Figure 49 Attempts to synthesize 1-Bromoacetyl-1'-trifluoroacetyl ferrocene.

Although the typical purple colour of the acylium ion occurred upon addition of the acylation reagent to the ferrocene derivative, after reaction at room temperature overnight no product formation was observed. Conducting the reaction under reflux yielded an insoluble brown precipitate. As Cottis and Rosenberg found in 1960, perfluorocarboxylic acid derivatives exclusively give monosubstituted products in Friedel-Crafts acylations on ferrocene.[39] This is probably due to the very strong electron withdrawal of the trifluoroacetyl group and following from this, strong deactivation for electrophilic substitutions. It was expected that for the reverse order, the acylation of acetylferrocene with trifluoroacetic anhydride, the reaction would proceed. However, no product formation could be observed.

At this point, it was decided to try and get an alkyl substituted ferrocene derivative to decrease the redox potential. It is well known that Friedel-Crafts alkylations are less favourable since the product of the reaction is activated towards further alkylations. With an already activated system like ferrocene, this would lead to a strong overreaction and thus to many by-products. A better way was to try and reduce the already obtained acylation products. In the literature, the decarboxylation of similar compounds is reported to succeed with $ZnCl_2$ and $NaBH_4$.[40] Applying the conditions to **18-Br** gave a yellow oil that was not stable overnight in the NMR tube. It is

expected that the bis-alkylferrocene is sensitive to oxidation, thus this finding was expected. A fresh NMR sample gave a complicated spectrum with broad signals that could not be analysed. An aspired Wolff-Kishner reduction was also unsuccessful.

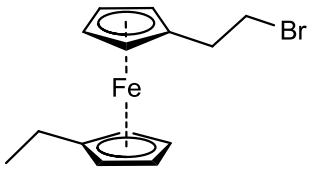

Figure 50 1-ethyl-1'-(2.bromoethyl) ferrocene.

Interesting redox active molecules can also be found among polycyclic homo- and heteroaromatic systems. Therefore, a series of aromatic redox cofactors were synthesized. Naphthalic anhydride was brought into reaction with ethanolamine[41] and subsequently with NaN_3 in glacial acetic acid to form **19-N_3** in 83% yield (Figure 51).

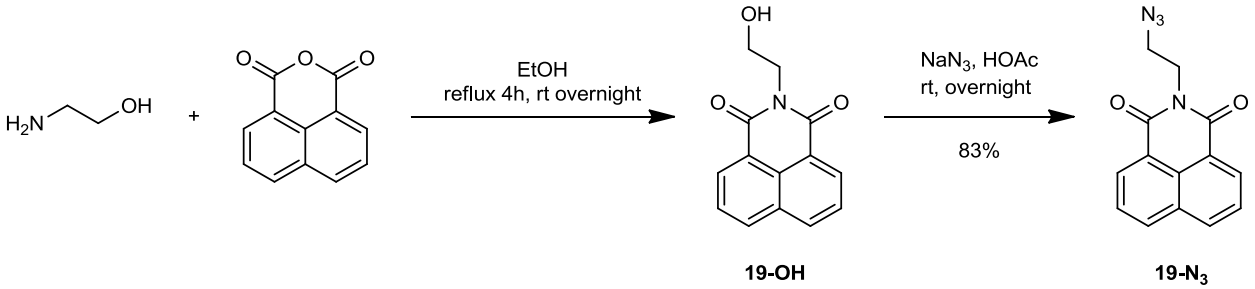

Figure 51 Synthesis of 19-N_3 from naphthalic anhydride in two steps.

1-Pyrenemethylamine was successfully converted into the corresponding azide **20-N_3** in 60% yield (Figure 52)

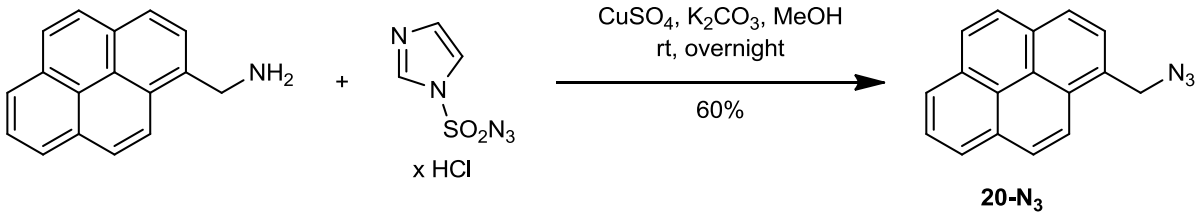

Figure 52 Synthesis of 20-N_3 in one step from commercially available 1-Pyrenemethylamine.

21-Cl (Figure 53) was obtained by a microwave reaction of phenothiazine **ptz** and 3-chloropropionyl chloride[42]. Other efforts to obtain **21-N_3** were unsuccessful. The reaction with

NaN_3 in DMF overnight did not give the desired product **21-N_3**. Instead, the NMR spectrum showed signs of decomposition in form of many small signals over a wide range of chemical shift (Figure 53)

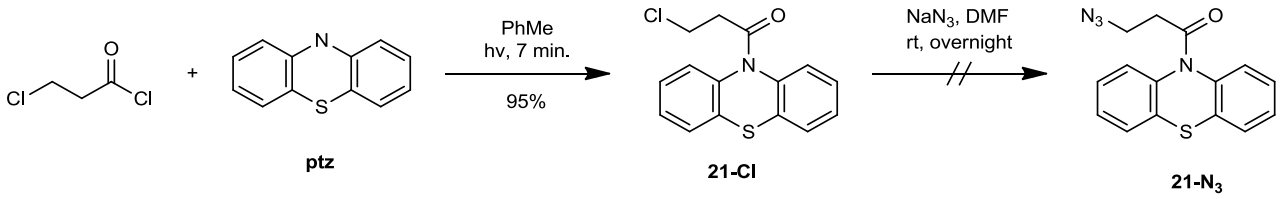

Figure 53 attempted synthesis of 21-N_3 from ptz in two steps.

3.6.2 Electrochemical characterization of cofactors

The above described simple redox cofactors were now characterized electrochemically. First, the azides **9-N_3** and **20-N_3** were characterized using cyclic voltammetry. It turned out that the oxidation reactions were irreversible under the applied conditions (Figure 54).

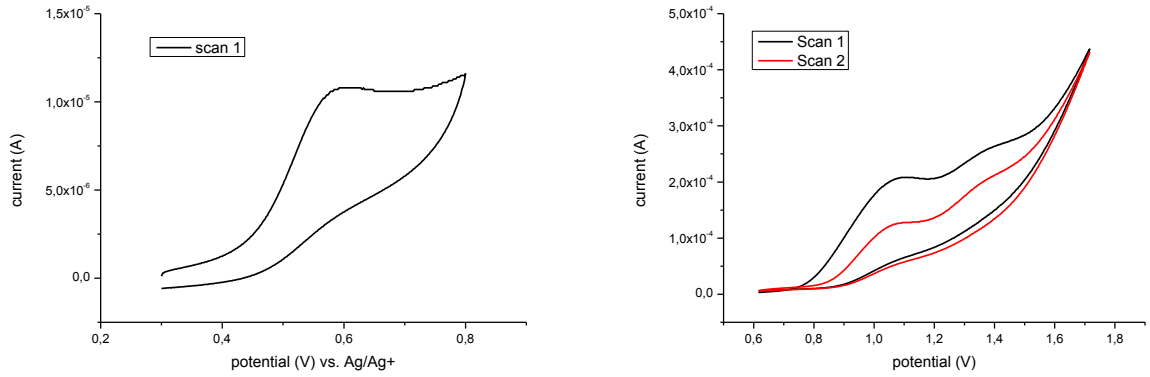

Figure 54 Irreversible oxidation of $FcCH_2N_3$ 19-N_3 and azidomethyl pyrene 21-N_3 in DMF at 100 mV/s.

These results were particularly unexpected for ferrocene, since it is famous for its stability. The same measurement was performed on the precursor for **19-N_3**, hydroxymethylferrocene, and here the oxidation turned out to be reversible. It follows that after oxidation of **19-N_3** the oxidized species undergoes a chemical conversion that is fast compared to the scan rate. The same behaviour was observed with the pyrene analogue. Since pyrene is also known to show reversible redox reactions in voltammetry,[43] it was concluded that the azide moiety is responsible for the observed outcome. In order to both show successful click chemistry on the cofactors as well as being able to accurately measure the redox potentials of the molecules, all cofactors were brought into reaction with 2,2-dimethylbut-3-yne under $CuSO_4$ / ascorbic acid catalysis (Figure 55).

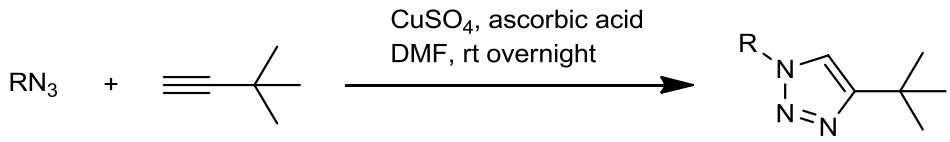

Figure 55 Click reaction prior to electrochemical characterization.

The cyclic voltammograms of the resulting 4-(*tert*-butyl)-1*H*-1,2,3-triazoles are shown and discussed below.

3.6.3 4-(tert-butyl)-1-ferrocenyl-1H-1,2,3-triazole 9-trz

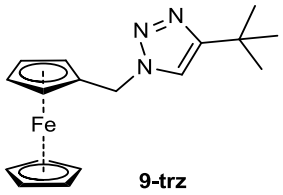

9-trz

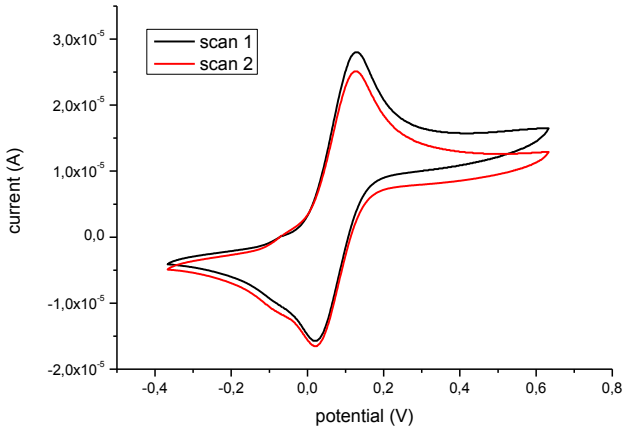

Figure 56 cyclic voltammogram of 9-trz vs. Fc in DMF, 100mV/s with 0.01M $[Bu_4N]PF_6$.

Table 7 parameters for the cv of 9-trz.

	9-trz
E_{pa} [mV]	133
E_{pc} [mV]	25
I_{pa} [µA]	25.25
I_{pc} [µA]	23.44
$E_{1/2}$ [mV]	79
ΔE [mV]	108

As can be seen in Figure 56, the clicked species shows both half waves, which confirms the assumption that azide causes irreversibility of the oxidation. For the pyrene derivative however, the reduction wave did not show.

3.6.4 4-(tert-butyl)-1-(pyren-2-ylmethyl)-1H-1,2,3-triazole 21-trz

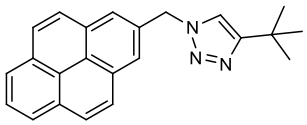

21-trz

The parameters for the cv of **21-trz** are summarized in Table 8.

Table 8 Parameters for cv of 21-trz at 100 mV/s.

	reduction		oxidation	
	wave 1	**wave 2**	**wave 3**	**wave 4**
E_{pa} [mV]	-2507		993	1233
E_{pc} [mV]	-2637	-2479		
I_{pa} [µA]	21,7			
I_{pc} [µA]	48,78	40,53		
$E_{1/2}$ [mV]	-2572			
ΔE [mV]	130			

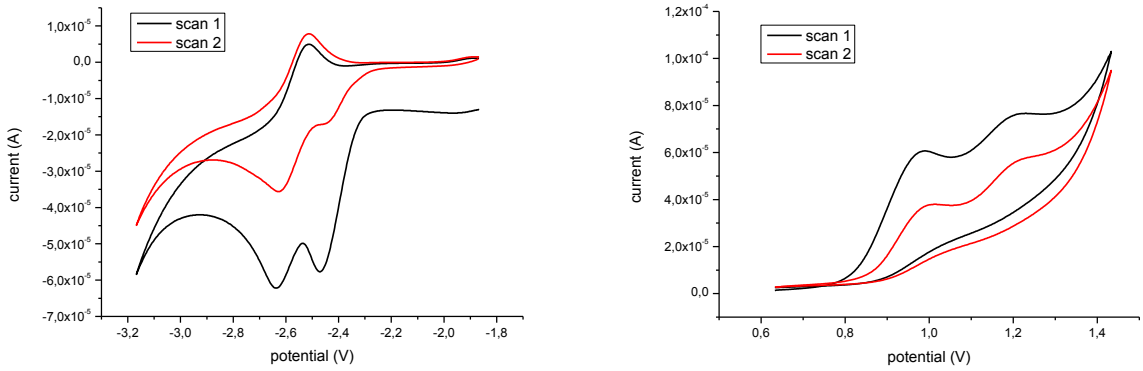

Figure 57 cv of 21-trz, negative (left) and positive scans (right).

Even after clicking, the oxidation waves did not become reversible for **21-trz** (Figure 57). Although the oxidation half wave at 1233 mV now shows a maximum and can therefore be analysed, clicking the cofactor did not give the desired reversibility. The negative scan shows an irreversible reduction with a half wave at -2479 mV and a pseudo-reversible reduction at $E_{1/2}$ = -

2572 mV. This behaviour can be cause by either precipitation or a subsequent chemical reaction after the first wave. In this way, the oxidised or reduced species is not present for the reverse reaction. It should also be noted that the second scan cycles show considerable decrease in intensity, which further confirms this conclusion.

The instability of the synthesized acyl ferrocene derivatives in solution was already pointed out in the previous section. The conditions that were applied to click the cofactors did not produce the desired product in case of **17-N_3** and **18-N_3**. In order to be able to assess their redox behaviour, it was decided to measure the precursors, the halides instead of the azides, which are stable in solution. The resulting voltammograms are shown in Figure 58

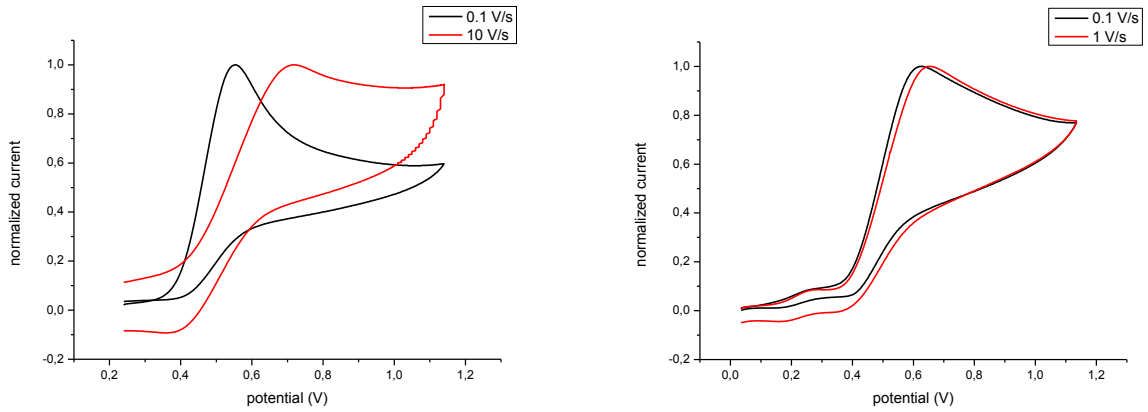

Figure 58 cv of 17-Br (left) and 18-Br (right) recorded at 0.1 and 10 V/s, currents normalized for comparison.

Since in neither of the reverse scan a minimum could be found, the reduction half waves could not be analysed. In both cases the second scans show considerably smaller half waves.

Figure 59 shows the cyclic voltammogram of 2-(2-hydroxyethyl)-1H-benzo[de]isoquinoline-1,3(2H)-dione **19-OH**.

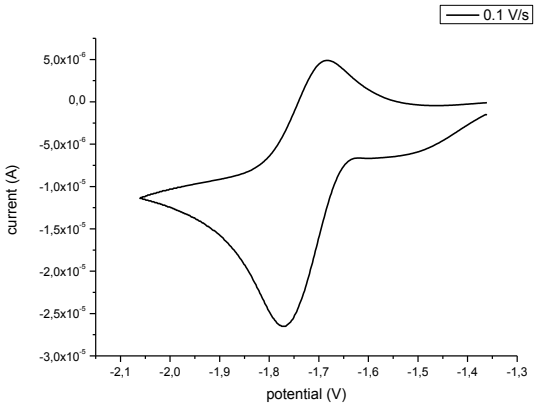

Figure 59 cv of 19-OH at 0.1 V/s scan rate.

Table 9 parameters for the cv of 19-OH and comparison between FcCH2OH and corresponding 4-(*tert*-butyl)-1*H*-1,2,3-triazole.

	19-OH	**9-trz**	**9-OH**
E_{pa} [mV]	-1683	133	40
E_{pc} [mV]	-1771	25	-108
I_{pa} [µA]	11,62	25,25	60,96
I_{pc} [µA]	19,59	23,44	60,32
$E_{1/2}$ [mV]	**-1727**	**79**	**-34**
ΔE [mV]	88	108	148

In Table 9, the parameters for the cv measurements of 4-(*tert*-butyl)-1-ferrocenyl-1*H*-1,2,3-triazole and hydroxymethyl ferrocene are shown. The hydroxyl- and triazole group are separated from ferrocene by only one CH_2 unit. The electronic effect of these groups is therefore considerable and causes the rather large difference of the redox potentials of 113 mV. In case of **19-N_3** the click reaction did not give the triazole. It is possible that due to long storage of the azide, the compound decomposed. In order to still get information about its redox behaviour, the alcohol **19-OH** was characterized instead. Considering the longer distance between the functional groups and the naphthalic imide due to an additional CH_2 unit, the difference between the redox potentials of the triazole and the alcohol is expected to be much smaller.

3.6.4.1 Styrylpyridinium fluorophores

The fluorophores described in section 3.5.1 were also subjected to the above described click reaction and characterized by cyclic voltammetry. The results are shown below (Figure 60).

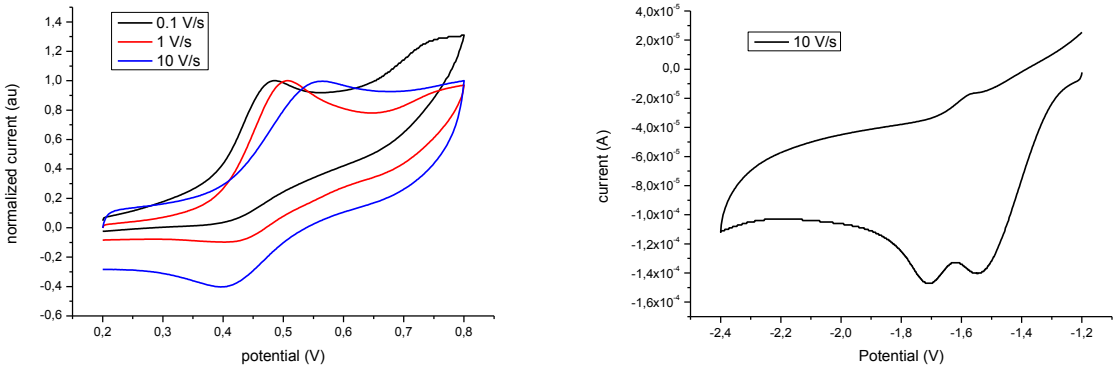

Figure 60 left: cv of oxidation of 7-trz at different scan rates. Currents normalized to the individual peak anodic currents for better comparison, right: negative scan showing two irreversible reduction waves.

.

Table 10 shows the parameters for the scans without normalization.

Table 10 Parameters from cv scans of 7-trz

	Epa [mV]	Ipa [µA]	Epc [mV]	Ipc [µA]	E1/2	dE	Ipa/Ipc
0.1 V/s	486	7.99					
1 V/s	508	18.04	400	3.39	454*	108	5.32
10 V/s	566	43.72	396	17.25	481	170	2.53
	-1546						
	-1708						

The currents of the different curves were normalized to the peak anodic current for better comparison. At a scan rate of 100 mV/s the voltammogram of **7-trz** shows irreversible oxidation. Raising the scan rate to 1 V/s showed a very small wave in the reverse scan, whereas 10 V/s clearly showed a minimum and therefore could be analyzed. In the reduction scan, two irreversible waves were observed at -1.546 V and -1.708 V. Even at 10 V/s scan rate, the rudimentary wave in the forward scan at about -1600 mV did not show a maximum.

Figure 61 shows the cv scans for **10-trz**.

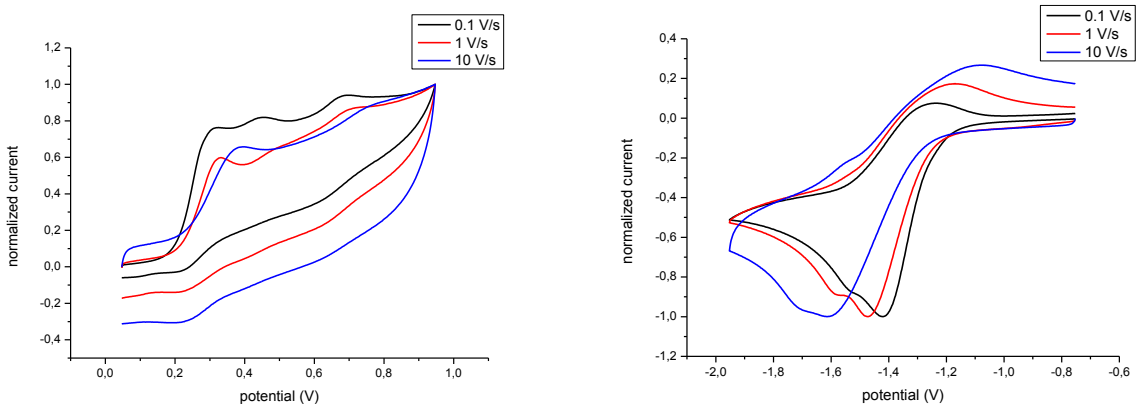

Figure 61 cv of 10-trz at different scan rates, positive (left) and negative (right) scan.

Table 11 parameters of cv of 10-trz.

Scan rate	E_{pa} [mV]	I_{pa} [µA]	E_{pc} [mV]	I_{pc} [µA]	$E_{1/2}$	ΔE
0.1 V/s	325	9,558				
	455	9,92				
	697	10,84				
	-1235	9,954	-1421	26,17	-1328	186
1 V/s	333	14,87				
	-1173	28,52	-1473	73,83	-1323	300
10 V/s	397	39,92				
	-1077	66,65	-1615	196,7	-1346	538

Increasing the scan rate did not lead to a defined minimum for the backward scan. The reduction part however showed a reversible wave at $E_{1/2}$ = -1328 mV even at 100 mV/s.

For **11-trz**, the positive scan (Figure 62) showed no distinct peaks and varying the scan rate could not improve the result. The negative scan showed only irreversible reductions without distinct minima.

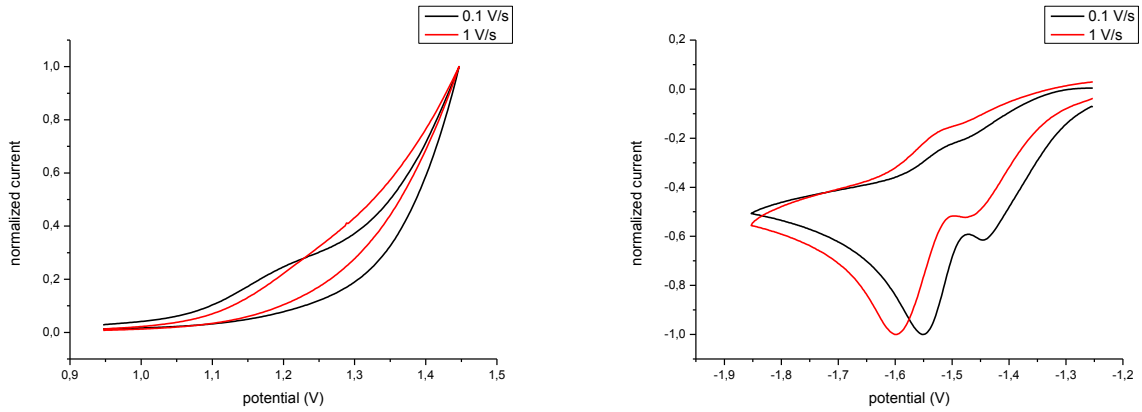

Figure 62 cv of 11-trz at different scan rates, positive (left) and negative (right) scan.

Table 12 Parameters for cv of 11-trz vs. Fc.

	Epc [mV]	Ipc [µA]
0.1 V/s	-1457	8,65
	-1561	15,68
1 V/s	-1609	45,03

An investigation of the redox processes of **7-trz**, **10-trz** and **11-trz** by means of spectroelectrochemistry would be interesting. It is likely that the redox processes influence the fluorescence of the molecules. Characterizing this influence could lead to a method to use them as probe for redox processes. It is important to notice that all the above described measurements show the situation only in DMF solution. The solvent has an effect on the stability of the redox active species as well.

3.7 Coordination Clusters as redox cofactors

3.7.1 Synthesis of azide-modified clusters

Coordination clusters consist of metal centres joined by bridging groups and are enclosed in a shell of ligands. These ligands can be modified to perform click reactions. A series of μ_3-oxo-Fe_3 compounds ($[Fe_3O(L)_6(H_2O)_3]^+$ where L is a carboxylate) with various para-substituted benzoic acids as ligands have been thoroughly studied in our workgroup.[5] The reliable synthesis and tolerance for many functional groups in the ligand qualify these systems for modification. Dirk Schray published in his PhD thesis a series of Fe_nLn_m coordination clusters with various core structures that contain 2-naphthoic acid as co-ligand.[44] The synthetic route to these complexes is robust and the compounds show interesting magnetic properties.

The goal of this part of the project was to test a strategy to graft clusters like these onto peptides. The first step was to prepare modified complex ligands that contain azide groups (Figure 63) and used to synthesise clickable complexes.

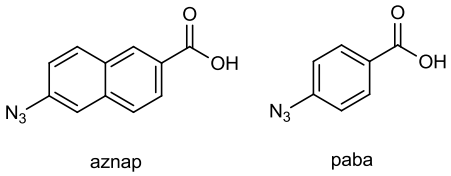

Figure 63 Modified ligands for the synthesis of clickable coordination clusters.

6-azido-2-naphthoic acid (aznap) was synthesized by diazo transfer on 6-amino-2-naphthoic acid. Thin layer chromatography showed that separation of the product mixture was not feasible. Proton and carbon NMR were recorded, but due to the poor purity of 90% of the commercially available starting material, the data could not be analysed conclusively. However, IR spectroscopy showed the presence of an organic azide function, different from the band in the diazo transfer reagent. Synthesis of complexes yielded no single crystals. Most probably, the impurities present prevent the formation of uniform clusters and crystallization of the same. 6-bromo-2-naphthoic acid is available in higher purity than the amino derivative. Attempts to substitute Br with N_3 did not give the desired product.

P-Azidobenzoic acid (paba) was synthesized by diazo transfer onto the corresponding amine in high yield.[45] The corresponding $[Fe_3O(L)_6L_3]^+$ cluster **22-paba** was synthesized by dissolving the ligand and an equimolar amount of NaOH in ethanol and then adding iron nitrate. The material obtained with this method did not give single crystals. However, the crystal structure (Figure 64) could be determined by Dr. Thomas Biet from crystals grown with an optimized procedure.

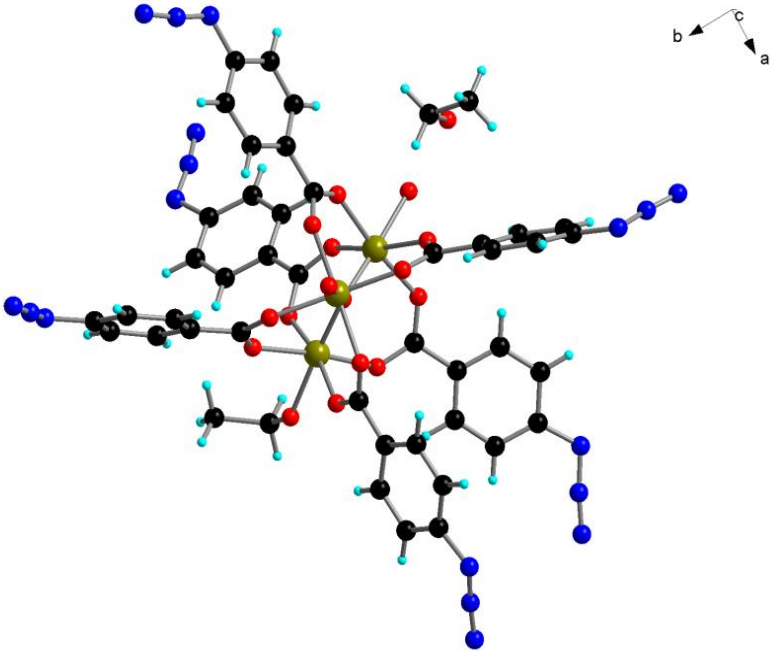

Figure 64 Crystal structure of $[Fe_3O(paba)_6(EtOH)(H_2O)_2]ClO_4$ by Dr Thomas Biet,

The identity of the substances could be confirmed by comparing the infrared spectra (Figure 65)

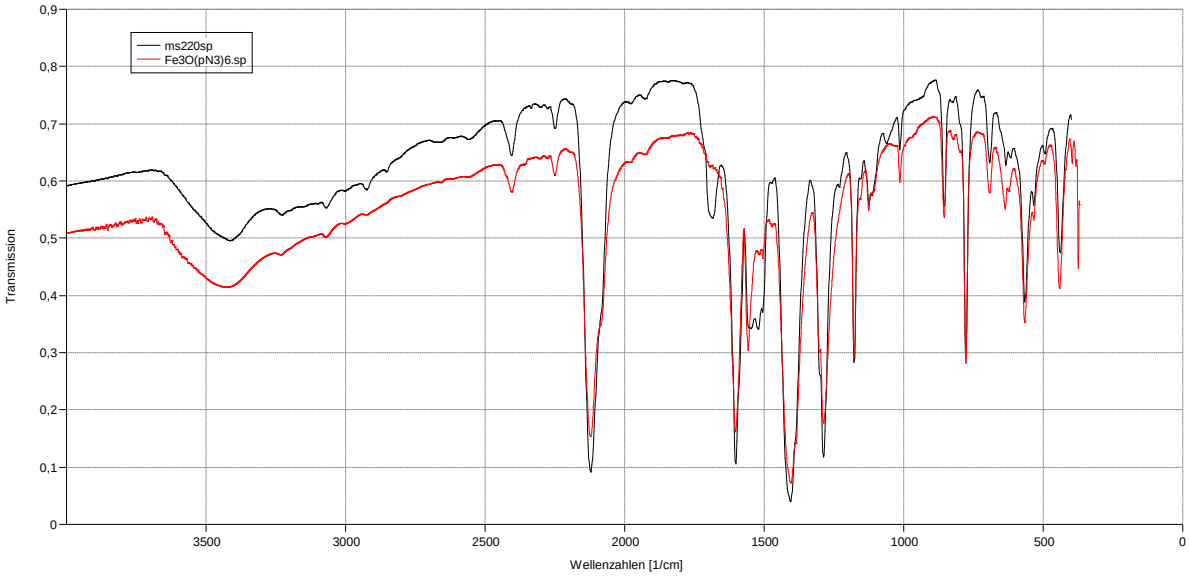

Figure 65 IR comparison between $[Fe_3O(paba)_6L_3]NO_3$ 22-paba and $Fe_3O(pamba)_6(H_2O)_2EtOH]$ by Dr Thomas Biet.

This cluster was subjected to click reaction conditions using propargyl alcohol as coupling partner. Because the click reaction with $CuSO_4$ produced a solid on the glass slide that had to be removed by washing with water, this step was also included in the click reactions tested on the complexes. This step led to hydrolysis of the complex. In order to avoid aqueous workup, $[Cu(CH_3CN)_4]BF_4$ was used as catalyst. The reaction proceeded slowly at room temperature, but was accelerated considerably at 70°C. At this temperature, the reaction was completed overnight, which was confirmed by IR spectroscopy (Figure 66).

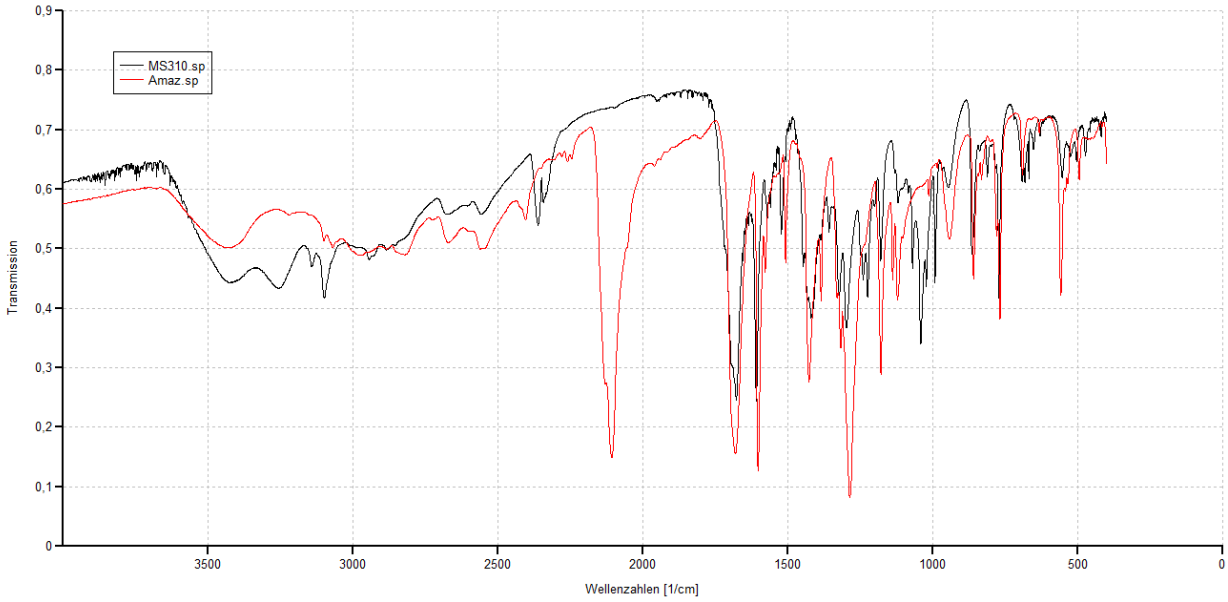

Figure 66 comparison of Fe3O(paba)6 before (red) and after (black) click reaction with propargylic alcohol.

The red spectrum shows the complex before the click reaction. Azide is represented by two very intensive bands at 1287cm^{-1} (sym. Stretching) and 2107 cm^{-1} (asym. Stretching). These bands are absent in the black spectrum, which is from the product of the click reaction. A band at 1035 cm^{-1} shows the C-O stretching of the CH_2OH unit in the former propargyl alcohol that is now incorporated into the ligand. The group of bands between 600cm^{-1} and 700 cm^{-1} show that the complex is still intact after the reaction. The solid product could only be dissolved in DMF and it was not possible to obtain single crystals. This could be due to the hydroxyl groups in the propargyl alcohol forming intermolecular hydrogen bonds and thus cause the quick formation of a precipitate. In cooperation with Dr Thomas Biet, the reaction was repeated with hex-1-yne as reaction partner, and the resulting product could be characterized by X-ray diffraction. The resulting structure is shown in Figure 67.

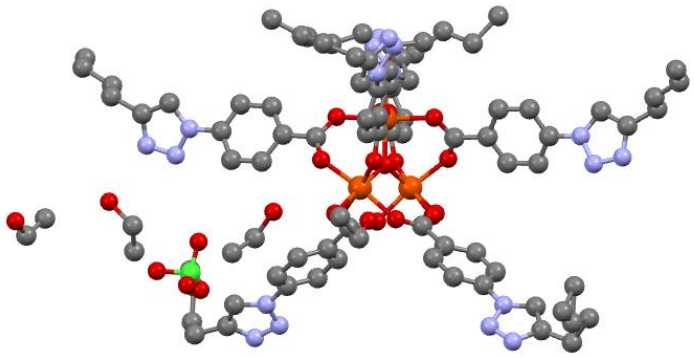

Figure 67 $[Fe_3O(paba)_6L_3]ClO_4$ clicked with hex-1-yne.

Pegma coated glass-slides can be sensitive to elevated temperatures. Hence a second modified version of the ligand was synthesized where the azide function is isolated from the aromatic system. P-azidomethylbenzoic acid (pamba, Figure 68) was synthesised by diazo transfer to the corresponding amines in high yield.

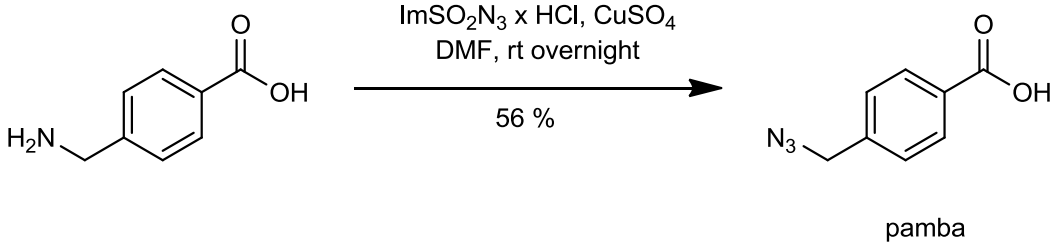

Figure 68 synthesis of p-azidomethylbenzoic acid (pamba).

This ligand was used to obtain complex **22-pamba** (Figure 69) by first obtaining the sodium salt of the ligand with NaH and then combining a solution of the same with a solution of $Fe(NO_3)_3$. Again, the synthetic procedure was optimized in cooperation with Dr Thomas Biet to finally grow single crystals that were characterized by single crystal X-ray diffraction (Figure 69).

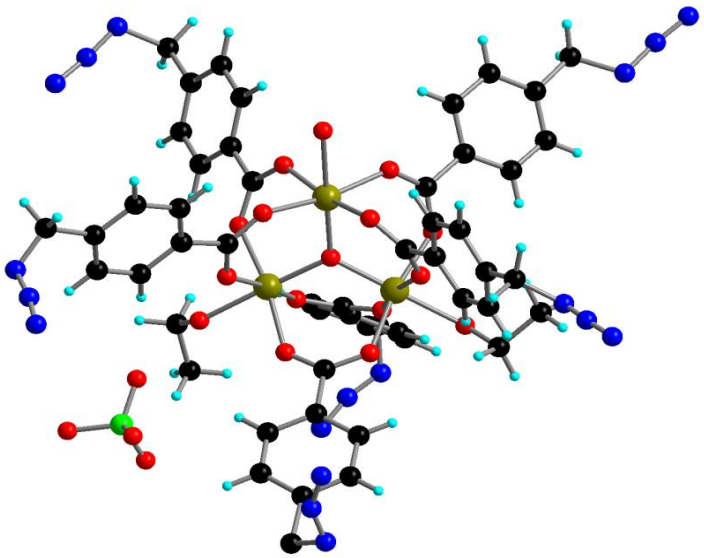

Figure 69 Crystal structure of $[Fe_3O(pamba)_6(EtOH)_2(H_2O)]ClO_4$ by Dr Thomas Biet.

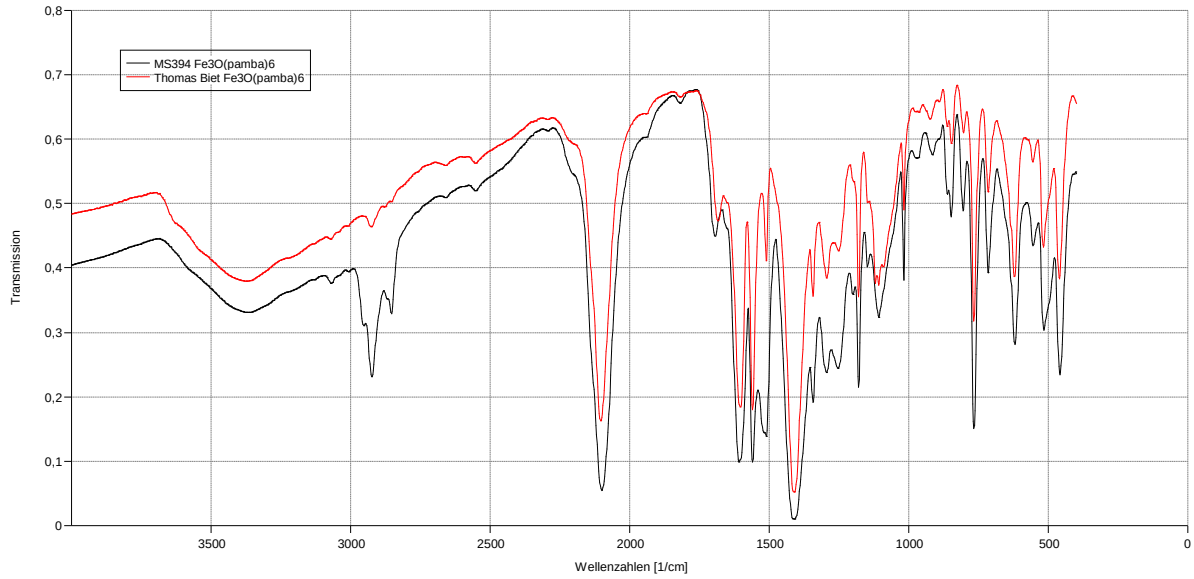

Figure 70 IR comparison between synthesis by DrThomas Biet (structure in Figure 69, red) and 22.pamba (black).

Figure 70 shows a comparison between the IR spectra of the crystalline material by Dr Thomas Biet and the product of the synthesis described here. With exception of the group of bands between 2800 cm^{-1} and 3000 cm^{-1}, which belongs to residual ethanol in the amorphous material, the spectra are identical, which confirms the identity of both substances. The resulting cluster was expected to undergo CuAAC click reactions at lower temperatures than the **paba**

analogue. Therefore, a click reaction was performed on a glass slide with Fmoc-Pra under $Cu(CH_3CN)_4BF_4$ catalysis overnight at room temperature.

No Fe could be detected on the surface. It was suspected that the click grafting was successful, but a subsequent reaction decomposed the complex, so that Fe was removed by the washing process and could not be detected in the sample. Fe_3O hexacarboxylate complexes are widely used as precursors for larger clusters. This is due to the fact that they readily react further. The analogous chromium clusters have been shown to undergo reactions only under much harsher conditions.[46] An analogous Cr_3O cluster was synthesized in the same way and subjected to the same click reaction conditions. The resulting Cr 2p XPS scans are shown in Figure 71.

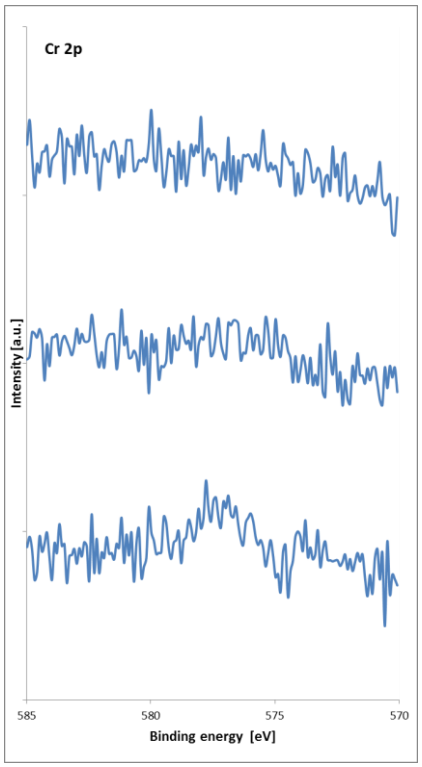

Figure 71 XPS results for $[Cr_3O(pamba)_6L_3]NO_3$, blank sample (top), click conditions with Fmoc-Ser(OPrg) (centre) and Fmoc-Pra (bottom).

Although too small to be analysed, a rudimentary line can be seen centred at 577 eV in the Fmoc-Pra experiment. Neither the blank nor the control sample showed any trace of Cr. It follows that a very small amount of the coordination cluster was clicked onto the surface. Taking into consideration the size of the coordination clusters, it cannot be assumed that the surface is completely smooth. It is likely that due to this, many of the alkyne functions are not accessible

for the clusters. Apparently, a different approach had to be found to investigate the reactions. Since after successful click reaction, the complex would still contain azide (Figure 72).

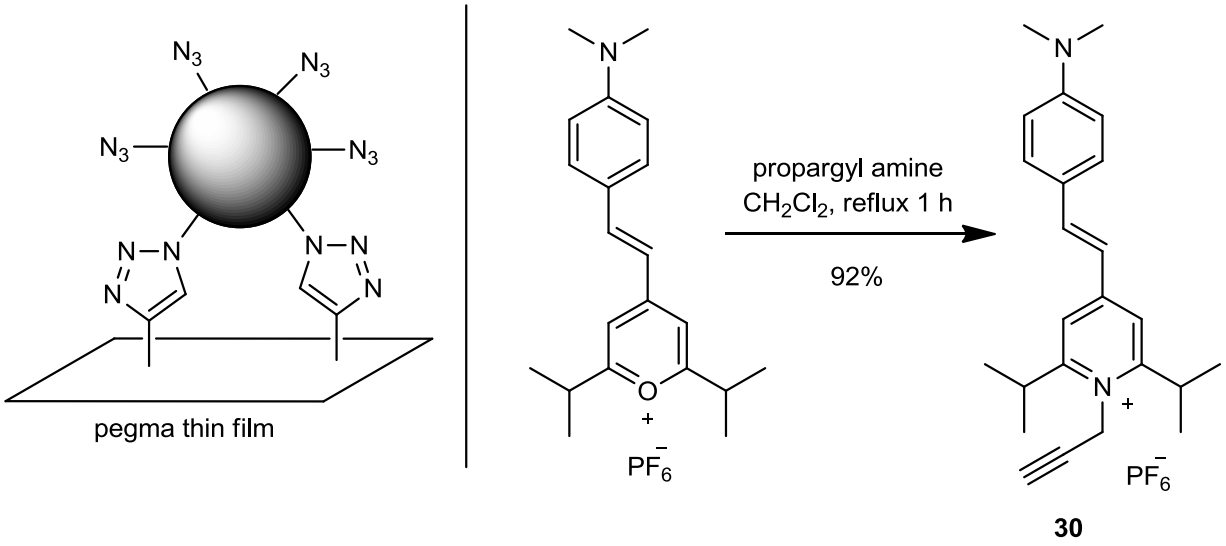

Figure 72 Left: cofactor (black ball) clicked to alkyne on pegma thin film, with azides still available for reaction; right: synthesis of alkyne modified fluorophore 30 to click to complex.

It would be possible to conduct a second reaction involving an alkyne modified fluorophore **30** to stain the complex on the surface and make it visible for fluorescence scanning. A glass slide surface was first reacted with $[Cr_3O(pamba)_6L_3]NO_3$ and subsequently with the modified fluorophore that was obtained by reacting propargyl amine with the corresponding styrylpyryllium salt (Figure 72, right). The scanner was unable to detect fluorescence on the surface. Considering the very short link between the fluorophore and alkyne, this could be the result of fluorescence quenching. In this case it would be necessary to increase the distance between fluorophore and cluster by using a longer chain alkynyl amine.

In parallel, $[Fe_6Dy_3(\mu\text{-}OMe)_9(vanox)_6(paba)_9]$ **23**, a ring-shaped complex, which was synthesized by Irina Kühne with paba as ligand, was reacted with propargyl glycine on a glass slide. The complex could not be obtained with pamba as ligand, which means that the click reaction needed to be performed at elevated temperatures under $Cu(CH_3CN)_4BF_4$ catalysis. XPS showed comparable amounts of Fe, Dy and Cu on the surface after the reaction (Figure 73, top).

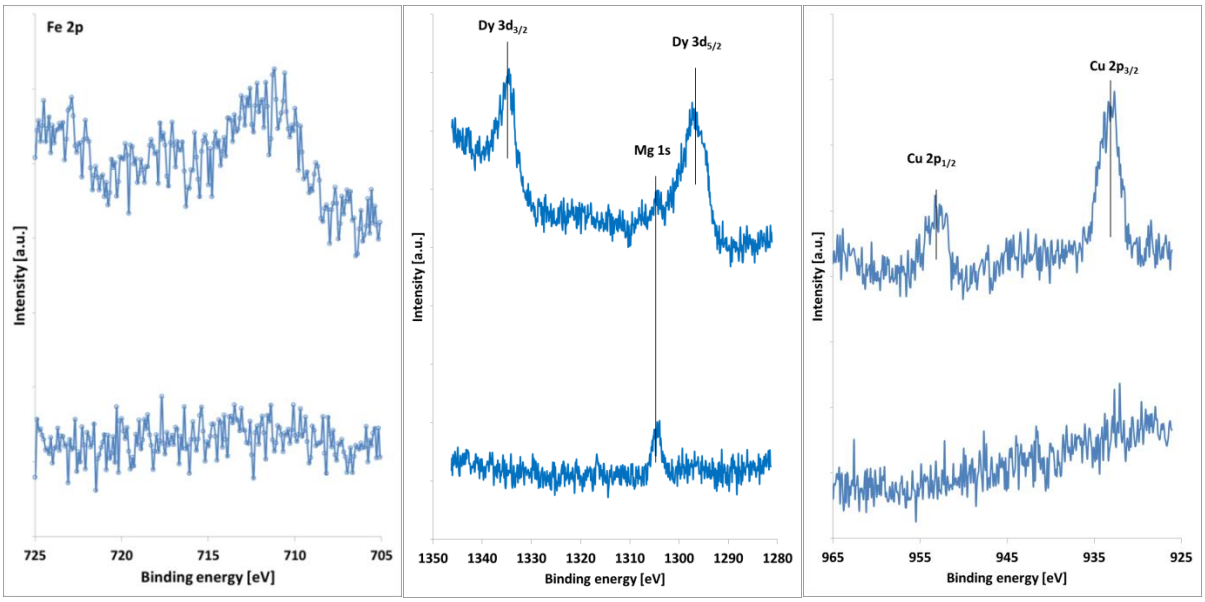

Figure 73 XPS scans of click experiments with 23 for Fe 2p (left), Dy 3d (middle) and Cu 2p (right), with (top) and without (bottom) catalyst.

The parameters determined for Fe, Cu and Dy from the measurement are shown in Table 13.

Table 13 Parameters for Fe, Cu and Dy lines found in 23 on pegma 10/90.

	BE [eV]	Atomic %
Fe 2p3/2	710,7	0,1
	713,2	0,1
Cu 2p3/2	933,0	0,1
	934,6	0,1
Dy 3d5/2	1295,6	0,2
	1298,5	0,1

The control sample, which was exposed to **23** for the same time and at the same temperature, showed no Fe or Dy contamination. These findings can be explained either by a reaction of the azide groups from the ligands with the nitrile to tetrazole derivatives that still coordinate copper, or by incorporation of Cu into the complex.

3.7.2 Ferrocenophane ligand

In 2009, two coordination clusters were published by Mereacre et al. that contains a single ferrocenedicarboxylate ligand.[47] This is particularly interesting because a modification of this ligand could yield a cluster that carries one single clickable function instead of six in case of the Me_3O carboxylates. The first step towards grafting these complexes onto peptides was the modification of the ligand.

Diacetylferrocene was reacted with p-bromobenzaldehyde using a protocol by Tarraga et al.[48] to produce ferrocenophane dione **24** in quantitative Yield. Due to its insolubility, the product could only be characterized by infrared spectroscopy. Subsequently, a reduction with $LiAlH_4$ was performed to give tetrahydropyrane derivative **25** in quantitative yield, by first reducing both carbonyl functions and subsequent condensation (Figure 74).

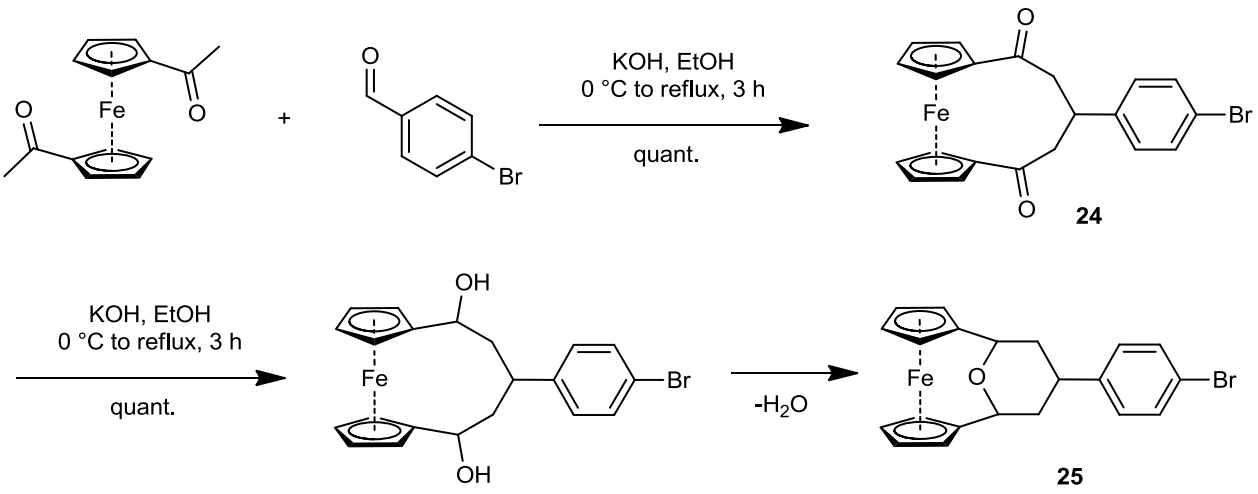

Figure 74 Synthesic route to 25.

From the crystal structure (Figure 75) could be determined that the Cp rings are not coplanar anymore, but are angled towards each other in a 12.9° angle. This will have an influence on the formation of the complex, because the carboxylic acid groups will be spaced further apart.

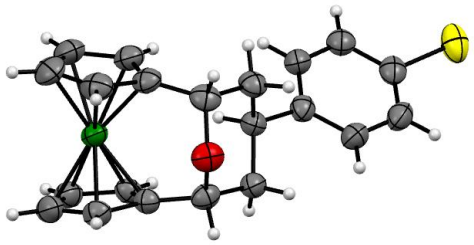

Figure 75 crystal structure of 25.

Because NMR spectroscopy could not conclusively be analysed and the product took a long time to crystallize and finally be identified, the approach could not be followed further. The next steps that need to be done are lithiation of the cp rings with *n*-Butyllithium and tetramethylethylenediamine and subsequent exchange of bromine with azide (Figure 76).

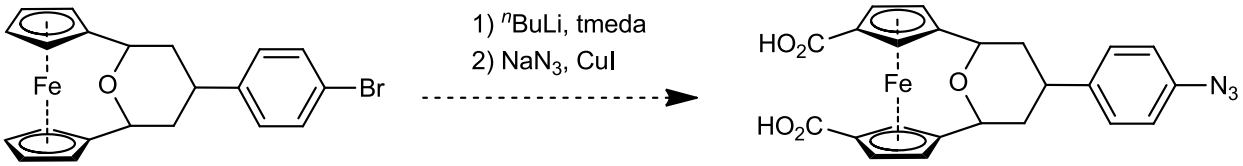

Figure 76 further reactions necessary for obtaining a modified ligand for ferrocenedicarboxylate complexes.

3.8 Metal clusters with redox active ligands

3.8.1 Optimization of $Fe_3O(fcmc)_6$ synthesis

Closely related to the above mentioned clusters and ferrocene derivatives, a complex with a Fe_3O triangular centre and six ferrocenecarboxylate ligands was published by Mereacre et al. in 2006.[49] This complex is interesting because it contains both a redox active cluster core and redox active organometallic ligands.

At first, it was difficult to get single crystals from the published method. Original samples from the substance were available for comparison, which was done by Infrared spectroscopy as well as Mößbauer spectroscopy. The latter was expected to show a 2:1 ratio of Fe(II) from the fcmc ligands to Fe(III) in the cluster core. The results from the measurements at room temperature showed a different situation (Figure 77).

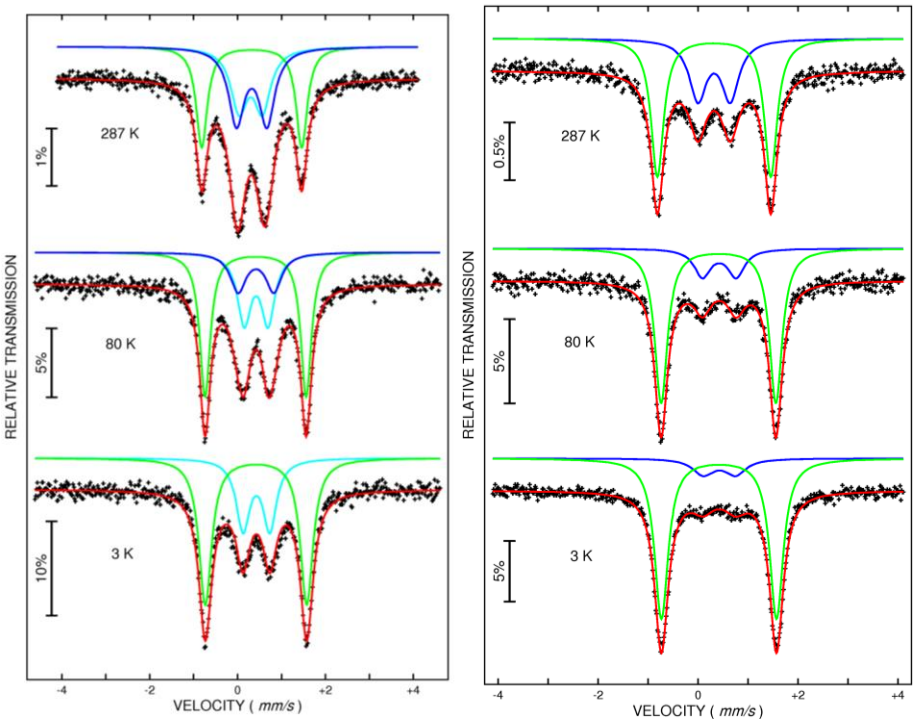

Figure 77 Mößbauer spectra of $[^{nat}Fe_3O(OOCCp^{nat}FeCp)_6L_3]^+$ (26, left) and $[^{56}Fe_3O(OOCCp^{nat}FeCp)_6L_3]^+$ (^{56}26, right) at different temperatures with fitted doublets for Fe(II) low spin (green), Fe(III) low spin (blue) and Fe(III) high spin (turquoise).

The hyperfine parameters for the fitting are given in Table 14

Table 14 Hyperfine parameters for the Mößbauer measurements shown in Figure 77.

Compound	T, K	δ,[α] mm/s	ΔE_Q, mm/s	Γ, mm/s	area,%	assignment
nat-26	287	0.41(1)	0.64(1)	0.53(2)	33.1	$Fe^{III}_{Fe_3O}$
		0.42(1)	2.27(1)	0.29(2)	32.6	Fe^{II}_{Fcmc}
		0.42(2)	0.61(2)	0.41(1)	34.3	Fe^{III}_{Fcmc}
	80	0.52(1)	0.60(1)	0.40(2)	30.1	$Fe^{III}_{Fe_3O}$
		0.51(1)	2.29(1)	0.29(2)	49.6	Fe^{II}_{Fcmc}
		0.48(2)	0.67(2)	0.43(1)	20.3	Fe^{III}_{Fcmc}
	3	0.53(1)	0.63(1)	0.46(1)	38.2	$Fe^{III}_{Fe_3O}$
		0.52(1)	2.31(1)	0.31(2)	61.8	Fe^{II}_{Fcmc}
^{56}26	287	0.42(1)	0.61(1)	0.32(2)	37.0	Fe^{III}_{Fcmc}
		0.42(1)	2.26(1)	0.32(1)	63.0	Fe^{II}_{Fcmc}
	80	0.51(1)	0.67(2)	0.40(2)	19.1	Fe^{III}_{Fcmc}
		0.51(1)	2.29(2)	0.31(2)	80.9	Fe^{II}_{Fcmc}
	3	0.52(1)	0.64(1)	0.51(1)	13.2	Fe^{III}_{Fcmc}
		0.52(1)	2.30(1)	0.33(2)	86.8	Fe^{II}_{Fcmc}

[a]The isomer shifts are given relative to the value for room temperature α-iron foil.

It was found that at room temperature the ratio was 4:5 respectively. The spectrum recorded at 3 K without external magnetic field shows two quadrupole doublets, an inner one with quadrupole splitting ΔE_Q = 0.65 mm/s and isomer shift δ = 0.53 mm/s, and an outer doublet

with ΔE_Q = 2.31 mm/s, δ = 0.52 mm/s, respectively. The ratio between the integral of both doublets is temperature dependent, where at low temperatures the ratio converges to the expected value.

With the interesting electronic situation found by Mößbauer spectroscopy, it was now important to get information about the redox behaviour of the compound. Figure 78 shows the cyclic voltammogram of nat-25 in DMF on platinum electrodes with ferrocene as internal reference.

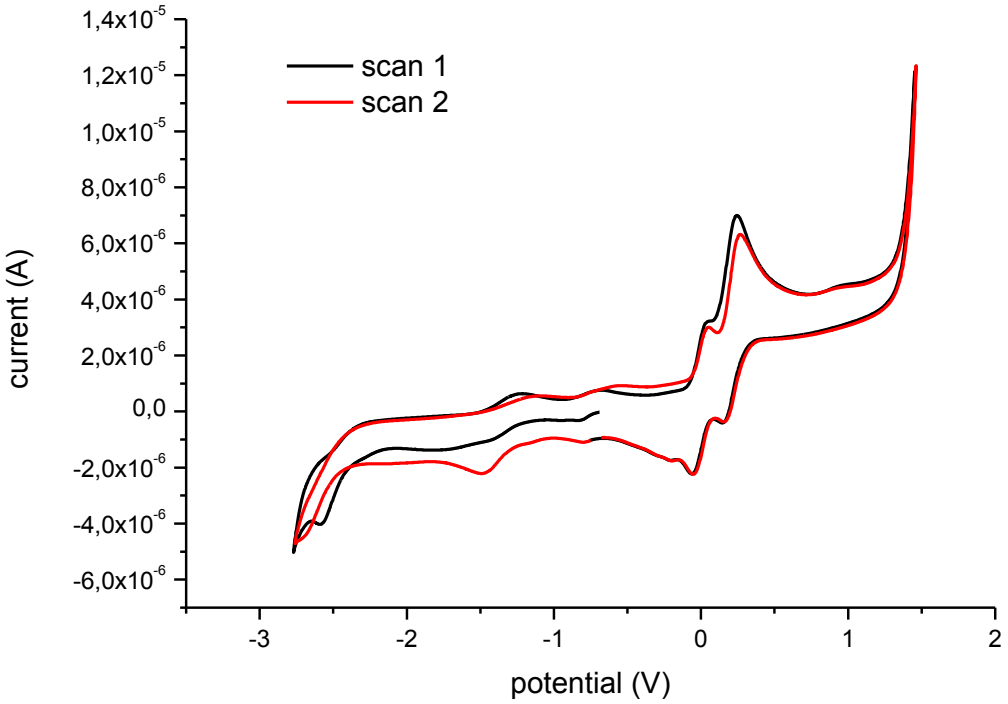

Figure 78 cyclic voltammogram of 26 in DMF vs. Fc/Fc^+ (wave at 0 V).

The calculated values for the respective peaks are given in Table 15.

Table 15 Parameters from cv of 26.

	E	ΔE [V]
wave 1	-2.591	-
wave 2	-1.359	0.291
wave 3	-0.743	0.129
wave 4	0.195	0.099

The peak at $E_{1/2}$ = +0.195V corresponds to the fcmc ligands. By comparing the above values with a study by Alexandru et al.[50], the redox processes observed in the acetate $[Fe_3O(OAc)_6(H_2O)_3]^+$ can also be identified in complex **26**. At -0.743 V, the first reduction occurs to $Fe^{III}_2Fe^{II}O(fcmc)_6L_3]^{2+}$, and at -1.359 V both remaining Fe^{III} are reduced in one step, which can also be seen on the peak sizes. The irreversible reduction wave at E = -2.591 V belongs to the reduction of Fe^{2+} to Fe^{+} in the ferrocenecarboxylates, as can be seen in comparison with the corresponding potential for ferrocene.[51]

It was intended to synthesize a network containing complex **26** as motif to study how intermolecular interactions influence the intramolecular electronic interaction between the ligand's iron atoms and the central Fe_3O cluster core. 4,4'-bipyridine (bipy) should be used to substitute the equatorial solvent molecules and serve as intermolecular bridge. Therefore, an experiment was conducted using ferric nitrate, ferrocenemonocarboxylic acid (fcmc) and bipy. When dissolving the former two compounds in ethanol, a drastic colour change to almost black blue occurred quickly, indicating that the reaction proceeds readily. The addition of bipy immediately generated an off-white solid while the colour of the solution remained unchanged. Single crystals grown from this solution were found to contain complex **26** (Figure 79).

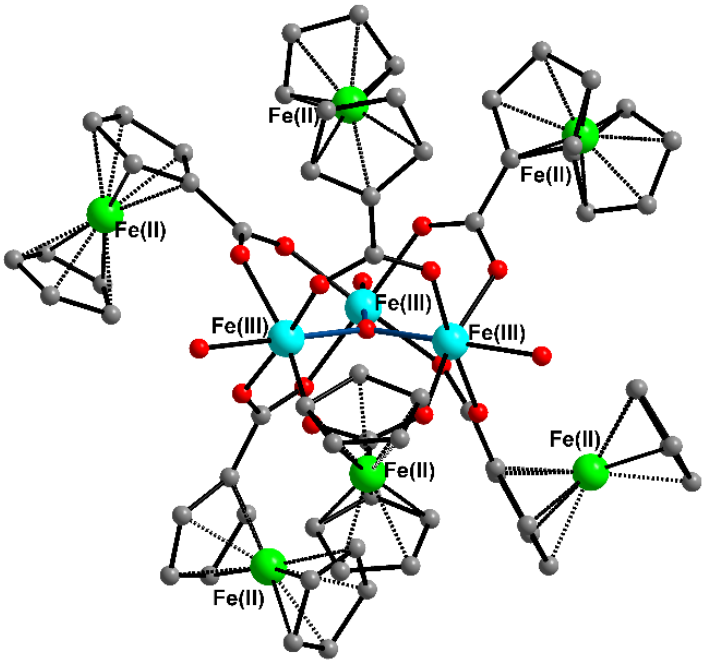

Figure 79 Crystal structure of $[Fe_3O(fcmc)_6L_3]NO_3$ complex 26 from the reaction of Iron nitrate with fcmc and bipy.

Similar observations were made when adding NaOMe as base to the reaction. It was concluded that bipy scavenges the nitric acid that is liberated in the reaction and precipitates as bipyridinium nitrate.

3.8.2 Mixed-metal $[Fe_2MeO(fcmc)_6L_3]$ complexes

The mixed-metal clusters are neutral and therefore even harder to crystallize than the ionic analogue. Powder diffraction showed no crystallinity in the solids. Elemental analyses for the compounds deviate from the prediction, which is probably due to the complex precipitating various impurities from the solution. Nevertheless, it was possible to identify the compounds as the desired products using infrared spectroscopy. Figure 80 shows the detailed comparison of the ferrocenecarboxylate (black) and acetate (red) complexes for $[Fe_2MeO(RCOO)_6L_3]$ with Me = Mn, Co, Ni. Between 550 and 750 cm^{-1}, the spectra show groups of four signals that occur slightly shifted in both the fcmc complex and acetate. According to the literature,[52] this group is correlated to the triangular centre of the complex.

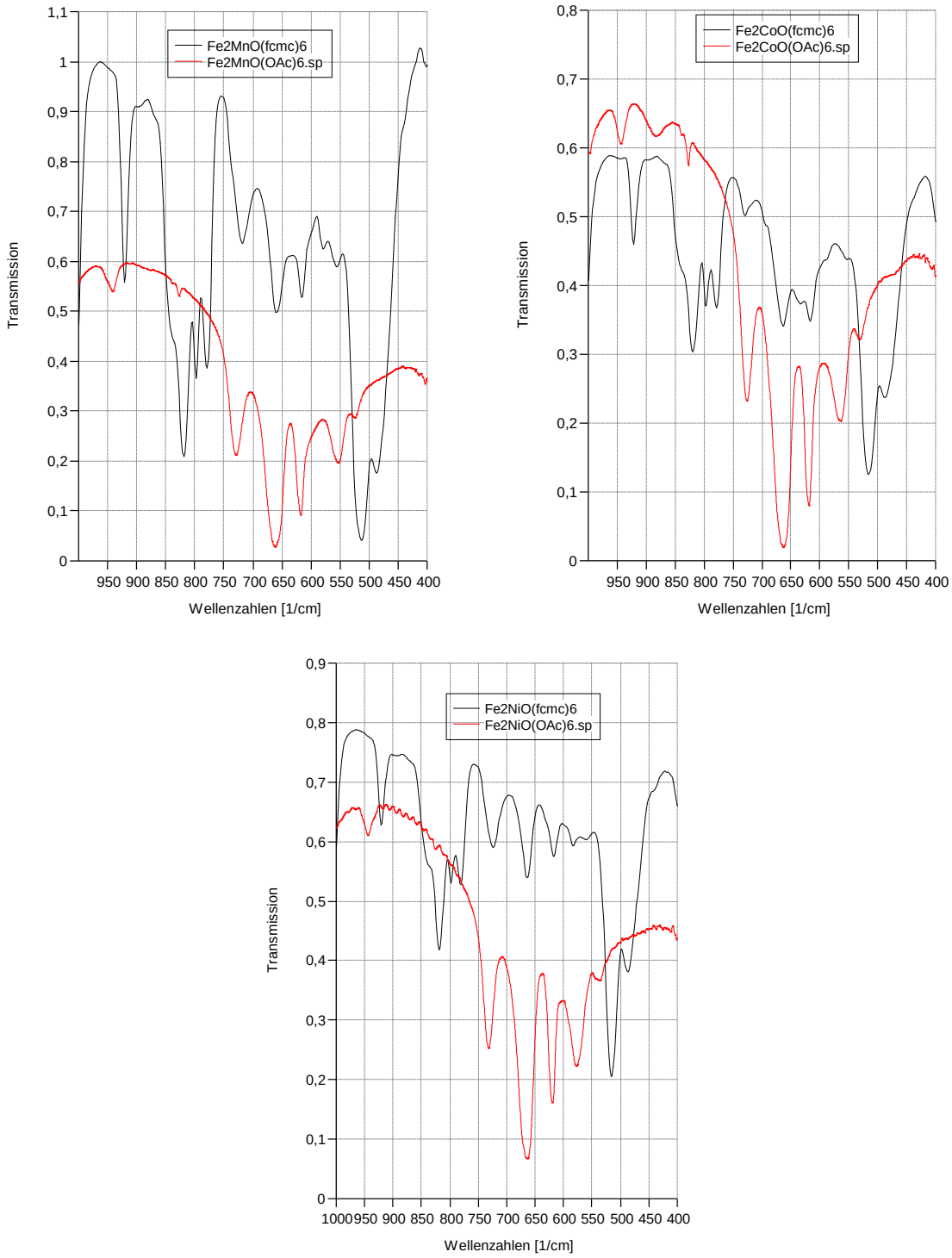

Figure 80 Details of Infrared spectra of the Fe2MeO(fcmc)6 complexes (black) and the corresponding acetate complexes (red) for M3 = .Mn (top left), Co (top right), Ni (bottom).

Mößbauer measurements of the mixed-metal clusters at room temperature are shown in Figure 81.

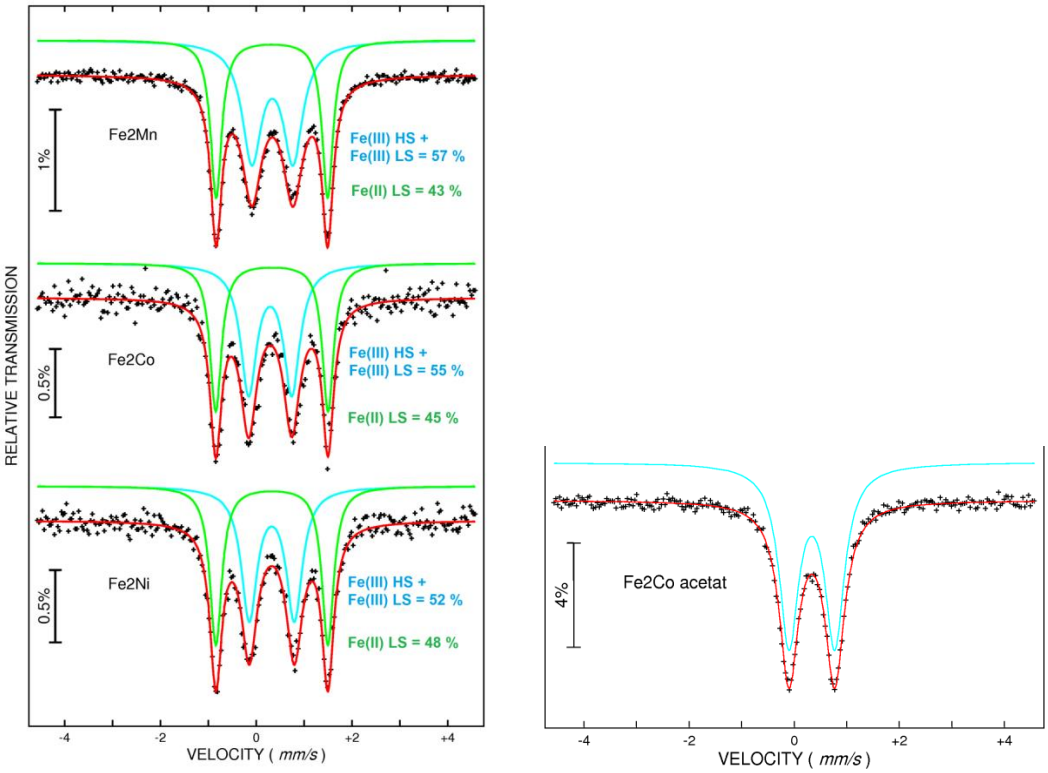

Figure 81 Room temperature Mößbauer spectra of the mixed-metal μ3-oxo $Fe_2Me(fcmc)_6(H_2O)_3$ clusters (left) and Fe2Co(OAc)6 (right) for comparison.

The hyperfine parameters determined from the measurements are given in Table 16.

Table 16 Hyperfine parameters for $[Fe_2MeO(fcmc)_6(H_2O)_3]$ 27-Me and $Fe_2Co(OAc)_6(H_2O)_3$ mixed-metal clusters. Isomer shifts are given relative to value at room-temperature for α-iron foil.

compound	$\delta,^{\alpha}$ mm/s	ΔE_Q, mm/s	Γ, mm/s	rel. area,%	assignment
Fe_2Mn	0.44(1)	0.86(1)	0.49(1)	57	$Fe^{III}_{fcmc} + Fe^{III}_{Fe2MnO}$
	0.43(1)	2.32(1)	0.28(2)	43	Fe^{II}_{Fcmc}
Fe_2Co	0.39(1)	0.90(1)	0.41(2)	55	$Fe^{III}_{fcmc} + Fe^{III}_{Fe2CoO}$
	0.43(1)	2.34(1)	0.29(2)	45	Fe^{II}_{Fcmc}
Fe_2Ni	0.42(1)	0.94(1)	0.40(1)	52	$Fe^{III}_{fcmc} + Fe^{III}_{Fe2NiO}$
	0.43(1)	2.34(1)	0.30(1)	48	Fe^{II}_{Fcmc}

The blue curves show a fitted doublet which corresponds to Fe(III) (blue) and one that corresponds to Fe(II) (green). The ratio between the integral for the Fe(III) and Fe(II) doublet are

close to equal in all cases. If the coordination cluster core contained only Fe^{3+} and the ligands only Fe^{2+}, the ratio would be expected to be 3:1. The measured values can be explained in two ways. First, this ratio would occur if only two of the six acetate ligands would have been substituted with fcmc in the complex synthesis. This explanation can be ruled out by comparing the full spectra of $Fe_2Ni(fcmc)_6$ **27-Ni** and $Fe_2Ni(OAc)_6$ (Figure 82)

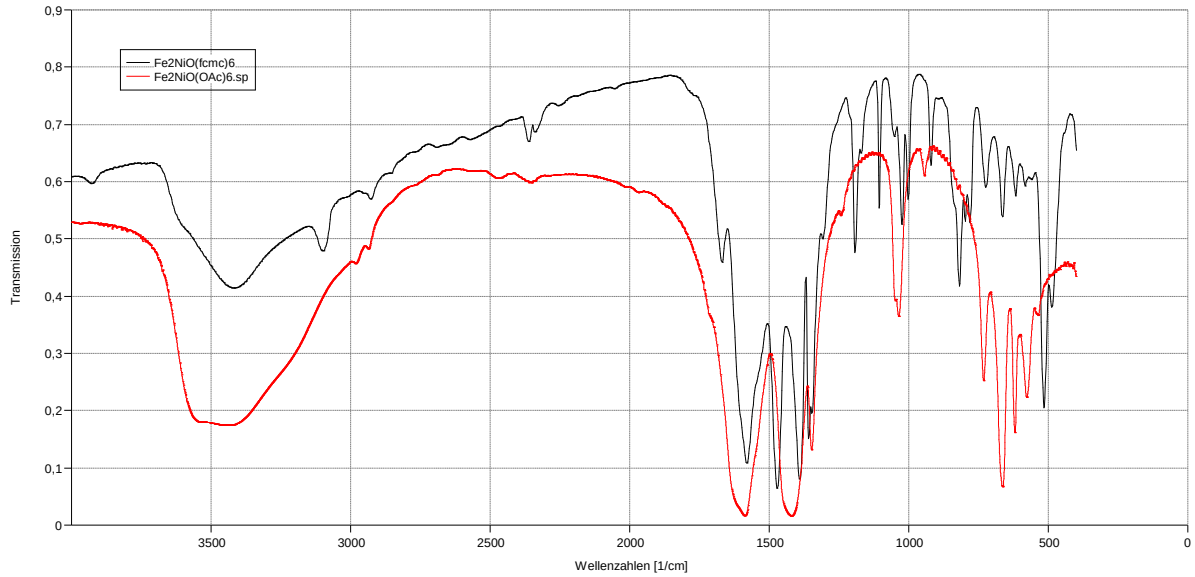

Figure 82 Infrared spectra of [Fe2NiO(fcmc)$_6$L$_3$] (27-Ni, black) and [Fe2NiO(OAc)$_6$L$_3$] (red) for comparison.

The acetate spectrum shows two bands for the carboxylate vibrations at 1421cm^{-1} (symmetric OCO stretching vibration) and 1588 cm^{-1} (asymmetric OCO stretching vibration). For **27-Ni**, this region shows three bands that are located at 1391, 1471 and 1580 cm^{-1}, which is in good agreement with the spectrum of $[Fe_3O(fcmc)_6L_3]NO_3$ (L = solvent). The second reasoning is that in two of the fcmc ligands Fe is oxidised. The electrons were not transferred to Fe(III) in the coordination cluster core, since no Fe(II) high spin signal was observed.

3.8.3 Chromium complex

It was now very interesting to see the behavior of a complex with similar structure with a core that is not active in ^{57}Fe Mößbauer spectra and electrochemically inert in the region of ferrocene/ferrocenium. Considering the crystallization behaviour of the hexaferrocene complexes as described above, it was also necessary to find a system that can be characterized without crystallization. Chromium was the metal of choice because an extensive study on µ3-oxo bridged $[Cr_3O(OOCR)_6L_3]$ complexes with regard to their Infrared spectra, published by Johnson et al. in 1981[53] allows for the identifaction of the complexes from amorphous material.

The synthesis of $[Cr_3O(fcmc)_6(H_2O)_3]NO_3$ **28** was conducted in the same way as the iron analogue. First, the acetate was synthesized from chromium nitrate and glacial acetic acid and subsequently, acetate was substituted with fcmc.

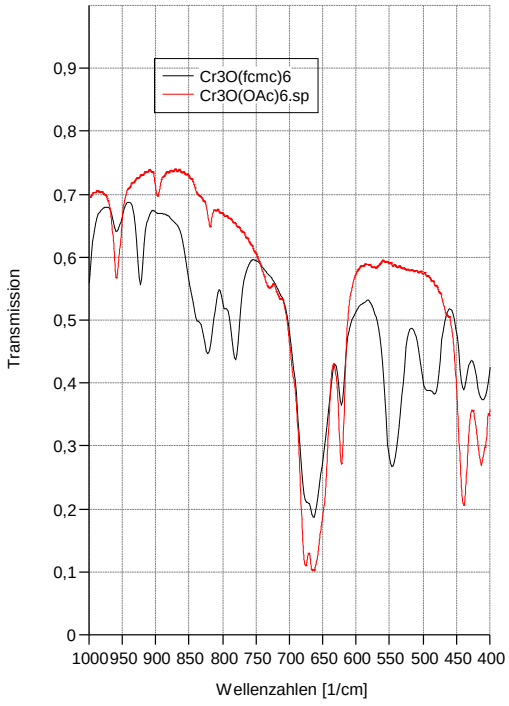

Figure 83 Comparison of infrared spectra of Cr3O(fcmc)6 (28, black) and Cr3O(OAc)6 (red).

This compound was then converted to **28** in a ligand substitution with ferrocene monocarboxylic acid under reflux in benzene. Mößbauer spectra of the resulting complex at different temperatures are shown in Figure 84, the corresponding data in Table 17.

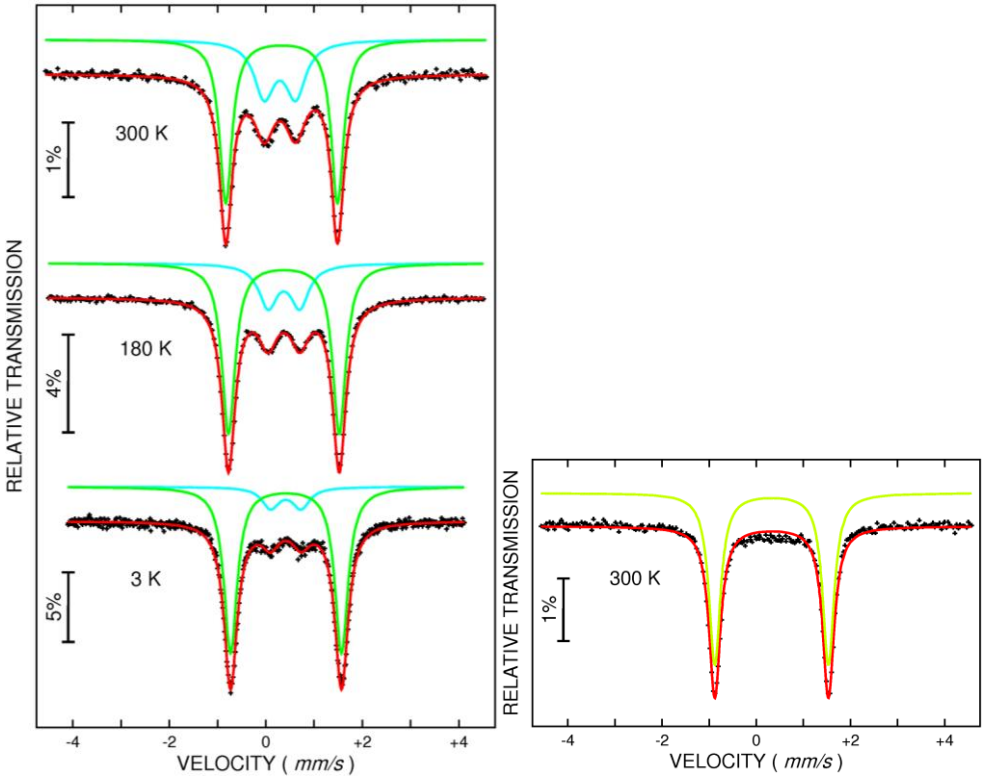

Figure 84 ^{57}Fe Mößbauer spectra of $[Cr_3O(fcmc)_6(H_2O)_3]NO_3$ at 300k, 180k and 3k, green lines represent Fc, blue lines represent Fc^+ (left) and FcCOOH at room temperature (right) for comparison

Table 17 Hyperfine parameters of $[Cr_3O(fcmc)_5(H_2O)_3]NO_3$ and $Cr(NO_3)_3$/fcmc mechanical mixture (mm).

Compound	T, K	$\delta,^{\alpha}$ mm/s	ΔE_{Θ}, mm/s	Γ, mm/s	area,%	assignment
28	300 K	0.42(1)	2.31(1)	0.31(2)	65.0	Fe^{II}
		0.39(2)	0.65(1)	0.50(1)	35.0	Fe^{III}
	180 K	0.47(1)	2.29(1)	0.33(1)	74.1	Fe^{II}
		0.47(2)	0.65(2)	0.46(1)	25. Sep	Fe^{III}
	3 K	0.52(1)	2.30(1)	0.32(1)	85.2	Fe^{II}
		0.51(1)	0.63(4)	0.42(2)	14. Aug	Fe^{III}
mm	300 K	0.42(1)	2.33(1)	0.29(1)	100	Fe^{II}

The spectrum recorded at 3 K without external magnetic field shows two quadrupole doublets, an inner one with quadrupole splitting ΔE_Q = 0.63 mm/s and isomer shift δ = 0.51 mm/s, and an outer one with ΔE_Q = 2.30 mm/s and δ = 0.52 mm/s. The ratio between the surface area above the curves of both doublets is temperature dependent and at low temperatures the Fe^{III} signal decreased considerably. This is in agreement with the findings in **26**.

Transition metal ions like Fe^{3+} are strong lewis acids. In order to investigate if this property is related to the above described findings, a complex with a weaker lewis acid like lanthanides had to be synthesized. A series of similar compounds was found in the literature that contain lanthanides and fcmc ligands. In the publication, no dysprosium complex is described. Because Dy complexes often show interesting magnetic behaviour, it was decided to synthesise the Dy analogue by the method described in the literature.[54] The crystal structure of $[Dy_2(fcmc)_6OMe_2(H_2O)_2]$ **29** and the corresponding Mößbauer spectra at different temperatures are shown in Figure 85.

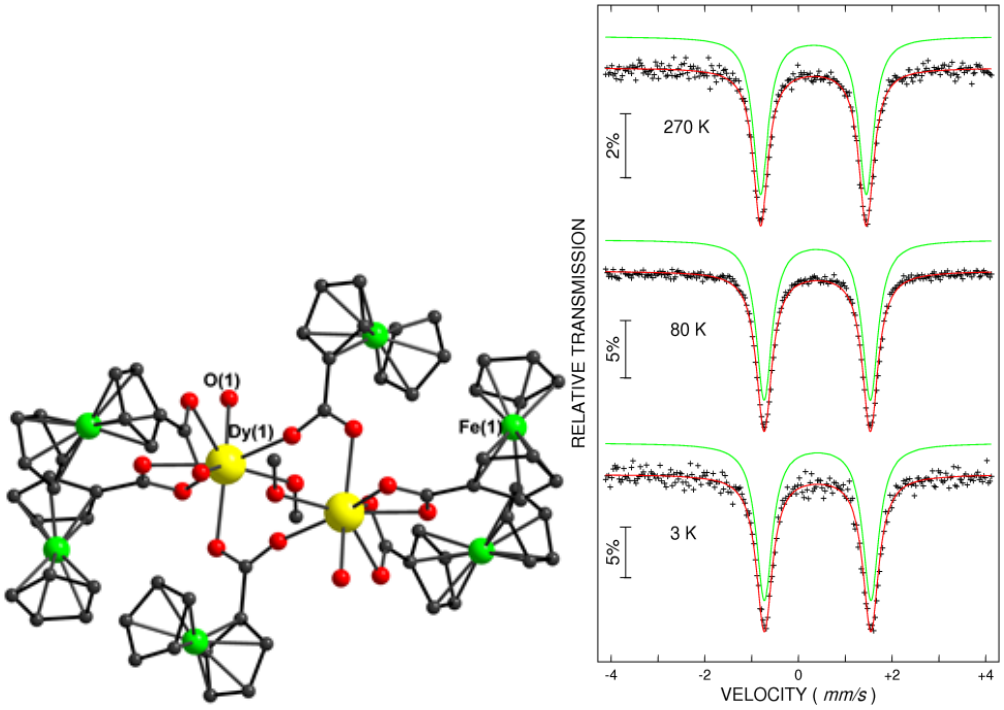

Figure 85 Crystal structure (left) and Mößbauer spectra at different temperatures (right) of 29.

The Mößbauer spectra show exclusively Fe^{II} low spin which represents the unaltered fcmc. From this finding follows that only strong Lewis acids cause oxidation of Fe in the ligands.

3.8.4 Modification of clusters with redox-active ligands for click grafting

At an early stage of the project, the synthesis of a modified version of **26** was attempted. To this point it was not yet decided whether to place the alkyne on the peptide and the azide on the cofactor or vice versa. Literature research showed a synthetic route to a ferrocene derivative (Figure 86) that was accessible in five steps from ferrocenecarboxylic acid.[55] It was therefore decided to test the complex synthesis with 1'-ethynylferrocenecarboxylic acid as ligand.

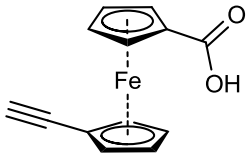

Figure 86 1'-ethynylferrocenecarboxylic acid (etfcmc).

As described in section 3.8.1, crystallization was hard to achieve for this kind of complex, which turned out to be true for $[Fe_3O(etfcmc)_6L3]NO_3$ **30** as well. Nevertheless, an IR comparison between the original complex and its modified version could confirm its identity (Figure 87).

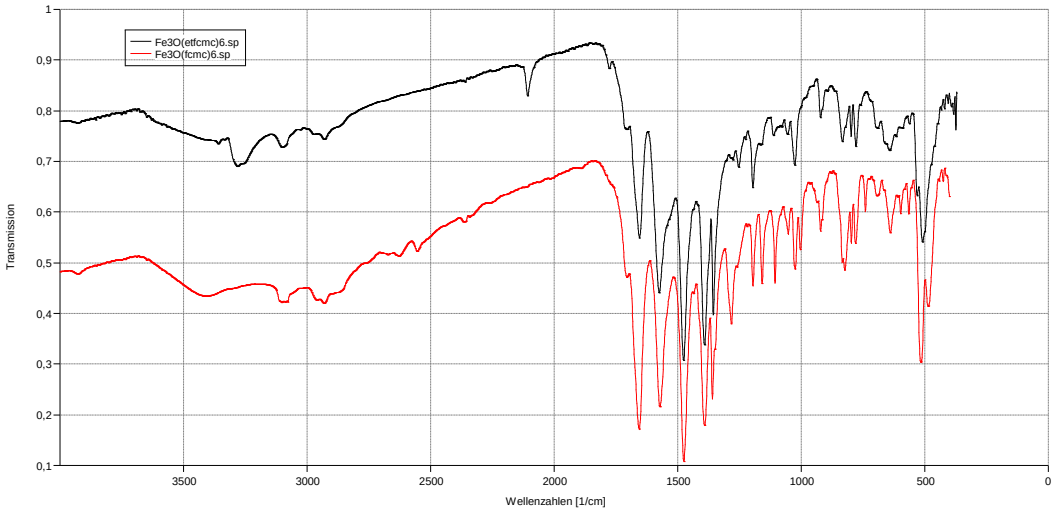

Figure 87 Comparion of IR spectra of 30 (black) and 26 (red).

The band at 2100 cm^{-1} represents the alkyne function whereas the cluster core shows signals between 550 and 750 cm^{-1}. Because this complex is not suited for grafting with the above described approach, it could not be put into reaction with an amino acid. However, this means that this complex is also modifiable. With an azide containing fcmc derivative, the complex could be used as an interesting electroactive species.

4 Conclusion and outlook

In section 3.1 it was shown that it is necessary to find a new strategy to graft redox cofactors onto peptides, since the existing strategies require multi-step syntheses that are not suitable for producing large amounts of cofactor amino acids.

A series of experiments is described in section 3.2, designed to test the simple one-step conversion of ferrocene into an amino acid using Friedel-Crafts acylation with aspartic anhydride. Ferrocene was chosen as a model system because of its known stability and the fact that its redox potential can be tuned with substituents on the Cp ligands. Variation of the solvent, catalyst and residue on the amine function in the amino acid anhydride did not result in identification of the necessary conditions to give the desired product. Therefore it was decided to follow a different approach.

In section 3.3, the feasibility of post-synthetic grafting on a surface-mounted peptide was demonstrated. This was achieved through fluorescent imaging of a structured surface using a new clickable derivative of a fluorophore. Further evidence was gained through xps measurements of pegma 10/90 thin films, where propargylglycine was reacted with azidomethyl ferrocene using two different catalysts.

In section 3.4 the click grafting approach was extended to a two-step consecutive click sequence. Initially, a series of experiments was performed to synthesize triisopropylsilyl (TIPS) propargylglycine. Propargylglycine was successfully protected with TIPS-Cl, but in only 30 % yield, which is reasonable given the high steric demand of the protecting group. A recently published method by Maier et al.[27] was adopted to give the desired product from far less expensive reactants, however in an overall yield of only 17 %. In order to apply this amino acid to particle-based peptide synthesis, it will be necessary to optimize the synthesis of the protected amino acid. Probably a completely new synthetic strategy needs to be found in order to overcome the very high steric demand of TIPS and obtain acceptable yields with less expensive starting materials.

It was found that in a peptide with both protected and unprotected alkyne on neighbouring amino acids, the click reactions proceeded, but with much less efficiency. This was verified by

sequentially clicking a ferrocene and ruthenocene derivative on the same peptide. The function of the protecting group and the feasibility of deprotection were tested in a series of experiments and could be verified. No fluoride could be detected on the surface after deprotection, which means that the surface is not compromised by this reaction. The click reaction of azidomethyl ruthenocene gave comparable results, both with and without protection of the alkyne. Without deprotection of the TIPS alkyne, no reaction was observed. Thus, in order to apply consecutive click chemistry, it will be necessary to conduct studies on how far apart both alkynes have to be in a peptide sequence to retain their function.

The synthesis and electrochemical characterization of a number of redox cofactors is shown in section 3.6. Ferrocene was used as motif as well as aromatic homo- and heteroaromatics. The fluorophores described previously were also characterized electrochemically.

The synthesis and click reaction experiments of a number of coordination clusters are reported in section 3.7. It was found that the clusters with an Fe_3O core are not robust enough to withstand the click reaction on the surface. For $[Cr_3O(pamba)_6L_3]NO_3$, which is considerably more stable, a line was observed in the XPS, which was however too small to be analysed quantitatively, but gives a clear indication that the species has been clicked onto the surface. It was concluded that this finding can be explained by limited access to the alkyne groups on the surface by the coordination clusters. Future work should thus involve mapping the landscape of the surface, including depth profiling, in order to suggest how to improve surface coverage. Nevertheless, the findings indicate that the click reaction worked to some extent on the surface. Further optimization is necessary to investigate this, e.g. with the use of 100% pegma surfaces that have a much higher surface coverage with the amino acid.

In section 3.8, a series of clusters with ferrocenemonocarboxylic acid as ligand was synthesized and characterized via ^{57}Fe Mößbauer spectroscopy. It was found that in complexes with strong Lewis acids, $[Fe(III,III)_2MeO(fcmc)_6L_3]$ where Me = Fe^{3+} or Mn^{2+} or Co^{2+} or Ni^{2+} and $[Cr_3O(fcmc)_6L_3]NO_3$, signals were different from what was expected. The observed effect is temperature dependent. It was also found that in the absence of strong Lewis acids, this effect could not be observed. From this it was concluded that in two of the ligands a reversible

oxidation occurs and that the electrons are not transferred to the Fe ions in the cluster core. It is unclear where the electrons are shifted to. This will be subject to future studies. In addition, the crystallization of $[Fe_3O(fcmc)_6L_3]NO_3$ could be optimized by the addition of base during the synthesis.

Finally, it was demonstrated that it is possible to obtain derivatives of $[Fe_3O(fcmc)_6L_3]NO_3$ with modified ferrocenecarboxylate ligands. Combined with the above described electronic properties, a plethora of possibilities arise from this. The synthesized alkyne complexes could be used to click redox cofactors. The electronic interactions of the aggregates could then be investigated. Alternatively an azide derivative could be obtained to use as cofactor on peptides using the click chemistry described in this thesis.

4.1 Zusammenfassung

In Abschnitt 3.1 der vorgelegten Arbeit konnte gezeigt werden, dass die Notwendigkeit besteht, eine neue Strategie zur Verknüpfung von Redox-Cofaktoren und Peptiden besteht.

Abschnitt 3.2 zeigt eine Reihen von Experimenten zur Friedel-Crafts Acylierung von Ferrocen als Modellverbindung mit Asparagiinsäureanhydrid zur Erzeugung eines Ferrocen-Peptidkonjugats in einem Schritt. Es konnten jedoch keine Rekationsbedingungen gefunden werden, die eine erfolgreiche Umsetzung ermöglichen.

In Abschnitt 3.3 wurde die Machbarkeit Post-synthetischer Verknüpfungen an pegma 10/90-Dünnfilmen durch Click-Chemie mit Hilfe eines für Klick-Reaktionen modifizierten Fluorophors und Fluoreszenz-Bildgebung belegt. Weitere Belege dafür wurden durch Reaktionen mit Azidomethylferrocen und anschließender XPS-Spektroskopie gewonnen.

Die Click-Strategie wurde zu einer zweistufigen Click-Sequenz erweitert (Abschnitt 3.4), indem eine Alkin-Aminosäure mit einer Triisopropylsilyl (TIPS)-Schutzgruppe versehen wurde. Aufgrund des erheblichen sterischen Anspruchs von TIPS waren die Ausbeuten nur gering. Wie in Abschnitt 3.5 gezeigt, wurde die zweistufige Reaktion zunächst an einem oberflächengebundenen Peptid mit geschützter und ungeschützter Alkin-Aminosäure in direkter Nachbarschaft untersucht, indem nach einander Azidomethylferrocen und –ruthenocen geklickt wurden und die Oberfläche anschließend mittels XPS charakterisiert wurde. Obwohl deutlich weniger als erwartet, wurden Fe^{2+} und Ru^{2+} nachgewiesen. Nach der Entschützung mit Tetrabutylammoniumfluorid konnte kein Fluor auf der Oberfläche festgestellt werden, was zeigt, dass die Methode geeignet ist.

Eine Reihe von einfachen Redox-Cofaktoren wurden synthetisiert und elektrochemisch charakterisiert (Abschnitt 3.6) Im Weiteren wurden einige Koordinationscluster mit modifizierten Liganden dargestellt und deren Eignung zur Click-Chemie untersucht (3.7)

Schließlich wurde eine Reihe von Koordinationsclustern mit Ferrocencarboxylat-Liganden dargestellt und mittels Mößbauer-Spektroskopie untersucht, wobei interessante Effekte beobachtet wurden.

5 Experimental Part

5.1 Methods

Nuclear magnetic resonance (NMR) spectra were recorded by Helga Berberich on a Bruker AV 300, AV 400 and AV600 spectrometer. Chemical shifts were referenced to the respective solvent residual peak. Solvent impurities were identified according to Gottlieb et al.[56] Proton NMR signals were assigned based on multiplicity, by comparison with similar known compounds or by spectral simulation with the Program ChemBioOffice Ultra 10.

Fourier-Transform Infrared spectroscopy (FTIR) was performed on a Perkin Elmer Spektrum GX FT-IR System. Samples were measured in form of KBr pellets that were produced immediately prior to measurement from pre-dried, IR grade KBr. Prior to each measurement session, a background spectrum was recorded and substracted from the sample spectra. Data were handled using the program SpekWin.[57] Bands were designated as very strong (vs), strong (s), medium (m) or weak (w). Signals were assigned by comparison with spectral database

Electron Impact (EI) mass spectrometry was performed by Petra Smie on a Thermo Fischer DFS EI GC-MS double-focused sector field electron impact GC/MS mass spectrometer.

Electrospray ionization time-of-flight (ESI-TOF) mass spectrometry was performed by Petra Smie on an Ionspec FT-ICR fourier-transform ion cyclotron resonance mass spectrometer.

X-ray photoelectron spectroscopy (XPS) measurements were performed by Vanessa Trouillet using a K-Alpha XPS spectrometer (ThermoFisher Scientific, East Grinstead, UK). Data acquisition and processing using the Thermo Avantage software is described elsewhere.[58] All Pegma thin films were analyzed using a microfocused, monochromated Al Kα X-ray source (400 µm spot size). The K-Alpha charge compensation system was employed during analysis, using electrons of 8 eV energy, and low-energy argon ions to prevent any localized charge build-up. The spectra were fitted with one or more Voigt profiles (BE uncertainty: +0.2eV) and Scofield sensitivity factors were applied for quantification.[59] All spectra were referenced to the C1s peak assumed

to originate from surface hydrocarbon contamination at 285.0 eV binding energy controlled by means of the well-known photoelectron peaks of metallic Cu, Ag, and Au, respectively.

Fluorescence images were recorded using a GenePix 4000B scanner with excitation wavelengths of 532 nm (green scans) and 635 nm (red scans) with a resolution of 5 µm.

Cyclic voltammetry was performed on a Gamry Interface 1000 Potentiostat using a three-electrode setup of Pt working and counter electrode and Ag/Ag^+ reference electrode (0.01M $AgNO_3$ with 0.1M Tetrabutylammonium hexafluorophosphate (TBAP) in acetonitrile with silver wire electrode). All potential curves were subsequently referenced to Ferrocene / Ferrocenium. Measurements were performed using the following procedure:

137 mg of the auxillary electrolyte TBAP was dissolved in 7 mL of the respective dry solvent in the measurement cell. The cover with the electrodes in place was closed and a constant stream of dry N_2 gas was bubbled through the solution for 1 min. A background spectrum of the solution was recorded for later comparison. The sample was added and the desired voltammograms recorded. At last, Ferrocene was added and another voltammogram was added to reference all potentials.

X-Ray single crystal diffraction measurements were performed on a Stoe IPDS II single crystal diffractometer equipped with a molybdenum x-ray source (Mo-Kα = 0.71073 Å) at room temperature and an Agilent Supernova dual source single crystal diffractometer equipped with a microfocused molybdenum and copper x-ray source (Cu-Kα = 1.5405 Å) and a CCD X-ray detector at 150 K.

X-Ray powder diffraction was performed on a Stoe Stadi P diffractometer equipped with a copper x-ray source with Cu-Kα = 1.5405 Å. All spectra were recorded at room temperature.

Variable temperature Mössbauer spectra were recorded by Dr. Valeriu Mereacre using a conventional spectrometer in a constant–acceleration mode equipped with a ^{57}Co source (3.7 GBq) in a rhodium matrix. Isomer shifts are given relative to α-Fe at 300 K. The fitting of the experimental data was performed using the Software NORMOS.

5.2 Synthesis and characterization

5.2.1 Coupling of OPfp activated amino acids to pegma 10/90 coated glass slides

Coupling of Pfp activated amino acids onto pegma 10/90 coated glass slides was performed according to a procedure developed by Christopher Schirwitz.[28] The amino acid to be coupled to the surface (0.03 mol/L) was dissolved in 250µL DMF. The solution was dropped carefully onto the functionalized and deprotected side of the slide surface until complete coverage. A blank microscope slide was put onto the solution to completely cover the surface. After 16 h, the slides were separated and the functionalised slide washed with DMF (3 x 5 mL, 5 min. ultrasound) and acetone (2 x 5 mL, 5 min. ultrasound) and left to dry in air. The slide was stored at 5 °C until further use. Eventually the Fmoc protecting group was removed by immersing the slide in a 20% (v/v) solution of piperidine in DMF for 20 min. and subsequent washing as described above.

5.2.2 Click reactions on glass slide surfaces

5.2.2.1 Catalysis with $CuSO_4$ and ascorbic acid

The glass slide was immersed in 5 mL DMF for 5 min. During that time, $CuSO_4$ x $5H_2O$ (2.50 mg, 0.01 mmol, 0.10 eq.) and β-ascorbic acid (35.0 mg, 0.20 mmol, 2.00 eq.) were stirred for 5 min. in 5 mL DMF, during which a yellowish solution formed. The azide to be clicked (0.10 mmol, 1.00 eq.) was put into a 20 mL snap-cap flask and 5 mL of the catalyst solution was added. After complete solution, the glass slide was immersed in the reaction solution overnight. The slide was removed and rinsed with dist. H_2O until no more crystalline solid on the surface is visible. The slide was washed with portions of DMF (3 x 5 mL, 5 min. ultrasound) and acetone (2 x 5 mL, 5 min. ultrasound) and dried in air. It was stored at 5 °C under air.

5.2.2.2 Catalysis with $Cu(CH_3CN)_4BF_4$

The glass slide was immersed in 5 mL DMF for 5 min. The azide to be clicked (0.10 mmol, 1.00 eq.) and $Cu(CH_3CN)_4BF_4$ (3.15 mg, 0.01 mmol, 0.10 eq.) were dissolved in 5 mL wet DMF.. The glass slide was immersed in the reaction solution overnight. The slide was removed and rinsed with dist. H_2O until no more crystalline solid on the surface is visible. The slide was

washed with portions of DMF (3 x 5 mL, 5 min. ultrasound) and acetone (2 x 5 mL, 5 min. ultrasound) and dried in air. It was stored at 5 °C under air.

5.2.3 Deprotection of TIPS alkynes on glass slide surfaces

The glass slide was immersed in 2 mL of a solution of tetra-*N*-butylammonium fluoride in THF (0.1 mol/L) and left to react for 30 min. at room temperature. The slide was subsequently washed with THF (3 x 5 mL , 5 min. ultrasound) and dried in air. The following click reaction was performed according to 5.2.2.

5.2.4 (S)-prop-2-yn-1-yl-2-((((9H-fluoren-9-yl)methoxy)carbonyl)amino)-3-hydroxypropanoate (4)

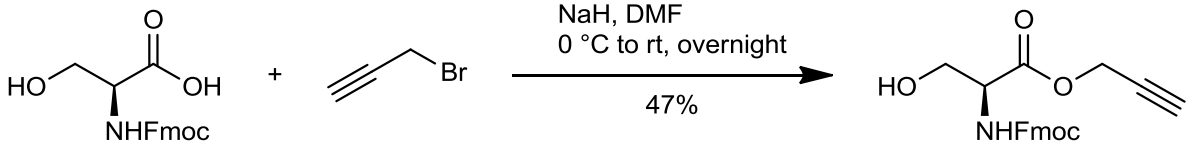

In a flame-dried 100 mL Schlenk flask, Fmoc-Ser-OH (1.00 g, 3.06 mmol, 1.00 eq.) was dissolved in 10 mL dry DMF. After cooling in an ice bath for 5 min, NaH (250 mg, 6.25 mmol, 2.05 eq.) was added in small portions over 5 min. Stirring was continued at 0 °C for 30 min. Propargyl bromide (681 µL, 909 mg, 6.11 mmol, 2.00 eq.) was added in one portion and the mixture was allowed to warm up to room temperature overnight. The reaction was quenched with 6 eq. 1M HCl and after stirring for 10 min, extracted with ethyl acetate (3 x 50 mL). Column chromatography (Silica gel, 3 x 20 cm, CH_2Cl_2/Acetone 9:1 to 1:1) of the crude product yielded colorless oil (520 mg, 1.42 mmol, 47 %) that solidified upon standing.

^{1}H-NMR (300 MHz, $CDCl_3$): δ(ppm) = 2.51 (t, *J* = 2.47 Hz, 1 H, CC*H*), 4.01 (dd, *J* = 47 Hz, 11 Hz, 2 H, Propargyl-OCH_2), 4.24 (t, *J* = 6.87 Hz 1 H, Fmoc-C*H*), 4.38-4.55 (m, 3 7.33 (t, *J* = 7.54 Hz, 2 H, Fmoc-H_{ar}), 7.41 (t, *J* = 7.35 Hz, 2 H, Fmoc-H_{ar}), 7.53-7.66 (m, 2 H, Fmoc-H_{ar}), 7.77 (d, *J* = 7.51 Hz, 2 H, Fmoc-H_{ar}).

5.2.5 (S)-perfluorophenyl-2-((((9*H*-fluoren-9-yl)methoxy)carbonyl)amino)pent-4-ynoate (Fmoc-Pra-OPfp)

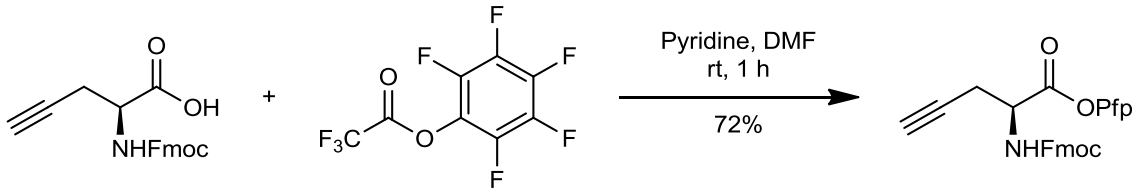

In a 100 mL round-bottomed flask, Fmoc-Propargylglycine (200 mg, 0.596 mmol, 1.00 eq.) was dissolved in 5 mL DMF. Under stirring, pentafluorophenyl trifluoroacetate (205 µL, 334 mg, 1.19 mmol, 2.00 eq.) and Pyridine (52.9 µL, 51.9 mg, 0.656 mmol, 1.10 eq.) were added and stirring continued for 1 h at room temperature, after which TLC control indicated complete conversion. The reaction was quenched with 0.1N HCl (50 mL) and the product extracted from the aqueous phase with CH_2Cl_2 (3 x 25 mL). The united organic phases were dried over Na_2SO_4 and the solvent removed in vacuo, yielding a white powder (215 mg, 0,429 mg, 72%).

^{1}H-NMR (300 MHz, $CDCl_3$): δ(ppm) = 2.22 (t, J = 2.6 Hz, 1 H, CC*H*), 2.87 to 3.12 (m, 2 , 4.31 (t, J = 7.0 Hz, 1 H, C*H*CO_2R) , 4.51 (d, J = 7.3 Hz, 2 H, Fmoc-CH_2), 4.99 (dt, J = 8.7, 4.8 Hz, 1 H, Fmoc-C*H*), 5.71 (d, J = 9.6 Hz, 1 H, N*H*), 7.36 (t, J = 7.4 Hz, 2 H, Fmoc-H_{ar}), 7.45 (t, J = 7.4 Hz, 2 H, Fmoc-H_{ar}), 7.65 (d, J = 7.6 Hz, 2 H, Fmoc-H_{ar}), 7.82 (d, J = 7.2 Hz, 2 H, Fmoc-H_{ar}).

^{13}C-NMR (75 MHz, $CDCl_3$): δ(ppm) = 22.83, 47.1, 52.4, 67.6, 72.9, 120.1, 125.1, 127.1, 127.8, 141.4, 143.7, 155.5.

^{19}F-NMR (282 MHz, $CDCl_3$): δ(ppm) = -151.7 (d, J = 17.5 Hz, 2 F), -156.8 (t, J = 21.8 Hz, 1 F), -161.7 (dd, J = 21.5, 17.3 Hz, 2 F).

5.2.6 (S)-perfluorophenyl-2-((((9H-fluoren-9-yl)methoxy)carbonyl)amino)-3-(prop-2-yn-1-yloxy)propanoate (Fmoc-Ser(OPrp)-OPfp)

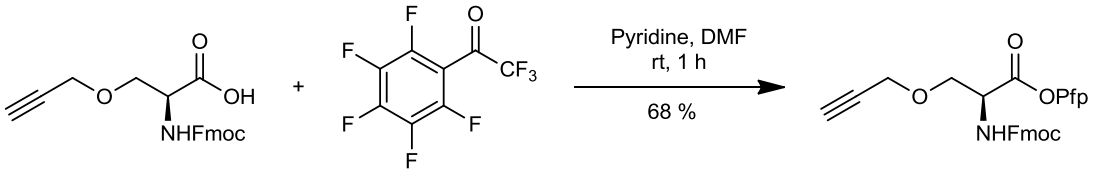

In a 100 mL round-bottomed flask, Fmoc-Ser(OPrp)-OH (100 mg, 0.274 mmol, 1.00 eq.) was dissolved in 5 mL DMF. Under stirring, pentafluorophenyl trifluoroacetate (94.0 µL, 153 mg, 0.547 mmol, 2.00 eq.) and Pyridine (200 µL, 196 mg, 2.48 mmol, 1.10 eq.) were added and stirring continued for 1 h at room temperature, after which TLC control indicated complete conversion. The reaction was quenched with 0.1N HCl (50 mL) and the product extracted from the aqueous phase with CH_2Cl_2 (3 x 25 mL). The united organic phases were dried over Na_2SO_4 and the solvent removed in vacuo, yielding a colorless oil (99.0 mg, 0.186 mmol, 68%).

^{1}H-NMR (300 MHz, $CDCl_3$): δ(ppm) = 2.53 (t, *J* = 2.4 Hz, 1 H, CC*H*), 3.99 (dd, J = 9.5 Hz, 3.0 Hz, 1 H, CH_2COOR), 4.23 (dd, J = 9.5 Hz, 2.9 Hz, 1 H, CH_2COOR), 4.26 to 4.32 (m, 2 H, CH_2), 4.42 to 4.65 (m, 2 H, CH_2), 4.98 (dt, J = 9.0 Hz, 2.7 Hz, 1 H, C*H*), 5.80 (d, *J* = 9.1 Hz, 1 H, N*H*), 7.35 (td, J = 7.5 Hz, 1.1 Hz, 2 H, Fmoc-CH_{ar}), , 7.45 (t, J = 7.5 Hz, 2 H, Fmoc-CH_{ar}), 7.65 (dd, J = 7.4 Hz, 3.2 Hz, 2 H, Fmoc-CH_{ar}), 7.81 (d, J = 7.6 Hz, 2 H, Fmoc-CH_{ar}).

^{13}C-NMR (75 MHz, $CDCl_3$): δ(ppm) = 31.0, 47.1, 54.3, 58.6, 67.6, 69.2, 75.7, 78.3, 120.1, 125.1, 127.8, 136.4, 141.3, 143.6, 143.7, 156.1, 166.6.

^{19}F-NMR (282 MHz, $CDCl_3$): δ(ppm) = -151.9 (d, J = 17.1 Hz, 2 F), -157.1 (t, J = 21.4 Hz, 1 F), -161.9 (dd, J = 21.6, 17.3 Hz, 2 F).

5.2.7 (S)-3-(but-2-yn-1-yloxy)-((*tert*-butoxycarbonyl)amino)propanoic acid (16)

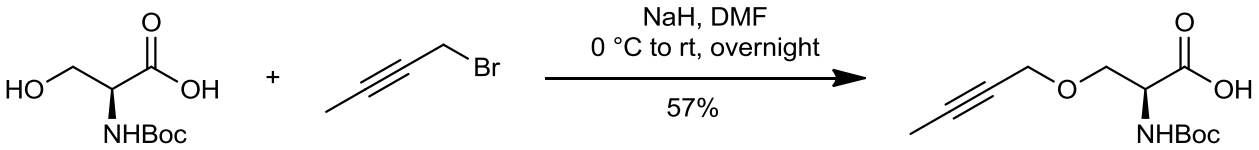

In a flame-dried 100 mL Schlenk flask, Boc-Ser-OH (490 mg, 2.39 mmol, 1.00 eq.) was dissolved in 10 mL dry DMF. After cooling in an ice bath for 5 min, NaH (225 mg, 5.36 mmol, 2.36 eq.) was added in small portions over 5 min. Stirring was continued at 0 °C for 30 min. 1-Bromo-2-propyne (250 µL, 380 mg, 2.86 mmol, 1.20 eq.) was added in one portion and the mixture was allowed to warm up to room temperature overnight. The reaction was quenched with 6 eq. 1M HCl and after stirring for 10 min, extracted with ethyl acetate (3 x 50 mL). Column chromatography (Silica gel, 3 x 20 cm, CH_2Cl_2/Acetone 9:1 to 1:1) of the crude product yielded colorless oil (348 mg, 1.35 mmol, 57 %).

^{1}H-NMR (300 MHz, $CDCl_3$): δ(ppm) = 1.43 to 1.49 (m, 9 H, Boc-C*H*$_3$), 1.86 (t, *J* = 2.4 Hz, 3 H, CCC*H*$_3$), 3.72 to 4.24 (m, 2 H, C*H*$_2$), 4.32 to 4.56 (m, 1 H, C*H*), 4.66 to 4.84 (m, 2 H, C*H*$_2$), 5.49 (dd, *J* = 32.2 Hz, 8 Hz, 1 H, N*H*).

^{13}C-NMR (75 MHz, $CDCl_3$): δ(ppm) = 3.78 (CC*C*H$_3$), 28.4 (Boc-*C*H$_3$), 54.0, 54.1, 56.0, 59.3, 63.5, 69.5, 72.8, 72.9, 74.5, 80.2, 80.4, 83.3, 83.6, 84.0, 155.7, 155.9, 170.2, 170.5.

5.2.8 6-Azido-2-naphthoic acid (aznap)

In a 100 mL round-bottomed flask, 2-Amino-6-naphthoic acid (1.00 g, 5.34 mmol, 1.00 eq.) was dissolved in 50 mL MeOH. K_2CO_3 (1.69 g, 12.2 mmol, 2.30 eq.), Imidazolesulfonic azide hydrochloride (1.34 g, 6.41 mmol, 1.20 eq.) and $CuSO_4$ x $5H_2O$ (50.0 mg, 0.200 mmol, 0.037 eq.)

were added and the mixture stirred overnight at room temperature. After TLC indicated complete conversion (SiO_2, MeOH), the solvent was removed in vacuo. The residue was dissolved in 50 mL H_2O. The solution was extracted with CH_2Cl_2 until TLC spots of the organic phase showed no more blue fluorescence. The aqueous phase was acidified with acetic acid and extracted with ethyl acetate (3 x 50 mL). The united organic phases were washed with H_2O (2 x 50 mL), dried over Na_2SO_4 and evaporated to dryness in vacuo, yielding an orange-brown powder (863 mg, 4.05 mmol, 76 %).

IR (KBr): (NapN3.sp) 2122 (s, N_3), 2104 (s, N_3), 1690 (vs, Ar-COO^-), [1627, 1477, 1424, 1377, 1344, 1296, 1230, 1215, 1185 (all typical for 6-substituted 2-naphthoic acids)].

5.2.9 (E)-1-(2-azidoethyl)-4-(4-(dimethylamino)styryl)-2,6-diisopropylpyridin-1-ium hexafluorophosphate (6-N_3)

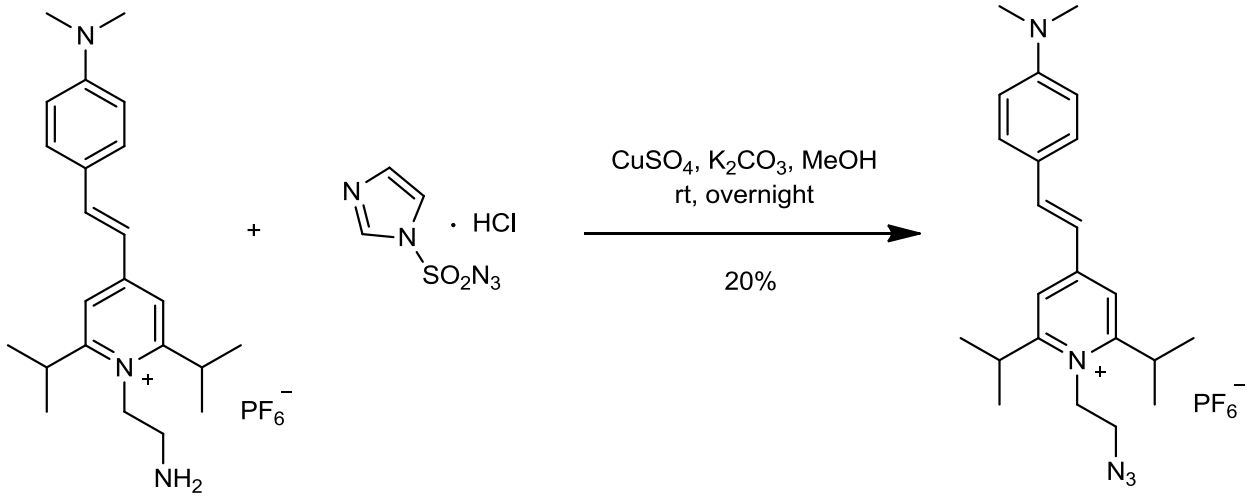

In a 25 mL round-bottomed flask, Styrylpyridinium fluorophore **6-NH_2** (43.0 mg, 0.086 mmol, 1.00 eq.) was dissolved in 10 mL Methanol. K_2CO_3 (20.0 mg, 0.145 mmol, 1.67 eq.), $CuSO_4$ x $5H_2O$ (6.00 mg, 0.086 mmol, 0.28 eq.) and imidazolesulfonyl azide hydrochloride (29.0 mg, 0.138 mmol, 1.60 eq.) were added and the reaction mixture was stirred overnight at room temperature. Volatiles were removed in vacuo and the crude product was purified by filtration through a short silica gel plug (3.5x3 cm) using acetonitrile as eluent. Evaporation of the solvent yielded a red fluorescent solid (9.00 mg, 0.017 mmol, 20%)

^{1}H-NMR (300 MHz, $CDCl_3$): δ(ppm) = 1.46 to 1.54 (m, 12 H, ^{i}Pr-CH_3), 3.13 (s, 6 H, NCH_3), 3.62 (hept, *J* = 6.8 Hz, 2 H, ^{i}Pr-C*H*), 4.00 (t, J = 5.7 Hz, 2 H, CH_2), 4.80 (t, J = 5.5 Hz, 2 H, CH_2), 6.76 (d, H = 9.0 Hz, 2 H, H_{Ar}), 6.89 (d, J = 16 Hz, 1 ^{13}C-NMR (75 MHz, $CDCl_3$): δ(ppm) = 31.5, 40.4, 51.3, 77.4, 112.2, 118.5, 130.8, 142.9, 154.2, 164.1.IR (KBr): 2151 (s, N_3),

HRMS (ESI-TOF): m/z = 378.2764 (calc. 378.2658 $[C_{23}H_{32}N_5]^+$).

5.2.10 (E)-1-(3-azidopropyl)-4-(4-(dimethylamino)styryl)-2,6-diisopropylpyridin-1-ium hexafluorophosphate (7-N_3)

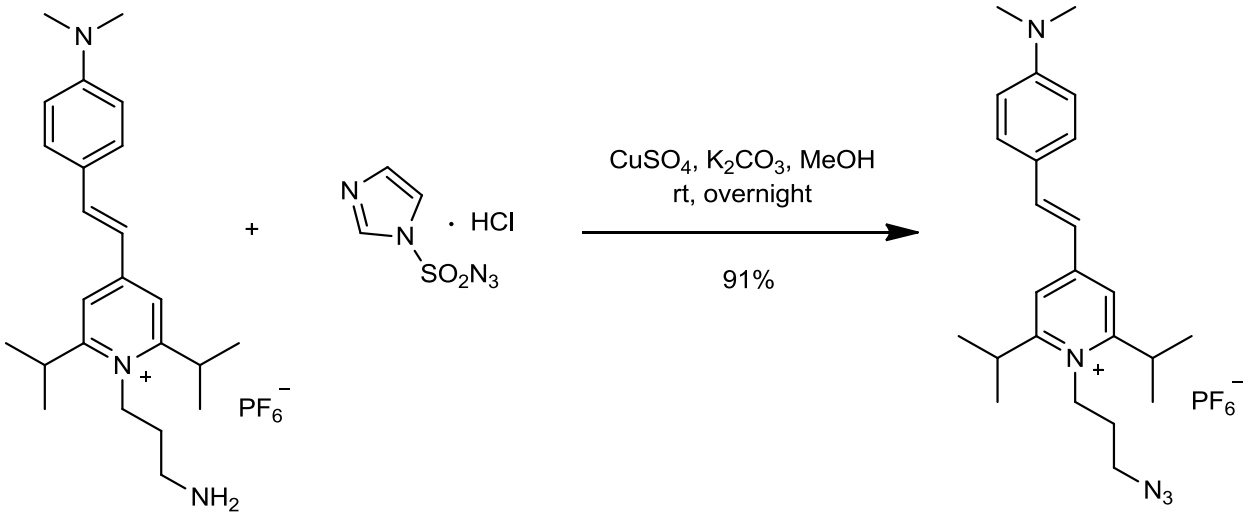

In a 50 mL round-bottomed flask, Styrylpyridinium fluorophore **7-NH_2** (100 mg, 0.195 mmol, 1.00 eq.) was dissolved in 20 mL Methanol. K_2CO_3 (178 mg, 1.29 mmol, 6.60 eq.), $CuSO_4$ x $5H_2O$ (7.00 mg, 0.027 mmol, 0.14 eq.) and imidazolesulfonyl azide hydrochloride (102 mg, 0.487 mmol, 2.49 eq.) were added and the reaction mixture was stirred overnight at room temperature. Volatiles were removed in vacuo and the crude product was purified by filtration through a short silica gel plug (3.5x3 cm) using acetonitrile as eluent. Evaporation of the solvent yielded a red fluorescent solid (96.0 mg, 0.017 mmol, 91%)

^{1}H-NMR (300 MHz, $CDCl_3$): δ(ppm) = 1.47 to 1.58 (m, 12 H, ^{i}Pr-CH_3), 2.05 to 2.15 (m, 2 H, CH_2), 3.11 (s, 6 H, NCH_3), 3.62 (hept, *J* = 6.7 Hz, 2 *H*, ^{i}Pr-C*H*), 3.72 (t, J = 5.7 Hz, 2 *H*, CH_2), 4.49 to 4.62 (m, 2 H, CH_2), 6.75 (d, H = 8.8 Hz, 2 H, H_{Ar}), 6.90 (d, J = 16 Hz, 1 ^{13}C-NMR (75 MHz, $CDCl_3$): δ(ppm)

= 23.2, 30.8, 40.2, 48.2, 112.0, 118.5, 130.5, 163.1.HRMS (ESI-TOF): m/z = 392.2935 (calc. 392.2814 for $[C_{24}H_{34}N_5]^+$)

5.2.11 1-(3-azidopropyl)-4-((1E,3E)-4-(4-(dimethylamino)phenyl)buta-1,3-dien-1-yl)-2,6-diisopropylpyridin-1-ium hexafluorophosphate(10-N_3)

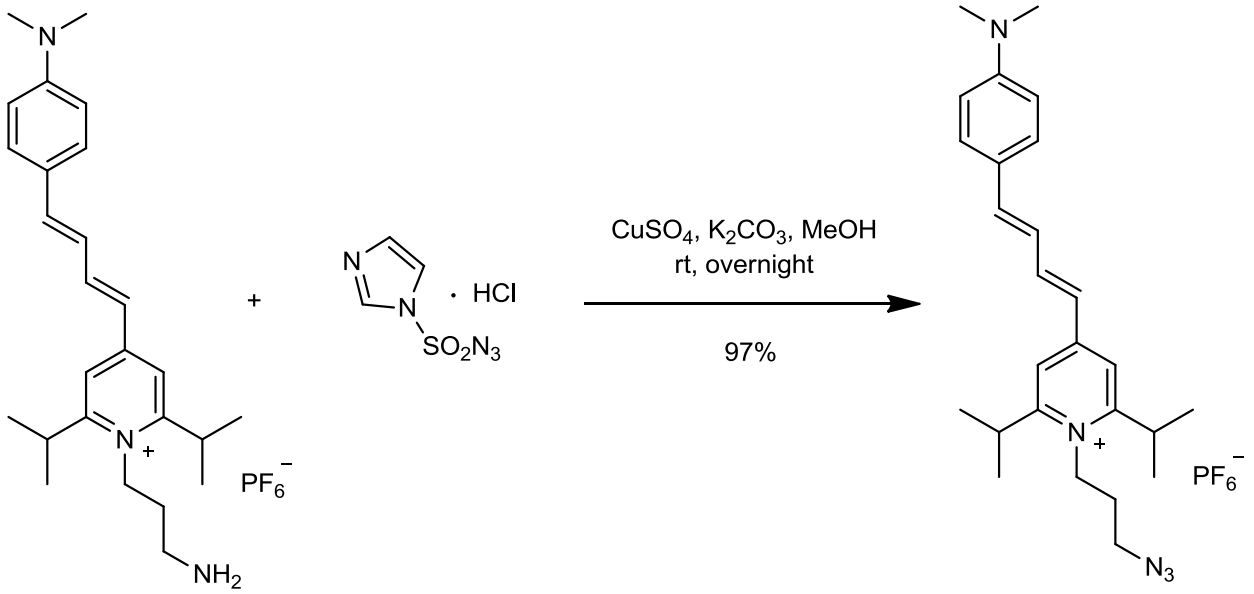

In a 25 mL round-bottomed flask, Styrylpyridinium fluorophore **10-NH_3** (98.0 mg, 0.182 mmol, 1.00 eq.) was dissolved in 10 mL Methanol. K_2CO_3 (166.0 mg, 1.20 mmol, 6.60 eq.), $CuSO_4$ x $5H_2O$ (7.00 mg, 0.028 mmol, 0.15 eq.) and imidazolesulfonyl azide hydrochloride (102.0 mg, 0.487 mmol, 2.67 eq.) were added and the reaction mixture was stirred overnight at room temperature. Volatiles were removed in vacuo and the crude product was purified by filtration through a short silica gel plug (3.5x3 cm) using acetonitrile as eluent. Evaporation of the solvent yielded a red fluorescent solid (100 mg, 0.177 mmol, 97%)

^{1}H-NMR (300 MHz, $CDCl_3$): δ(ppm) = 1.52 (d, *J* = 6.6 Hz, 12 H, ^{i}Pr-C*H*$_3$), 2.07 to 2.18 (m, 2 H, C*H*$_2$), 3.09 (s, 6 H, NC*H*$_3$), 3.52 to 3.62 (m, 2 *H*, ^{i}Pr-C*H*), 3.75 (t, *J* = 5.7 Hz, 2 *H*, C*H*$_2$), 4.55 to 4.63 (m, 2 H, C*H*$_2$), 6.53 (d, H = 15.4 Hz, 2 H), 6.75 (d, H = 8.5 Hz, 2 H, *H*$_{Ar}$), 6.81 to 6.89 (m, 2 H), 7.07 (d, *J* = 15 Hz, 1 ^{13}C-NMR (75 MHz, $CDCl_3$): δ(ppm) = too weak, no signals visible

HRMS (ESI-TOF): m/z = 418.3087 (calc. 418.2971 for $[C_{26}H_{36}N_5]^+$)

5.2.12 (E)-1-(3-azidopropyl)-2,6-diisopropyl-4-(4-methoxystyryl)pyridin-1-ium hexafluorophosphate (11-N_3)

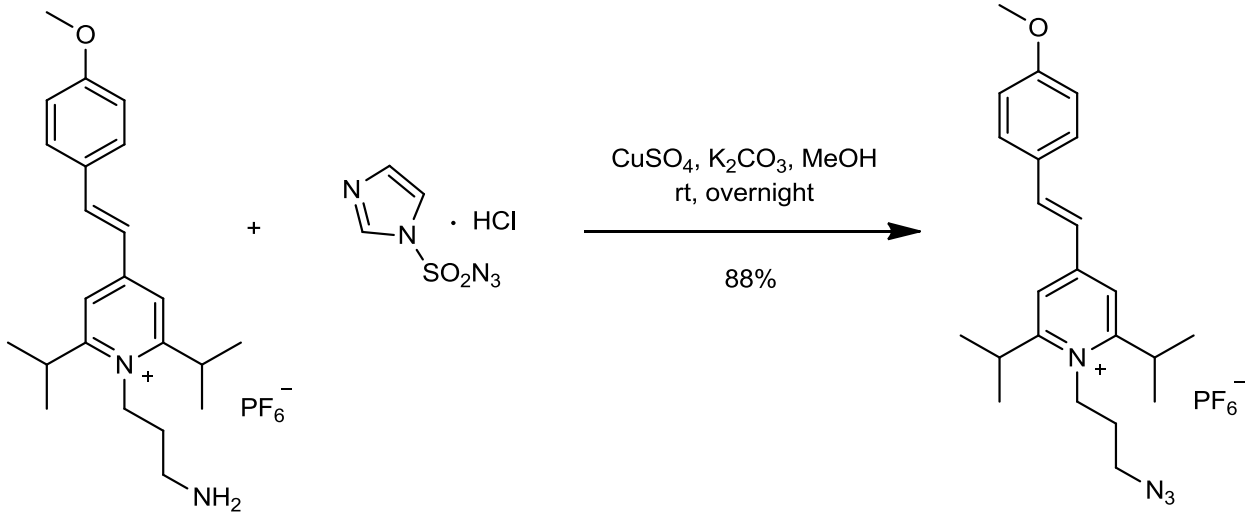

In a 25 mL round-bottomed flask, Styrylpyridinium fluorophore **11-NH_2** (43.0 mg, 0.086 mmol, 1.00 eq.) was dissolved in 10 mL Methanol. K_2CO_3 (20.0 mg, 0.145 mmol, 1.67 eq.), $CuSO_4$ x $5H_2O$ (6.00 mg, 0.086 mmol, 0.28 eq.) and imidazolesulfonyl azide hydrochloride (29.0 mg, 0.138 mmol, 1.60 eq.) were added and the reaction mixture was stirred overnight at room temperature. Volatiles were removed in vacuo and the crude product was purified by filtration through a short silica gel plug (3.5x3 cm) using acetonitrile as eluent. Evaporation of the solvent yielded a red fluorescent solid (94.0 mg, 0.179 mmol, 88%)

^{1}H-NMR (300 MHz, $CDCl_3$): δ(ppm) = 1.20 to 1.62 (m, 12 H, ^{i}Pr-C*H*$_3$), 1.71 to 1.89 (m, 2 H, C*H*$_2$), 2.00 to 2.21 (m, 2 H, C*H*$_2$), 3.32 to 3.64 (m, 2 H, ^{i}Pr-C*H*), 3.64 to 3.81 (m, 2 H, CH), 3.82 to3.95 (m, 3 H, OC*H*$_3$),4.38 to 4.74 (m, 2 *H*, C*H*$_2$), 6.89 to 7.31 (m, 4 H, *H*$_{Ar}$), 7.41 to 7.77 (m, 4 ^{13}C-NMR (75 MHz, $CDCl_3$): δ(ppm) = 30.5, 31.0, 48.1, 55.5, 98.7, 114.7, 119.5, 120.2, 127.4, 130.2, 130.6, 141.2, 162.0, 163.7.

5.2.13 (1-ferrocenylmethyl-5-(methylthio)-1*H*-1,2,3-triazol-4-yl)methanol (14)

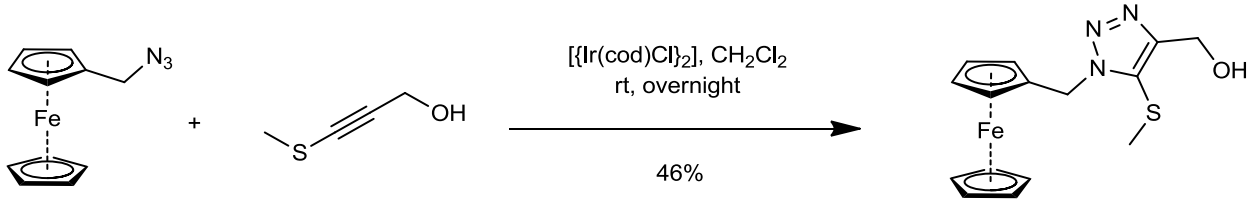

In a 50 mL round-bottomed flask, 3-(Methylthio)-2-propynol (27 mg, 0.255 mmol, 1.00 eq.), Azidomethylferrocene (63 mg, 0.261 mmol, 1.03 eq.) and $[\{Ir(cod)Cl\}]_2$ (4.00 mg, 0.006 mmol, 0.02 eq.) were dissolved in 5 mL CH_2Cl_2 and stirred overnight at room temperature. Volatiles were removed in vacuo and the crude product was purified by column chromatography (SiO_2, Hex/EE 2:1 to 1:0) to give yellow oil (40.0 mg, 0.117 mmol, 46%) that solidified upon standing.

^{1}H-NMR (300 MHz, $CDCl_3$): δ(ppm) = 2.29 (s, 3 H, SC*H*$_3$), 2.61 (br. s, 1 H, OH), 4.24 (s, 5 H, Cp-*H*), 4.40 (m, 2 H, Cp-*H*), 4.81 (m, 2 H, Cp-H).

^{13}C-NMR (75 MHz, $CDCl_3$): δ(ppm) = 20.3, 48.5, 56.2, 68.9, 69.1, 69.5, 81.9.

5.2.14 (S)-tert-butyl 2-((tert-butoxycarbonyl)amino)-5-(triisopropylsily)pent-4-ynoate (Boc-Pra(TIPS)-O^{t}Bu)

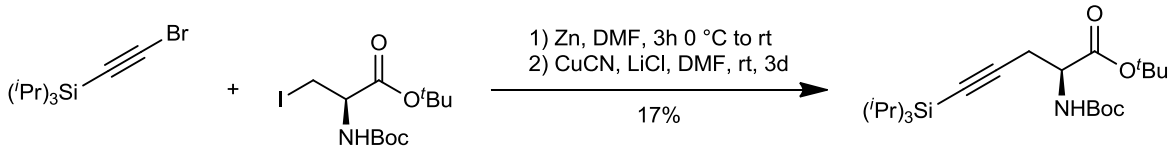

(S)-tert-butyl 2-((tert-butoxycarbonyl)amino)-5-(triisopropylsily)pent-4-ynoate was synthesized by a modified protocol from Maier et al.[27] In a flame-dried 100 mL schlenk flask, (R)-tert-butyl 2-((tert-butoxycarbonyl)amino)-3-iodopropanoate (1.15 g, 3.10 mmol, 1.00 eq.) was dissolved in 5 mL dry DMF and cooled down to 0 °C in an Ice bath. Activated Zinc dust (810 mg, 12.4 mmol, 4.00 eq.) was added. The cooling bath was removed and the Mixture was stirred for 3 h at room temperature, after which TLC control showed complete conversion. The solution was separated carefully from remaining Zn dust by schlenk filtration. A mixture of copper cyanide (278 mg,

3.10 mmol, 1.00 eq.) and lithium chloride (263 mg, 6.20 mmol, 2.00 eq.) were heated at 150 °C for 30 min. in a 10 mL schlenk tube under N_2 atmosphere. The resulting solid was dissolved in 10 mL dry DMF and added under stirring to the previous solution, which was cooled in an Ice/NaCl bath before. The reaction mixture was warm up to room temperature and stirred for three days. After addition of 50 mL H_2O, extraction with ethyl acetate (3 x 50 mL), drying the united organic phases over Na_2SO_4 and evaporation to dryness in vacuo, the crude product was yielded as a yellow oil. Purification by column chromatography (SiO_2, Hex/EE 10:1) gave a colorless oil (227 mg, 0.533 mmol, 17%).

^{1}H-NMR (300 MHz, $CDCl_3$): δ(ppm) = 1.05 to 1.12 (m, 21 H, Si(^{i}Pr)$_3$ C*H*$_3$, C*H*), 1.472 (s, 9 H, CH_3), 1.50 (s, 9 H, C*H*$_3$), 2.78 (dd, *J* = 16.8 Hz, 4 Hz, 1 H, C*H*$_2$) 2.89 (dd, J = 17.3 Hz, 5.1 Hz, 1 H, C*H*$_2$), 4.26 to 4.37 (m, 1 H, C*H*), 5.36 (d, *J* = 8.0 Hz, N*H*)

^{13}C-NMR (75 MHz, $CDCl_3$): δ(ppm) = 11.4, 18.8, 24.3, 28.2, 28.5, 79.8, 82.4, 84.4, 102.6, 155.2, 169.9.

MS(EI, 50 °C) m/z = 425.32 [M^+], 382.29 [$C_{20}H_{36}NO_4Si^+$], 326.21 [$C_{18}H_{36}NO_2Si^+$].

IR (KBr): 1732 (vs), 1491 (s), 1369 (vs), 1255 (s), 1163 (s), 1057 (m) cm^{-1}.

5.2.15 (S)-pentafluorophenyl-2-((tert-butoxycarbonyl)amino)-5-(triisopropylsily)pent-4-ynoate (Fmoc-Pra(TIPS)-OH and -O^{t}Bu)

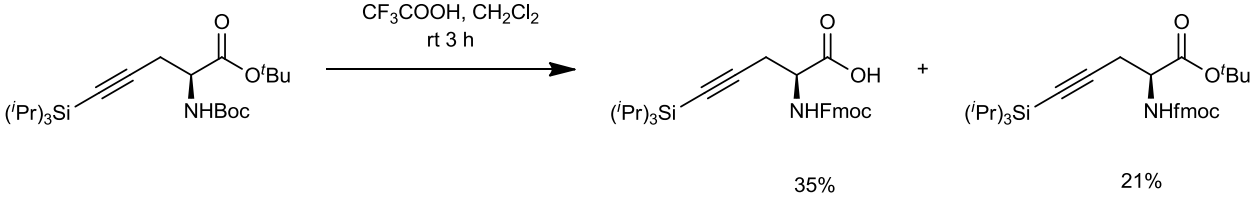

(S)-tert-butyl 2-((tert-butoxycarbonyl)amino)-5-(triisopropylsily)pent-4-ynoate (227 mg, 0.533 mmol, 1.00 eq.) was dissolved in 7 mL CH_2Cl_2. Trifluoroacetic acid (3.5 mL) was added to the solution and the reaction mixture stirred until TLC control showed complete conversion. Volatiles were removed in vacuo and the residue dissolved in 10 mL THF. 9-Fluorenylmethyl N-succinimidyl carbonate (181 mg, 0.537 mmol, 1.01 eq.) and $NaHCO_3$ (230 mg, 2.74 mmol,

5.13 eq.) were added and the mixture stirred for 4 days at room temperature. Water (100 mL) was added and extracted with CH_2Cl_2 (3 x 50 mL). The united organic phases were washed with H_2O (2 x 50 mL), dried over Na_2SO_4 and evaporated to dryness. The crude product was purified by column chromatography (SiO_2, Hex/EE 5:1 to 0:1) to yield the *tert*-butyl ester (60.0 mg, 0.110 mmol, 21%) and the free acid (92 mg, 0.187 mmol, 35%) of the title compound.

free acid Fmoc-Pra(TIPS)-OH

^{1}H-NMR (300 MHz, $CDCl_3$): δ(ppm) = 1.00 to 1.22 (m, 21 H, Si(^{i}Pr)$_3$ C*H*$_3$, C*H*), 2.85 to 3.05 (m, 2 H, C*H*$_2$), 4.28 (t, J = 7.6 Hz, 1 H, C*H*COOH)), 4.35 to 4.50 (m, 2 H, Fmoc-C*H*$_2$), 4.62 (d, J = 7.40 Hz, 1 H, Fmoc-C*H*), 5.69 (d, J = 8.2 Hz, 1 H, N*H*), 7.32 to 7.49 (m, 4 H, Fmoc-*H*$_{ar}$), 7.60 to 7.69 (m, 2 H, Fmoc-*H*$_{ar}$), 7.81 (d, J = 7.5 Hz, 2 H, Fmoc-*H*$_{ar}$).

^{13}C-NMR (75 MHz, $CDCl_3$): δ(ppm) = 11.1, 18.6, 47.1, 67.5, 85.2, 101.6, 120.0, 125.2, 127.1, 127.4, 127.8, 128.2, 141.3, 143.7, 143.8, 155.8, 168.6.

tert-butylester Fmoc-Pra(TIPS)-O^{t}Bu

^{1}H-NMR (300 MHz, $CDCl_3$): δ(ppm) = 1.02 to 1.22 (m, 21 H, Si(^{i}Pr)$_3$ C*H*$_3$, C*H*), 1.54 (s, 9 H, ^{t}Bu-C*H*$_3$), 2.81 to 2.87 (m, 2 H, C*H*$_2$), 4.28 (t, J = 7.2 Hz, 1 H, C*H*COOR), 4.26 to 4.44 (m, 2 H, Fmoc-C*H*$_2$), 4.62 (d, J = 7.4 Hz, 1 H, Fmoc-C*H*), 5.70 (d, J = 8.3 Hz, 1 H, NH), 7.30 to 7.50 (m, 4 H, Fmoc-*H*$_{ar}$), 7.60 to 7.70 (m, 2 H, Fmoc-*H*$_{ar}$), 7.78 to 7.85 (m, 2 H, Fmoc-*H*$_{ar}$).

^{13}C-NMR (75 MHz, $CDCl_3$): δ(ppm) = 11.2, 18.6, 24.3, 28.3, 47.2, 67.6, 82.6, 102.0, 120.0, 125.2, 127.1, 127.7, 141.3, 144.0, 155.6, 169.4.

5.2.16 (S)-perfluorophenyl-2-((((9*H*-fluoren-9-yl)methoxy)carbonyl)amino)-5-(triisopropylsilyl)pent-4-ynoate (Fmoc-Pra(TIPS)-OPfp)

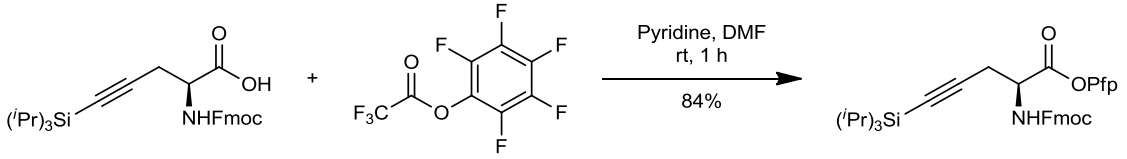

In a 100 mL round-bottomed flask, Fmoc-Propargylglycine (25 mg, 0.596 mmol, 1.00 eq.) was dissolved in 1 mL DMF. Pentafluorophenyl trifluoroacetate (17.5 µL, 28.5 mg, 0.102 mmol, 2.00 eq.) and Pyridine (4.92 µL, 4.83 mg, 0.061 mmol, 1.20 eq.) were added and stirring continued for 1 h at room temperature, after which TLC control indicated complete conversion. The reaction was quenched with 0.1N HCl (10 mL) and the product extracted from the aqueous phase with CH_2Cl_2 (3 x 5 mL). The united organic phases were dried over Na_2SO_4 and the solvent removed in vacuo, yielding a white powder (28 mg, 0,429 mg, 84%). The title compound was used to functionalize pegma thin films without further characterization.

5.2.17 Hydroxymethylruthenocene (12-OH)

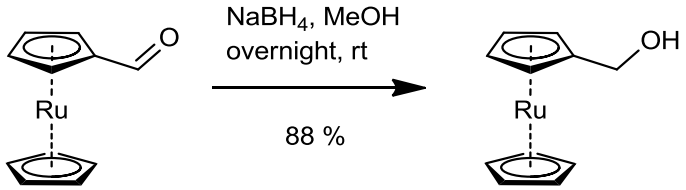

In a 100 mL Round-bottomed flask, Ruthenocenecarboxaldehyde (250 mg, 0.96 mmol, 1.00 eq.) was dissolved in 5 mL Methanol under stirring. $NaBH_4$ (91.0 mg, 2.41 mmol, 2.50 eq.) was added in one portion and stirring continued overnight at room temperature. The reaction mixture was put into 100 mL H_2O and extracted with Methylene chloride. The organic phases were united, dried over Na_2SO_4 and evaporated to dryness yielding an off-white solid (222 mg, 0.85 mmol, 88 %). Analytical data are in agreement with literature.

^{1}H-NMR (300 MHz, $CDCl_3$): δ(ppm) = 4.06 (s, 2 H, RcC*H*$_2$OH), 4.59 (t, *J* = 1.7 Hz, 2 H, Cp-H), 4.66 (s, 5 H, Cp-H), 4.71 (t, *J* = 1.7 Hz, 2 H, Cp-H)

5.2.18 Azidomethylruthenocene (12-N_3)

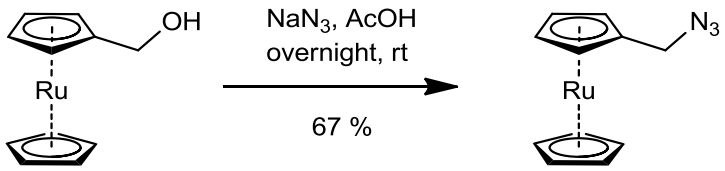

In a 100 mL Round-bottomed flask, Hydroxymethylruthenocene (222 mg, 0.85 mmol, 1.00 eq.) was dissolved in 10 m L glacial acetic acid. NaN_3 (340 mg, 5.23 mmol, 6.16 eq.) was added in one portion and stirred overnight at room temperature, during which the colorless solution turned yellow. The reaction mixture was put into 50 mL H_2O and extracted with Methylene chloride, yielding an orange liquid (164 mg, 0.57 mmol, 67 %) that crystallized upon standing. The analytical data are in agreement with literature.[38]

^{1}H-NMR (300 MHz, $CDCl_3$): δ(ppm) = 3.98 (s, 2 H, RcCH_2N_3), 4.58 to 4.62 (m, 7 H, Cp-*H*), 4.68 to 4.71 (m, 2 H, Cp-*H*).

5.2.19 Bromoacetylferrocene (17-Br)

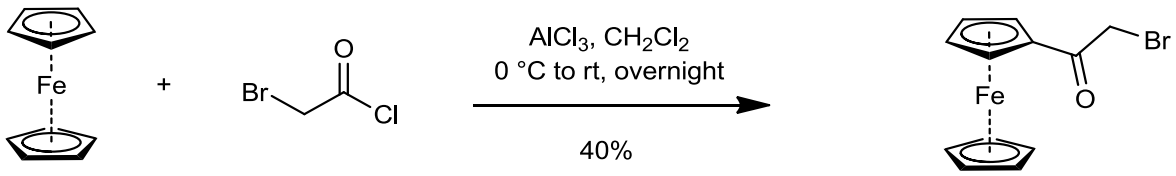

In a flame-dried 25 mL round-bottomed flask, $AlCl_3$ (3.30 g, 24.8 mmol, 0.97 eq.) was suspended in 20 mL dry CH_2Cl_2 under inert gas atmosphere and cooled in an ice bath for 10 min. Bromoacetic chloride (2.09 mL, 4.00 g, 25.4 mmol, 1.00 eq.) was added and stirred for further 10 min under cooling. Ferrocene (4.84 g, 26.0 mmol, 1.03 eq.) was added in one portion and the reaction mixture stirred overnight, allowing it to warm up to room temperature. The reaction was quenched with 20 mL H_2O and extracted with CH_2Cl_2 (3 x 50 mL). The united organic phases were dried over Na_2SO_4 and evaporated to dryness. Purification by column chromatography (SiO_2, CH_2Cl_2/Acetone 1:0 to 4:1) yielded red oil (3.10 g, 10.1 mmol, 40%). Analytical data are in agreement with literature.[60]

^{1}H-NMR (300 MHz, $CDCl_3$): δ(ppm) = 4.24 (s, 2 H, CH_2), 4.30 (s, 5 H, Cp-H), 4.65(t, J = 1.9 Hz, 2 H, Cp-*H*), 4.89 (t, *J* = 1.9 Hz, 2 H, Cp-*H*).

5.2.20 Azidoacetylferrocene (17-N_3)

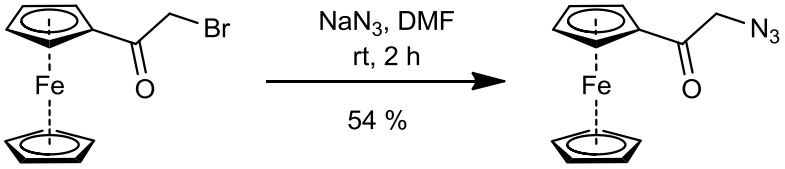

In a 10 mL round-bottomed flask, bromoacetylferrocene (80.0 mg, 0.261 mmol, 1.00 eq.) was dissolved in 2 mL DMF at room temperature. NaN_3 (33.9 mg, 0.521 mmol, 2.00 eq.) was added and the mixture was stirred for 2 h at room temperature. After TLC indicated complete conversion, the reaction mixture was partitioned between H_2O and CH_2Cl_2. The aqueous phase was extracted with CH_2Cl_2 (3 x 20 mL), the united organic phases dried over Na_2SO_4 and the solvent removed in vacuo. Purification by column chromatography (SiO_2, CH_2Cl_2/Acetone 1:0 to 4:1) gave a red solid (38.0 mg, 0.141 mmol, 54 %). The analytical data are in agreement with the literature.[61]

^{1}H-NMR (300 MHz, $CDCl_3$): δ(ppm) = 4.28 (m, 7 H, Cp-*H*, C*H*$_2$), 4.63 (m, 2 H, Cp-H), 4.83 (m, 3 H, Cp-H).

5.2.21 1-Acetyl-1'-bromoacetylferrocene (18-Br)

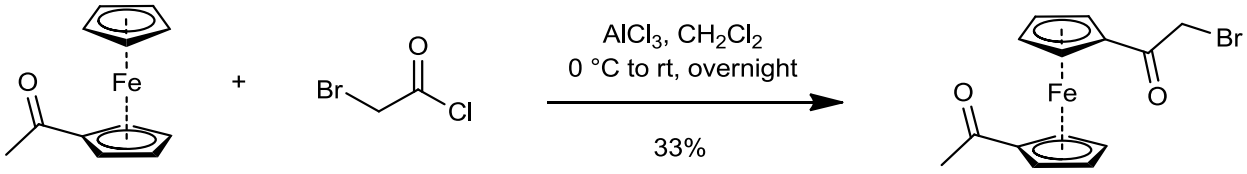

In a flame-dried 25 mL round-bottomed flask, $AlCl_3$ (0.805 g, 6.04 mmol, 1.00 eq.) was suspended in 20 mL dry CH_2Cl_2 under inert gas atmosphere and cooled in an ice bath for 10 min. Bromoacetic chloride (0.950 g, 6.04 mmol, 1.00 eq.) was added and stirred for further 10 min under cooling. Acetylferrocene (1.38 g, 6.04 mmol, 1.00 eq.) was added in one portion and the reaction mixture stirred overnight, allowing it to warm up to room temperature. The reaction was quenched with 10 mL H_2O and extracted with CH_2Cl_2 (3 x 50 mL). The united organic phases were dried ,over Na_2SO_4 and evaporated to dryness. Purification by column chromatography (SiO_2, CH_2Cl_2/Acetone 1:0 to 4:1) yielded red oil (690 mg, 1.98 mmol, 33%).

^{1}H-NMR (300 MHz, $CDCl_3$): δ(ppm) = 2.32 (s, 3 H, C*H*$_3$), 4.13 (s, 2 H, C*H*$_2$), 4.53 (t, J = 1.95 H 4.58 (t, J = 2.1 H 4.78 (t, J = 1.95 H 4.81 (t, J = 1.95 H^{13}C-NMR (75 MHz, $CDCl_3$): δ(ppm) =27.8, 31.9, 71.3, 71.3, 73.9, 74.2, 77.3, 80.8.

MS (EI, 70 °C): m/z (%) = 345.97 (7), 346.97 (1), 347.97 [M^+](100), 348.97 (19), 349.96 (94), 350.96 (18).

IR (KBr): 1683 (vs), 1656 (vs), 1453 (s), 1375 (s), 1281 (s), 1216 (s), 1118 (m), 1071 (s), 1033 (m).

5.2.22 1-Acetyl-1'-azidoacetylferrocene (18-N_3)

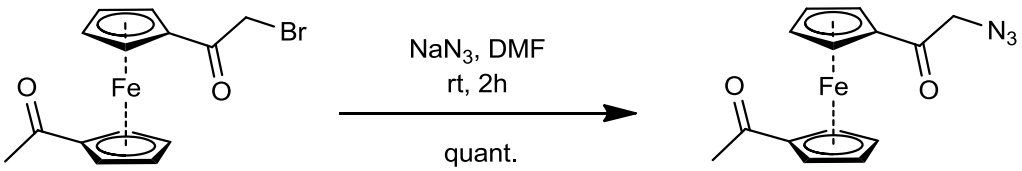

In a 10 mL round-bottomed flask, 1-Acetyl-1'-bromoacetylferrocene (99.0 mg, 0.284 mmol, 1.00 eq.) were dissolved in 2 mL DMF at room temperature. NaN_3 (46.1 mg, 0.709 mmol, 2.50 eq.) was added and the mixture was stirred for 2 h at room temperature. After TLC indicated complete conversion, the reaction mixture was partitioned between H_2O and CH_2Cl_2. The aqueous phase was extracted with CH_2Cl_2 (3 x 20 mL), the united organic phases dried over Na_2SO_4 and the solvent removed in vacuo, yielding a red solid (88 mg, 0.284 mmol, quant.).

^{1}H-NMR (300 MHz, $CDCl_3$): δ(ppm) = 2.38 (s, 3 H, C*H*$_3$), 4.20 (s, 2 H, C*H*$_2$), 4.50-4.70 (m, 4 H, Cp-*H*), 4.75-4.95 (m, 4 H, Cp-*H*).

^{13}C-NMR (75 MHz, $CDCl_3$): δ(ppm) = 27.8, 31.5, 36.5, 55.4, 70.4, 71.2, 73.7, 74.0, 80.8, 162.6, 197.0, 201.2.

IR (KBr): 2104 (vs, N_3), 1678 (vs), 1660 (vs), 1456 (s), 1420 (m), 1401 (m), 1376 (s), 1362 (w), 1280 (s), 1242 (s), 1116 (m), 1073 (s) cm^{-1}

5.2.23 CuAAC click reaction between redox cofactors and 2,2-dimethylbut-3-yne (trz)

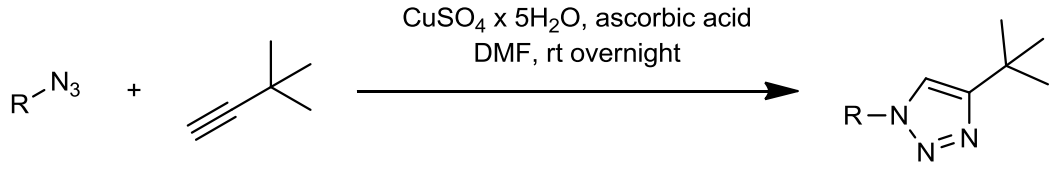

In a 25 mL round-bottomed flask, $CuSO_4$ x $5H_2O$ (12.5 mg, 0.05 mmol, 1.00 eq.) and ascorbic acid (88.1 mg, 0.50 mmol, 10.0 eq.) were dissolved in 10 mL DMF. 2,2-dimethylbut-3-yne (61.6 mg, 0.75 mmol, 15.0 eq.) was added and the resulting solution stirred for 5 min. The cofactor (0.05 mmol, 1.00 eq.) was dissolved in 1 mL DMF and 1 mL of the previous solution was added. The reaction mixture was stirred overnight at room temperature. 20 mL H_2O was added and the product extracted with CH_2Cl_2 (3 x 10 mL). The united organic phases were dried over Na_2SO_4 and the solvent removed in vacuo.

5.2.23.1 4-(tert-butyl)-1-(ferrocenylylmethyl)-1H-1,2,3-triazole (9-trz)

^{1}H-NMR (300 MHz, $CDCl_3$): (ppm) = 1.27 (s, 9 H, ^{t}Bu-CH_3), 4.19 (s, 5H, Cp-H_{Ar}), 4.23 (m, 2 H, Cp-H_{Ar}), 4.31 (m, 2 H, Cp-H_{Ar}), 5.31 (s, 2H,CH_2), 7.04 (s, 1 H, triazole-*H*).

5.2.23.2 4-(tert-butyl)-1-(pyren-2-ylmethyl)-1H-1,2,3-triazole (19-trz)

^{1}H-NMR (300 MHz, $CDCl_3$): δ(ppm) = 1.29 (s, 9 H, ^{t}Bu-CH_3), 6.24 (s, 2 H, CH_2), 7.06 (s, 1 H, triazole-*H*), 7.95 to 8.35 (m, 9 H, Ar-C*H*).

^{13}C-NMR (75 MHz, $CDCl_3$): δ(ppm) = 30.3, 30.8, 52.4, 118.5, 122.1, 124.5, 125.0, 125.1, 125.8, 125.9, 126.4, 127.1, 127.3, 127.7, 128.3, 129.0, 131.2, 132.1, 158.0.

5.2.23.3 (E)-1-(3-(4-(tert-butyl)-1H-1,2,3-triazol-1-yl)propyl)-4-(4-(dimethyl-amino)styryl)-2,6-diisopropylpyridin-1-ium hexafluorophosphate (7-trz)

^{1}H-NMR (300 MHz, $CDCl_3$): δ(ppm) = 1.37 to 1.52 (m, 21 H, CH_3), 2.46 to 2.62 (m, 2 H, CH2), 3.13 (s, 6 H, NCH_3), 3.22 to 3.38 (m, 2 H, ^{i}Pr-C*H*), 4.43 to 4.56 (m, 2 H, CH_2), 4.71 (t, J = 5.1 Hz, 2 H, CH_2), 6.72 to 6.92 (m, 3 H, CH), 7.40 to 7.80 (m, 6 H, CH).

^{13}C-NMR (75 MHz, $CDCl_3$): δ(ppm) = 30.4, 30.6, 30.8, 40.5, 47.7, 112.5, 118.4, 130.5.incomplete because of low intensity

5.2.23.4 1-(3-(4-(tert-butyl)-1H-1,2,3-triazol-1-yl)propyl)-4-(1E, 3E)-4-(dimethyl-amino)phenyl)buta-1,3-dien-1-yl)2,6-diisopropylpyridin-1-ium hexafluorophosphate (10-trz)

^{1}H-NMR (300 MHz, $CDCl_3$): δ(ppm) = 1.33 to 1.55 (m, 21 H, CH_3), 2.46 to 2.63 (m, 2 H, CH_2), 3.02 to 3.18 (m, 6 H, NCH_3), 3.21 to 3.39 (m, 2 H, ^{i}Pr-CH), 4.41 to 4.60 (m, 2 H, CH_2), 4.63 to 4.76 (m, 2 H, CH_2), 6.50 (d, J = 14.7 Hz, 1 H, CH), 6.68 to 6.98 (m, 2 H, CH_2), 7.06 (d, J = 15.4 Hz, 1 H, CH), 7.36 to 7.74 (m, 6 H, CH_{Ar}).

^{13}C-NMR (75 MHz, $CDCl_3$): δ(ppm) = 30.4, 30.6, 30.8, 31.2, 46.3, 118.5, 121.1, 129.4, 163.5. incomplete because of low intensity

5.2.23.5 (E)-1-(3-(4-(tert-butyl)-1H-1,2,3-triazol-1-yl)propyl)-4-(4-methoxystyryl)-2,6-diisopropylpyridin-1-ium hexafluorophosphate (11-trz)

^{1}H-NMR (300 MHz, $CDCl_3$): δ(ppm) = 1.16 to 1.58 (m, 21 H, CH_3), 2.50 to 2.68 (m, 2 H, CH_2), 3.88 (d, J = 19.7 Hz, 3 H, CH), 7.54 to 7.82 (m, 3 H, CH).

^{13}C-NMR (75 MHz, $CDCl_3$): δ(ppm) = 30.2, 114.7, 123.0, 130.4, 163.9. incomplete because of low intensity

5.2.24 3-(p-bromophenyl)[5]ferrocenophane-1,5-dione (24)

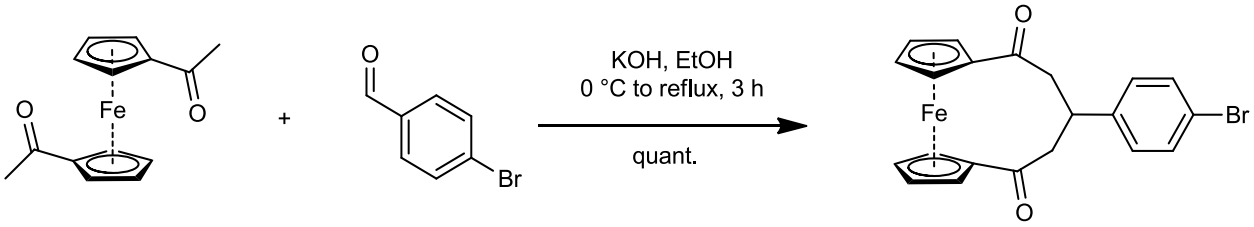

KOH (1.01 g, 18.0 mmol, 4.80 eq.) was dissolved in 30 mL dry EtOH and cooled down to 0 °C in an ice bath. 1,1'-Diacetylferrocene (1.01 g, 3.75 mmol, 1.00 eq.) was added and the resulting mixture stirred for 30 min. 4-bromobenzaldehyde (0.69 g, 3.75 mmol, 1.00 eq.) was added in on

portion and the cooling bath removed. The reaction mixture was stirred at room temperature for 2.5 h and subsequently was heated to reflux for 1 h. The newly formed orange solid was filtered off, washed with small portions of EtOH and dried in air to give the title compound (1.66 g, 3.75 mmol, quant.)

MS (EI): m/z = 435.98, 437.97, 269.97.

IR (KBr): 2927 (m), 2855 (m), 1747 (m), 1658 (vs), 1645 (m), 1488 (m), 1458 (m), 1401 (m), 1381 (m), 1316 (w), 1274 (m), 1093 (m), 1070 (m), 1008 (s), 704 (m).

5.2.25 1,1'-(tetrahydro-4-(p-bromophenyl)-2*H*-pyran-2,6-diyl)-ferrocene (25)

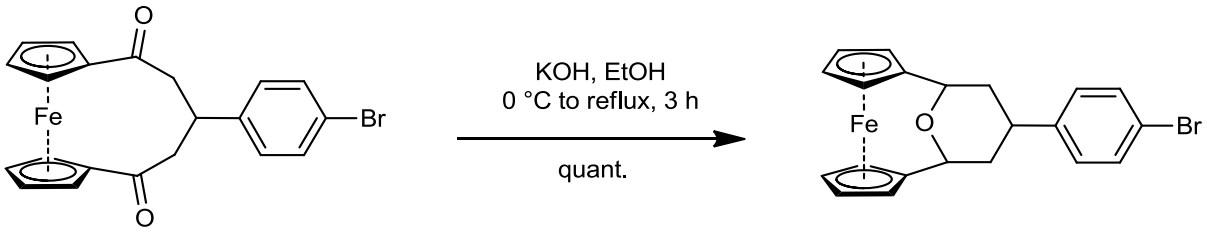

3-(p-bromophenyl)[5]ferrocenophane-1,5-dione (532 mg, 1.22 mmol, 1.00 eq.) was suspended in 20 mL THF. $LiAlH_4$ (120 mg, 3.16 mmol, 2.6 eq.) was added in small portions over 10 min. The resulting mixture was refluxed for 1 h. The reaction was quenched by the addition of 100 mL H_2O. The product was extracted with portions of CH_2Cl_2 (3 x 50 mL). The united organic phases were dried over Na_2SO_4 and evaporated to dryness. After standing for 3 days, TLC (SiO_2, CH_2Cl_2) showed a fraction at R_f = 0.8 and one on the baseline. The fractions were separated by a short column of silica gel, the higher running fraction eluated with CH_2Cl_2, the lower with Acetone. Both fractions were reduced to 5 mL volume in vacuo and put in snap cap flasks to slowly evaporate the residual solvent. After two weeks, crystals appeared in both flasks that were identified by X-Ray single crystal diffraction.

5.2.26 P-azidomethylbenzoic acid (pamba)

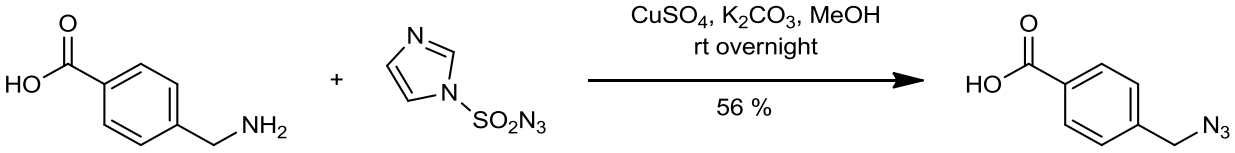

P-aminomethylbenzoic acid (1.37 g, 9.04 mmol, 1.00 eq.), K_2CO_3 (1.25 g, 9.04 mmol, 1.00 eq.), $CuSO_4$ x $5H_2O$ (60.0 mg, 0.24 mmol, 0.027 eq.) and imidazolesulfonyl azide hydrochloride (2.28 g, 10.9 mmol, 1.20 eq.) were stirred in 100 mL MeOH and the reaction mixture was stirred overnight at room temperature. The reaction was quenched by addition of 200 mL H_2O. MeOH was removed in vacuo and the aqueous solution carefully acidified and extracted with ethyl acetate (3 x 100 mL). The united organic phases were washed with 0.1M HCl (3 x 100 mL) and the solvent removed in vacuo, giving an off-white solid (1.61 g, 0.906 mmol, quant.). Analytical data are in agreement with the literature.[62]

^{1}H-NMR (300 MHz, $CDCl_3$): δ(ppm) = 4.49 (s, 2 H, CH_2), 7.43 to 7.52 (m, 2 H, CH_{Ar}), 8.15 to 8.21 (m, 2 H, CH_{Ar}).

5.2.27 $[Fe_3O(pamba)_6L_3]ClO_4$ (22-pamba)

p-Azidomethylbenzoic acid (258 mg, 1.46 mmol, 2.10 eq.) was dissolved in 5 mL dry EtOH. NaH (60% in paraffin, 58.3 mg, 1.46 mmol, 2.10 eq.) was added and the mixture stirred for 5 min. at room temperature, until gas evolution ceased. The newly formed yellow precipitate was dissolved by adding 15 mL H_2O. $Fe(ClO_4)_3$ x H_2O (258 mg, 0.693 mmol, 1.00 eq.) was dissolved in 2 mL H_2O and added drop wise under stirring to the previous solution over 2 min. A yellowish precipitate occurred that was filtered off and dried in air to give a pale orange-brown solid (189 mg, 56%).

IR (KBr): 2102 (vs, N3), 1689 (s), 1598 (vs), 1557 (vs), 1507 (s), 1417 (vs), 1344 (m), 1296 (m), 1251 (m), 1180 (m), 1122 (m), 1108 (m), 1019 (m), 845 (m), 765 (s), 713 (s) cm-1.

5.2.28 $[Cr_3(III,III,III)O(pamba)_6(H_2O)_3]NO_3$

$[Cr_3O(OAc)_6(H_2O)_3]NO_3$ (100 mg, 0.156 mmol, 1.00 eq.) and p-azidobenzoic acid (182 mg, 1.03 mmol, 6.60 eq.) were refluxed in 15 mL toluene for 2 h. The resulting green suspension was filtered off and the solid dried in air, giving green powder (145 mg, 0.108 mmol, 69 %)

IR (KBr): 2102 (vs, N_3), 1688 (s), 1597 (vs), 1556 (vs), 1418 (vs), 1294 (s), 1252 (s), 1179 (s), 1122 (s), 1020 (m-s).

5.2.29 (E)-4-(4-(dimethylamino)styryl)-2,6-diisopropyl-1-(prop-2-yn-1-yl)pyridine-1-ium hexafluorophosphate (30)

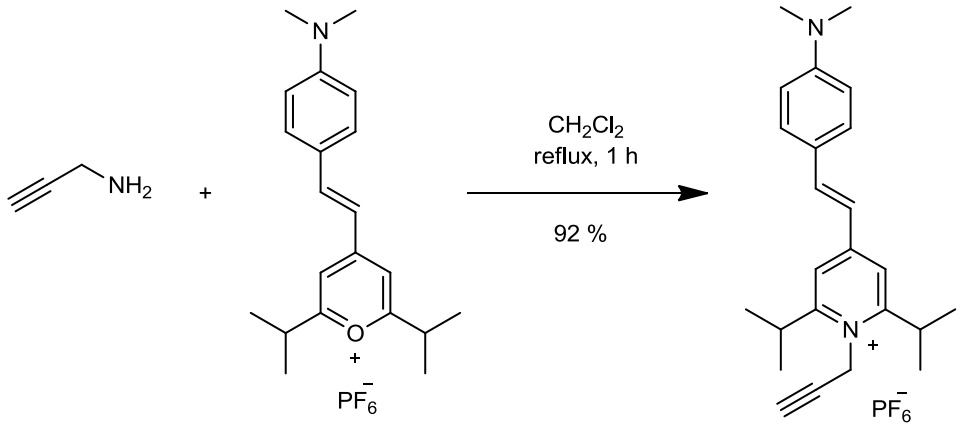

(E)-4-(4-(dimethylamino)styryl)-2,6-diisopropylpyridinium hexafluorophosphate (12.0 mg, 0.026 mmol, 1.00 eq.) and 1-aminoprop-2-yne (115 mg, 2.09 mmol, 79 eq.) were dissolved in 2 mL CH_2Cl_2 and heated to reflux under stirring for 1 h, until tlc showed no more styrylpyridinium salt. Volatiles were removed in vacuo to give the title compound as orange-red solid (12 mg, 0.024 mmol, 92 %).

^{1}H-NMR (300 MHz, $CDCl_3$): δ(ppm) = 1.19 to 1.55 (m, 12 H, ^{i}Pr-CH_3), 2.67 (br. S, 1 3.13 (s, 6 H, NCH_3), 3.45 to 3.80 (m, 2 H, ^{i}Pr-CH), 5.20 to 5.50 (br. s, 2 H, CH_2), 6.80 to 7.10 (m, 3 H_{Ar},

$[Fe_3(III,III,III)O(fcmc)_6L_3]NO_3$ (26)

In a 50 mL snap-cap flask, $Fe(NO_3)_3$ x $9H_2O$ (134 mg, 0.322 mmol, 1.00 eq.) and ferrocenemonocarboxylic acid (229 mg, 0.995 mmol, 3.00 eq.) were stirred under reflux in 20 mL EtOH for 5 min. A solution of 4,4'-bipyridine (78 mg, 0.498 mmol, 1.50 eq.) in 5 mL EtOH

was added in one portion. Immediately after addition, the formation of an off-white precipitate was observed. After stirring for 5 min, the solid was filtered off and the solution left to evaporate for crystallization. The product was obtained as black crystals (160 mg) The identity was confirmed via X-Ray single crystal diffraction and compared to the data from the literature.[49]

5.2.31 $[Fe_2(III,III)MnO(fcmc)_6L_3]\ NO_3$ (27-Mn)

$[Fe_2MnO(OAc)_6(H_2O)_3]$ (107 mg, 0.166 mmol, 1.00 eq.) and ferrocenemonocarboxylic acid (229 mg, 0.995 mmol, 6.00 eq.) were stirred under reflux in 20 mL benzene for 1 h. After cooling, hexane was added until no more solid formed, and the precipitate collected and dried in air to give a brown solid (190 mg).

IR (KBr): 3421 (m), 2977 (m), 1581 (vs), 1473 (vs), 1392 (vs), 1360 (vs), 1194 (m), 1107 (m), 1026 (m), 922 (w), 819 (m), 781 (m), 725 (m, Fe_2MnO), 665 (m, Fe_2MnO), 617 (m, Fe_2MnO), 584 (m, Fe_2MnO), 517 (s) cm^{-1}.

5.2.32 $[Fe_2(III,III)CoO(fcmc)_6L_3]\ NO_3$ (27-Co)

$[Fe_2CoO(OAc)_6(H_2O)_3]$ (110 mg, 0.169 mmol, 1.00 eq.) and ferrocenemonocarboxylic acid (234 mg, 1.02 mmol, 6.00 eq.) were stirred under reflux in 20 mL benzene for 1 h. After cooling, hexane was added until no more solid formed, and the precipitate collected and dried in air to give a brown solid (204 mg).

IR (KBr): 3097 (m), 2933 (m), 1568 (vs), 1475 (vs), 1392 (vs), 1360 (vs), 1196 (s), 1107 (m), 1026 (m), 922 (m), 819 (m), 779 (m), 731 (w, Fe_2CoO), 663 (m, Fe_2CoO), 617 (m, Fe_2CoO), 517 (vs) cm^{-1}

5.2.33 $[Fe_2(III,III)NiO(fcmc)_6L_3]\ NO_3$ (27-Ni)

$[Fe2NiO(OAc)_6(H_2O)_3]$ (104 mg, 0.160 mmol, 1.00 eq.) and ferrocenemonocarboxylic acid (221 mg, 0.962 mmol, 6.00 eq.) were stirred under reflux in 20 mL benzene for 1 h. After cooling, hexane was added until no more solid formed, and the precipitate collected and dried in air to give a brown solid (185 mg).

IR(KBr): 3097 (m), 2932 (w), 1576 (vs), 1473 (vs), 1390 (vs), 1360 (vs), 1194 (s), 1107 (m), 1024 (m), 922 (m), 819 (s), 719 (w, Fe_2NiO), 661 (m, Fe_2NiO), 617 (m, Fe_2NiO), 579 (w, Fe_2NiO), 513 (vs) cm^{-1}

5.2.34 $[Cr_3(III,III,III)O(fcmc)_6L_3]\ NO_3$ (28)

$[Cr_3O(OAc)_6(H2O)_3]NO_3$ (87 mg, 0.128 mmol, 1.00 eq.) and ferrocenemonocarboxylic acid (190 mg, 0.826 mmol, 6.44 eq.) were stirred under reflux in 20 mL benzene for 1 h. After cooling, hexane was added until no more solid formed, and the precipitate collected and dried in air to give a green solid (162 mg).

IR(KBr): 3091 (m), 2935 (w), 1605 (vs), 1544 (vs), 1483 (vs), 1453 (vs), 1402 (vs), 1362 (s), 1199 (s), 1105 (m), 1028 (m), 920 (m), 819 (m), 730 (w), 661 (m), 623 (m), 544 (s) cm^{-1}

6 X-Ray structural data

6.1 (1-ferrocenylmethyl-5-(methylthio)-1*H*-1,2,3-triazol-4-yl)methanol

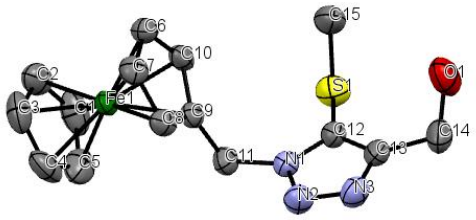

Table 18 Crystal data and structural refinement for 14.

Empirical formula	$C_{30}H_{34}Fe_2N_6O_2S_2$
Formula weight	686.45
Temperature/K	293(2)
Crystal system	monoclinic
Space group	$P2_1$
a/Å	9.780
b/Å	10.249
c/Å	7.529
α/°	90
β/°	96.30
γ/°	90
Volume/Å^3	750.0
Z	1
ρ_{calc}g/cm^3	1.520
μ/mm^{-1}	1.146
F(000)	356.0
Crystal size/mm^3	0.20 × 0.10 × 0.15
Radiation	MoKα (λ = 0.71073)
2Θ range for data collection/°	4.19 to 52.736
Index ranges	-12 ≤ h ≤ 12, -12 ≤ k ≤ 12, -9 ≤ l ≤ 9
Reflections collected	5855
Independent reflections	2828 [R_{int} = 0.0399, R_{sigma} = 0.0487]
Data/restraints/parameters	2828/1/192
Goodness-of-fit on F^2	0.995
Final R indexes [I>=2σ (I)]	R_1 = 0.0368, wR_2 = 0.0793
Final R indexes [all data]	R_1 = 0.0452, wR_2 = 0.0821
Largest diff. peak/hole / e Å^{-3}	0.24/-0.80
Flack parameter	0.021(19)

Table 19 Bond lengths for 14.

Atom	Atom	Length/Å	Atom	Atom	Length/Å
Fe1	C10	2.036(5)	N3	C13	1.356(8)
Fe1	C9	2.015(5)	O1	C14	1.388(9)
Fe1	C8	2.033(5)	C10	C9	1.425(7)
Fe1	C6	2.046(6)	C10	C6	1.427(8)
Fe1	C7	2.059(6)	C9	C8	1.421(7)
Fe1	C1	2.014(6)	C9	C11	1.498(7)
Fe1	C2	2.039(6)	C12	C13	1.372(8)
Fe1	C5	2.025(6)	C8	C7	1.425(8)
Fe1	C3	2.044(6)	C6	C7	1.411(8)
Fe1	C4	2.042(6)	C13	C14	1.499(8)
S1	C12	1.734(5)	C1	C2	1.392(10)
S1	C15	1.809(7)	C1	C5	1.396(11)
N1	N2	1.340(6)	C2	C3	1.396(10)
N1	C12	1.364(7)	C5	C4	1.370(11)
N1	C11	1.478(6)	C3	C4	1.395(10)
N3	N2	1.336(7)			

Table 20 Bond angles for 14.

Atom	Atom	Atom	Angle/˚	Atom	Atom	Atom	Angle/˚
C10	Fe1	C6	40.9(2)	N2	N1	C12	111.8(4)
C10	Fe1	C7	68.4(2)	N2	N1	C11	118.2(4)
C10	Fe1	C2	118.9(3)	C12	N1	C11	129.9(4)
C10	Fe1	C3	154.2(3)	N2	N3	C13	109.5(4)
C10	Fe1	C4	162.8(3)	C9	C10	Fe1	68.6(3)
C9	Fe1	C10	41.2(2)	C9	C10	C6	107.8(5)
C9	Fe1	C8	41.1(2)	C6	C10	Fe1	69.9(3)
C9	Fe1	C6	69.1(2)	N3	N2	N1	105.9(5)
C9	Fe1	C7	69.0(2)	C10	C9	Fe1	70.2(3)
C9	Fe1	C2	152.2(3)	C10	C9	C11	126.7(5)
C9	Fe1	C5	106.4(2)	C8	C9	Fe1	70.1(3)
C9	Fe1	C3	164.5(3)	C8	C9	C10	107.7(5)
C9	Fe1	C4	126.1(3)	C8	C9	C11	125.5(5)
C8	Fe1	C10	68.8(2)	C11	C9	Fe1	123.4(4)
C8	Fe1	C6	68.4(2)	N1	C12	S1	123.1(4)
C8	Fe1	C7	40.8(2)	N1	C12	C13	104.1(5)
C8	Fe1	C2	165.9(3)	C13	C12	S1	132.5(4)
C8	Fe1	C3	128.7(3)	C9	C8	Fe1	68.8(3)
C8	Fe1	C4	109.2(2)	C9	C8	C7	108.3(5)
C6	Fe1	C7	40.2(2)	C7	C8	Fe1	70.6(3)

Table 21 Bond angles for 14, continuation

Atom	Atom	Atom	Angle/˚	Atom	Atom	Atom	Angle/˚
C1	Fe1	C10	106.2(2)	C10	C6	Fe1	69.2(3)
C1	Fe1	C9	117.3(3)	C7	C6	Fe1	70.4(3)
C1	Fe1	C8	152.6(3)	C7	C6	C10	108.3(5)
C1	Fe1	C6	126.3(3)	N1	C11	C9	112.0(5)
C1	Fe1	C7	164.4(3)	N3	C13	C12	108.5(5)
C1	Fe1	C2	40.2(3)	N3	C13	C14	121.8(6)
C1	Fe1	C5	40.4(3)	C12	C13	C14	129.6(6)
C1	Fe1	C3	67.3(3)	C8	C7	Fe1	68.6(3)
C1	Fe1	C4	67.3(3)	C6	C7	Fe1	69.4(3)
C2	Fe1	C6	108.8(3)	C6	C7	C8	107.9(5)
C2	Fe1	C7	128.4(3)	C2	C1	Fe1	70.9(4)
C2	Fe1	C3	40.0(3)	C2	C1	C5	107.8(6)
C2	Fe1	C4	67.2(3)	C5	C1	Fe1	70.2(4)
C5	Fe1	C10	125.5(3)	C1	C2	Fe1	69.0(3)
C5	Fe1	C8	119.3(3)	C1	C2	C3	107.4(7)
C5	Fe1	C6	163.5(3)	C3	C2	Fe1	70.2(3)
C5	Fe1	C7	154.5(3)	C1	C5	Fe1	69.4(4)
C5	Fe1	C2	67.3(3)	C4	C5	Fe1	71.0(4)
C5	Fe1	C3	66.7(3)	C4	C5	C1	108.6(7)
C5	Fe1	C4	39.4(3)	C2	C3	Fe1	69.8(4)
C3	Fe1	C6	121.4(3)	C4	C3	Fe1	69.9(4)
C3	Fe1	C7	110.8(3)	C4	C3	C2	108.1(6)
C4	Fe1	C6	155.7(3)	C5	C4	Fe1	69.7(4)
C4	Fe1	C7	122.1(3)	C5	C4	C3	108.1(6)
C4	Fe1	C3	39.9(3)	C3	C4	Fe1	70.1(4)
C12	S1	C15	101.0(3)	O1	C14	C13	110.4(5)

6.2 1,1'-(tetrahydro-4-(p-bromophenyl)-2*H*-pyran-2,6-diyl)-ferrocene

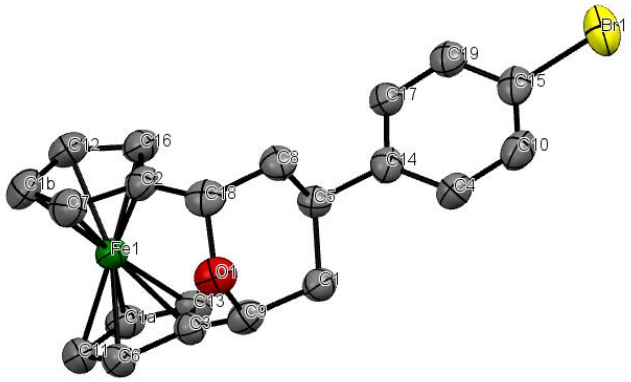

Table 22 Crystal data and structure refinement for 25.

Empirical formula	$C_{84}H_{76}Br_4Fe_4O_4$
Formula weight	1692.53
Temperature/K	293
Crystal system	orthorhombic
Space group	$P2_12_12_1$
a/Å	7.5061
b/Å	14.6414
c/Å	14.9359
α/°	90
β/°	90
γ/°	90
Volume/Å^3	1641.45261
Z	1
ρ_{calc}g/cm^3	1.7121
μ/mm^{-1}	3.357
F(000)	856.6
Crystal size/mm^3	0.30 × 0.10 × 0.15
Radiation	Mo Kα (λ = 0.71069)
2Θ range for data collection/°	5.46 to 52.18
Index ranges	-8 ≤ h ≤ 9, -18 ≤ k ≤ 17, -18 ≤ l ≤ 18
Reflections collected	10902
Independent reflections	3244 [R_{int} = 0.0718, R_{sigma} = 0.0585]
Data/restraints/parameters	3244/0/216
Goodness-of-fit on F^2	1.014
Final R indexes [I>=2σ (I)]	R_1 = 0.0491, wR_2 = 0.1153
Final R indexes [all data]	R_1 = 0.0677, wR_2 = 0.1291
Largest diff. peak/hole / e Å^{-3}	0.34/-0.92
Flack parameter	0.24(2)

Table 23 Bond lengths for 25.

Atom	Atom	Length/Å	Atom	Atom	Length/Å
Br1	C15	1.895(7)	C4	C14	1.395(8)
Fe1	C2	1.985(7)	C5	C14	1.508(9)
Fe1	C3	1.997(6)	C5	C1	1.536(9)
Fe1	C6	2.017(6)	C5	C8	1.528(8)
Fe1	C7	2.022(7)	C6	C11	1.397(10)
Fe1	C11	2.046(7)	C7	C1b	1.417(11)
Fe1	C12	2.078(7)	C10	C15	1.361(10)
Fe1	C13	2.038(6)	C11	C1a	1.432(10)
Fe1	C16	2.027(6)	C12	C16	1.426(10)
Fe1	C1a	2.065(7)	C12	C1b	1.415(12)
Fe1	C1b	2.049(7)	C13	C1a	1.420(9)
C2	C7	1.433(10)	C14	C17	1.380(9)
C2	C16	1.428(10)	C15	C19	1.395(9)
C2	C18	1.506(9)	C17	C19	1.368(9)
C3	C6	1.432(9)	C1	C9	1.526(9)
C3	C13	1.431(8)	C8	C18	1.525(10)
C3	C9	1.508(8)	C9	O1	1.435(8)
C4	C10	1.401(10)	C18	O1	1.448(8)

Table 24 Bond angles of 25.

Atom	Atom	Atom	Angle/˚	Atom	Atom	Atom	Angle/˚
C3	Fe1	C2	96.6(3)	C13	C3	Fe1	70.8(3)
C6	Fe1	C2	113.9(3)	C13	C3	C6	106.4(5)
C6	Fe1	C3	41.8(3)	C9	C3	Fe1	121.2(4)
C7	Fe1	C2	41.9(3)	C9	C3	C6	124.5(5)
C7	Fe1	C3	114.3(3)	C9	C3	C13	129.0(5)
C7	Fe1	C6	101.2(3)	C14	C4	C10	119.9(6)
C11	Fe1	C2	152.4(3)	C1	C5	C14	114.7(5)
C11	Fe1	C3	69.4(3)	C8	C5	C14	109.7(5)
C11	Fe1	C6	40.2(3)	C8	C5	C1	108.8(5)
C11	Fe1	C7	121.1(3)	C3	C6	Fe1	68.4(3)
C12	Fe1	C2	69.6(3)	C11	C6	Fe1	71.0(4)
C12	Fe1	C3	156.7(3)	C11	C6	C3	108.9(6)
C12	Fe1	C6	160.9(3)	C2	C7	Fe1	67.7(4)
C12	Fe1	C7	68.3(3)	C1b	C7	Fe1	70.7(4)
C12	Fe1	C11	130.8(3)	C1b	C7	C2	108.2(7)
C13	Fe1	C2	117.3(2)	C15	C10	C4	119.9(6)
C13	Fe1	C3	41.5(2)	C6	C11	Fe1	68.8(4)
C13	Fe1	C6	68.9(2)	C1a	C11	Fe1	70.3(4)

Table 25 Bond angles of 25, continuation.

Atom	Atom	Atom	Angle/˚	Atom	Atom	Atom	Angle/˚
C13	Fe1	C7	152.8(3)	C1a	C11	C6	108.7(6)
C13	Fe1	C11	68.2(3)	C16	C12	Fe1	67.8(4)
C13	Fe1	C12	127.6(3)	C1b	C12	Fe1	68.9(4)
C16	Fe1	C2	41.7(3)	C1b	C12	C16	107.4(7)
C16	Fe1	C3	116.9(3)	C3	C13	Fe1	67.7(3)
C16	Fe1	C6	152.3(3)	C1a	C13	Fe1	70.8(4)
C16	Fe1	C7	69.1(3)	C1a	C13	C3	109.0(5)
C16	Fe1	C11	165.9(3)	C5	C14	C4	123.3(6)
C16	Fe1	C12	40.6(3)	C17	C14	C4	117.9(6)
C16	Fe1	C13	107.4(3)	C17	C14	C5	118.6(5)
C1a	Fe1	C2	156.9(3)	C10	C15	Br1	119.5(5)
C1a	Fe1	C3	69.7(3)	C19	C15	Br1	119.3(5)
C1a	Fe1	C6	68.6(3)	C19	C15	C10	121.2(7)
C1a	Fe1	C7	160.6(3)	C2	C16	Fe1	67.6(4)
C1a	Fe1	C11	40.8(3)	C12	C16	Fe1	71.6(4)
C1a	Fe1	C12	116.2(3)	C12	C16	C2	108.7(6)
C1a	Fe1	C13	40.5(2)	C19	C17	C14	123.2(6)
C1a	Fe1	C16	127.4(3)	C17	C19	C15	117.8(6)
C1b	Fe1	C2	69.8(3)	C11	C1a	Fe1	68.9(4)
C1b	Fe1	C3	153.4(3)	C13	C1a	Fe1	68.7(4)
C1b	Fe1	C6	121.8(3)	C13	C1a	C11	106.9(6)
C1b	Fe1	C7	40.7(3)	C7	C1b	Fe1	68.6(4)
C1b	Fe1	C11	112.2(3)	C12	C1b	Fe1	71.0(4)
C1b	Fe1	C12	40.1(3)	C12	C1b	C7	108.7(7)
C1b	Fe1	C13	165.0(3)	C9	C1	C5	112.2(5)
C1b	Fe1	C16	68.4(3)	C18	C8	C5	113.3(5)
C1b	Fe1	C1a	130.0(3)	C1	C9	C3	116.0(5)
C7	C2	Fe1	70.4(4)	O1	C9	C3	111.7(5)
C16	C2	Fe1	70.7(4)	O1	C9	C1	110.9(5)
C16	C2	C7	106.9(6)	C8	C18	C2	115.4(6)
C18	C2	Fe1	121.8(5)	O1	C18	C2	111.7(5)
C18	C2	C7	124.4(6)	O1	C18	C8	110.1(5)
C18	C2	C16	128.7(6)	C18	O1	C9	115.5(5)
C6	C3	Fe1	69.8(3)				

6.3 $[Dy_2(fcmc)_6(OMe)_2(H_2O)_2]$ (29)

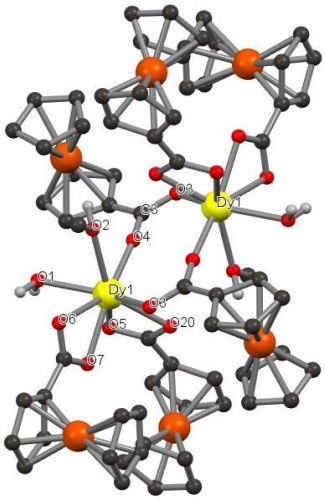

Table 26 Crystal data and structural refinement for 29.

Empirical formula	$C_{72}H_{80}Dy_2Fe_6O_{20}$
Formula weight	1925.46
Temperature/K	293(2)
Crystal system	triclinic
Space group	P-1
a/Å	10.884
b/Å	11.943
c/Å	15.112
α/°	76.53
β/°	88.16
γ/°	65.12
Volume/$Å^3$	1728.2
Z	1
$\rho_{calc}g/cm^3$	1.850
μ/mm^{-1}	3.430
F(000)	960.0
Crystal size/mm^3	0.15 × 0.20 × 0.10
Radiation	MoKα (λ = 0.71073)
2Θ range for data collection/°	3.874 to 55.22
Index ranges	$-14 \le h \le 14$, $-15 \le k \le 15$, $-19 \le l \le 19$
Reflections collected	16481
Independent reflections	7852 [R_{int} = 0.1721, R_{sigma} = 0.2067]
Data/restraints/parameters	7852/3/459
Goodness-of-fit on F^2	0.788
Final R indexes [I>=2σ (I)]	R_1 = 0.0884, wR_2 = 0.2140
Final R indexes [all data]	R_1 = 0.1545, wR_2 = 0.2514
Largest diff. peak/hole / e $Å^{-3}$	1.16/-3.00

Table 27 Bond lengths for 29.

Atom	Atom	Length/Å	Atom	Atom	Length/Å
Dy1	O7	2.341(10)	Fe2	C26	2.074(14)
Dy1	O6	2.554(8)	Fe2	C20	2.026(16)
Dy1	O4	2.279(9)	Fe2	C25	2.080(15)
Dy1	O3	2.345(9)	Fe2	C29	2.033(15)
Dy1	O20	2.398(9)	Fe2	C28	2.044(17)
Dy1	O2	2.395(9)	Fe2	C24	2.033(15)
Dy1	O5	2.442(9)	Fe2	C22	2.060(15)
Dy1	C1	2.815(14)	Fe2	C27	2.036(17)
Dy1	C2	2.766(14)	Fe2	C23	2.063(15)
Fe1	C12	2.068(16)	Fe3	C38	1.993(17)
Fe1	C19	2.022(14)	Fe3	C33	2.003(16)
Fe1	C13	2.025(17)	Fe3	C34	2.023(17)
Fe1	C15	2.029(15)	Fe3	C37	2.061(18)
Fe1	C17	2.064(16)	Fe3	C32	1.987(18)
Fe1	C10	2.035(15)	Fe3	C36	2.044(16)
Fe1	C18	2.001(14)	Fe3	C30	2.05(2)
Fe1	C14	2.048(16)	Fe3	C39	2.033(15)
Fe1	C16	2.078(16)	Fe3	C35	2.061(16)
Fe1	C11	2.066(16)	Fe3	C31	2.085(18)
Fe2	C21	2.054(17)			

7 appendix

7.1 List of Abbreviations

prp	**pr**o**p**argyl
pra	**pr**op**a**rgyl glycine
Fmoc	9-**f**luorenyl**m**eth**o**xy**c**arbonyl
Fmoc-OSu	fmoc **su**ccinimide
Boc	*tert*-**b**ut**o**xy**c**arbonyl
IR	**I**nfra**r**ed spectroscopy
MS	**M**ass **s**pectrometry
NMR	**N**uclear **M**agnetic **R**esonance spectroscopy
CV	**c**yclic **v**oltammetry
TBAP	**t**etra-*n*-**b**utyl**a**mmonium hexafluorophosphate (**p**erfluorophosphate)
Pfp	**p**enta**f**luoro**p**henyl
TIPS	**t**ri-**i**so**p**ropyl**s**ilyl
TFA	**t**ri**f**louru**a**cetic acid
Bipy	4,4'-**Bipy**ridine
Paba	**p**ara-**a**zido**b**enzoic **a**cid
Pamba	**p**ara-**a**zido**m**ethyl**b**enzoic **a**cid
pegma 10/90	**p**oly **e**thylene **g**lycol **m**eth**a**crylate (**10**%) / polymethylmethacrylate (**90**%) copolymer

7.2 References

[1] A. D. McNaught, A. Wilkinson, *IUPAC Compend. Chem. Terminol. (the "Gold Book")* **n.d.**, DOI http://dx.doi.org/10.1351/goldbook.P04479.

[2] R. B. Merrifield, *J. Am. Chem. Soc.* **1963**, *85*, 2149–2154.

[3] M. Lebl, N. F. Sepetov, S. Felder, K. S. Lam, **1995**, *37*, 177–198.

[4] V. Stadler, T. Felgenhauer, M. Beyer, S. Fernandez, K. Leibe, S. Güttler, M. Gröning, K. König, G. Torralba, M. Hausmann, et al., *Angew. Chemie - Int. Ed.* **2008**, *47*, 7132–7135.

[5] "PepPerPrint," can be found under http://pepperprint.com/high-content-peptide-microarrays/, **n.d.**

[6] V. V. Rostovtsev, L. G. Green, V. V. Fokin, K. B. Sharpless, *Angew. Chemie - Int. Ed.* **2002**, 2708–2711.

[7] H. C. Kolb, M. G. Finn, K. B. Sharpless, *Angew. Chemie - Int. Ed.* **2001**, *40*, 2004–2021.

[8] F. Himo, T. Lovell, R. Hilgraf, V. V. Rostovtsev, L. Noodleman, K. B. Sharpless, V. V. Fokin, *J. Am. Chem. Soc.* **2005**, *127*, 210–216.

[9] D. Noy, C. C. Moser, P. L. Dutton, *Biochim. Biophys. Acta - Bioenerg.* **2006**, *1757*, 90–105.

[10] "EU Project PepDiode," can be found under http://www.imt.kit.edu/projects/pepdiode/, **n.d.**

[11] C. R. Lindsay, Jacque K.; Hauser, *J. Org. Chem.* **1957**, *22*, 355–358.

[12] W. Lin, Z. He, H. Zhang, X. Zhang, A. Mi, Y. Jiang, *Synthesis (Stuttg).* **2001**, *2001*, 1007–1009.

[13] K. L. Rinehart Jr., R. J. Curby Jr., P. E. Sokol, **1957**, *3458*, 3420–3424.

[14] D. Bauer, A. Foucault, *J. Electroanal. Chem. Interfacial Electrochem.* **1972**, *39*, 385–394.

[15] P. G. M. Wuts, T. W. Greene, Eds. , *Protective Groups in Organic Synthesis*, Wiley, Hoboken, New Jersey, **1999**.

[16] J. E. Nordlander, M. J. Payne, F. G. Njoroge, V. M. Vishwanath, G. R. Han, G. D. Laikos, M. A. Balk, *J. Org. Chem.* **1985**, *50*, 3619–3622.

[17] W. Pieken, K. Hill, B. Eaton, D. McGee, K. Vagle, L. Gold, A. Stephens, *Derivatizing Oligonucleotides and Proteins Using Cycloaddition Reactions Including Diels-Alder Reaction or 1,3-Dipolar Cycloaddition Reactions*, **2004**, US6737236 B1.

[18] S. Ballet, C. Betti, A. Novoa, C. To, C. U. Nielsen, H. C. Helms, A. Lesniak, P. Kleczkowska, N. N. Chung, A. W. Lipkowski, et al., *ACS Med. Chem. Lett.* **2014**, *5*, 352–357.

[19] M. Green, J. Berman, *Tetrahedron Lett.* **1990**, *31*, 5851–5852.

[20] B. Rudat, E. Birtalan, I. Thomé, D. K. Kölmel, V. L. Horhoiu, M. D. Wissert, U. Lemmer, H. J. Eisler, T. S. Balaban, S. Bräse, *J. Phys. Chem. B* **2010**, *114*, 13473–13480.

[21] F. Maerkle, F. F. Loeffler, S. Schillo, T. Foertsch, B. Muenster, J. Striffler, C. Schirwitz, F. R. Bischoff, F. Breitling, A. Nesterov-Mueller, *Adv. Mater.* **2014**, *26*, 3730–3734.

[22] D. K. Wang, F. Rasoul, D. J. T. Hill, G. R. Hanson, C. J. Noble, A. K. Whittaker, *Soft Matter* **2012**, *8*, 435.

[23] V. Sai Sudhir, N. Y. Phani Kumar, S. Chandrasekaran, *Tetrahedron* **2010**, *66*, 1327–1334.

[24] T. Weidner, N. Ballav, M. Zharnikov, A. Priebe, N. J. Lon, R. Winter, A. Rothenberger, *Chem. - A Eur. J.* **2008**, *14*, 4346–4360.

[25] A. W. Taylor, P. Licence, *ChemPhysChem* **2012**, *13*, 1917–1926.

[26] R. Burai, J. Chatwichien, B. R. McNaughton, *Org. Biomol. Chem.* **2011**, *9*, 5056–5058.

[27] P. Danner, M. Morkunas, M. E. Maier, *Org. Lett.* **2013**, *15*, 2474–2477.

[28] C. Schirwitz, Purification of Peptides in High-Complexity Arrays, Ruprecht-Karls-Universität Heidelberg, **2012**.

[29] S. Ding, G. Jia, J. Sun, *Angew. Chemie - Int. Ed.* **2014**, *53*, 1877–1880.

[30] C. C. Schneider, B. Godoi, M. Prigol, C. W. Nogueira, G. Zeni, *Organometallics* **2007**, *26*, 4252–4256.

[31] N. a. Heaps, C. D. Poulter, *J. Am. Chem. Soc.* **2011**, *133*, 19017–19019.

[32] S. T. Kabanyane, D. I. MaGee, *Can. J. Chem.* **1992**, *70*, 2758–2763.

[33] L. W. Bieber, M. F. Da Silva, P. H. Menezes, *Tetrahedron Lett.* **2004**, *45*, 2735–2737.

[34] J. M. Casas-solvas, A. Vargas-berenguel, L. F. Capita, F. Santoyo-gonza, Ä. De Quı, *Synthesis (Stuttg).* **2004**, 671–673.

[35] C. G. Hardy, L. Ren, T. C. Tamboue, C. Tang, **2011**, *49*, 1409–1420.

[36] T. P. Smith, K. S. Kwan, H. Taube, A. Bino, S. Cohen, *Inorg. Chem.* **1984**, *23*, 1943–1945.

[37] M. R. Malachowski, M. F. Grau, J. M. Thomas, A. L. Rheingold, C. E. Moore, *Inorganica Chim. Acta* **2010**, *364*, 132–137.

[38] M. Patra, N. Metzler-Nolte, *Chem. Commun.* **2011**, *47*, 11444.

[39] H. Rosenberg, S. G. Cottis, *A Study of the Friedel-Crafts Axylation of Ferrrocene with Perfluorocarboxylic Acid Derivatives*, **1962**.

[40] S. Bhattacharyya, *Synth. Commun.* **1996**, *26*, 4647–4654.

[41] P. Guo, Q. Chen, T. Liu, L. Xu, Q. Yang, X. Qian, *ACS Med. Chem. Lett.* **2013**, *4*, 527–531.

[42] G. P. Sarmiento, G. Y. Moltrasio, A. G. Moglioni, **2009**, *2009*, 33–41.

[43] M. A. Tehfe, J. Lalevée, F. Morlet-Savary, B. Graff, N. Blanchard, J. P. Fouassier, *Macromolecules* **2012**, *45*, 1746–1752.

[44] D. Schray, *Darstellung Und Charakterisierung Eisen- Und Lanthanoidhaltiger Molekularer Nanomagnete*, Cuvillier-Verlag, Göttingen, **2013**.

[45] E. D. Goddard-Borger, R. V. Stick, *Org. Lett.* **2007**, *9*, 3797–3800.

[46] E. J. L. McInnes, C. Anson, A. K. Powell, A. J. Thomson, S. Poussereau, R. Sessoli, *Chem. Commun.* **2001**, *10*, 89–90.

[47] V. Mereacre, D. Prodius, A. M. Ako, S. Shova, C. Turta, K. Wurst, P. Jaitner, A. K. Powell, *Polyhedron* **2009**, *28*, 3551–3555.

[48] A. Tarraga, P. Molina, J. L. Lo, M. D. Velasco, P. G. Jones, **2002**, 2055–2065.

[49] V. Mereacre, M. Nakano, J. Gómez-Segura, I. Imaz, C. Sporer, K. Wurst, J. Veciana, C. Turta, D. Ruiz-Molina, P. Jaitner, *Inorg. Chem.* **2006**, *45*, 10443–10445.

[50] B. O. J. I. Alexandru MG, *Rev. Chim.* **2010**, *61*, 462–466.

[51] D. Astruc, in *Organomet. Chem. Catal.*, Springer, **1952**, p. 608.

[52] H. Vrubel, T. Hasegawa, E. De Oliveira, F. S. Nunes, *Inorg. Chem. Commun.* **2006**, *9*, 208–211.

[53] M. K. Johnson, D. B. Powell, R. D. Cannon, *Spectrochim. Acta Part A Mol. Spectrosc.* **1981**, *37*, 995–1006.

[54] H. Hou, G. Li, L. Li, Y. Zhu, X. Meng, Y. Fan, *Inorg. Chem.* **2003**, *42*, 428–435.

[55] D. Huber, H. Hubner, P. Gmeiner, *J. Med. Chem.* **2009**, *52*, 6860–6870.

[56] H. E. Gottlieb, V. Kotlyar, A. Nudelman, *J. Org. Chem.* **1997**, *62*, 7512–7515.

[57] F. Menges, "Spekwin32," can be found under http://www.effemm2.de/spekwin/, **n.d.**

[58] K. L. Parry, A. G. Shard, R. D. Short, R. G. White, R. G. Whittle, A. Wright, *Surf. Interface Anal.* **2006**, *38*, 1497–1504.

[59] J. H. Scofield, *J. Electron Spectros. Relat. Phenomena* **1976**, *8*, 129–137.

[60] H. Yang, Z. Zhou, K. Huang, M. Yu, F. Li, T. Yi, C. Huang, *Org. Lett.* **2007**, *9*, 4729–4732.

[61] C. V. Ursini, F. Mazzeo, J. A. R. Rodrigues, *Tetrahedron Asymmetry* **2006**, *17*, 3335–3340.

[62] H. Ankati, E. Biehl, *Tetrahedron Lett.* **2009**, *50*, 4677–4682.

7.3 List of Figures

7.4 List of Tables

7.5 Publications and presentations

Parts of the present work have already published or presented.

Publications:

V. Mereacre, M. Schlageter, A. K. Powell, “A temperature induced ferrocene–ferrocenium interconversion in a ferrocene functionalized μ_3-O chromium carboxylate”, Journal of magnetism and magnetic materials 2015, 381, 478-480.

Presentations:

“Unusual charge transfer in coordination clusters with ferrocenecarboxylate ligands” – Presentation at the 4th Schauinsland Meeting: Freiburg Physics meets Karlsruhe Chemistry, July 3rd to 5th, 2015.

Poster:

“Grafting redox cofactors onto surface-bound peptides using click chemistry” Poster at the 7th international Symposium on Bioorganometallic Chemistry, July 22nd to 25th, 2014

7.6 Acknowledgements

At this point I would like to express my thanks to a lot of people who made this thesis possible.

First and foremost, I would like to express my special appreciation and thanks to Prof. Annie K. Powell, for giving me the opportunity to work on this very interesting and challenging subject, for her trust and guidance and for many priceless lessons in serenity.

I would also like to thank Prof. Frank Breitling and Dr. Alexander Nesterov-Müller for giving me the opportunity to get an insight in application oriented research. Prof. Teodor Silviu Balaban was a great source of advice even over the long distance between Karlsruhe and Marseille, and gave me the opportunity to visit his laboratory. I would like to express my gratitude for his guidance in organic chemistry, his always kind words, and for introducing me to the beautiful city of Marseille and the amazing Bouillabaisse.

Dr. Valeriu Mereacre always had a sympathetic ear for all kinds of problems. He was very patient and provided guidance and advice whenever possible. I would like to thank him for letting me be a part of his project on clusters with electroactive ligands.

My special thanks go to Dr. Thomas Biet and Dr. Amer Baniodeh for the great cooperation on clickable M_3O clusters. Keep up the good work! I also wish Dr. Baniodeh the best of luck for his habilitation.

Prof. Richard Welter and Dr. Samir Mameri invited me to Strasbourg to work in their laboratory for a month and provided me with chemicals and scientific advice. I want to thank them for their kindness and hospitality, and for providing a pivot point for turning my project in the right direction. I also thank Dr. Khaled Ceaib and Dr. David Speckler from the Welter group for welcoming me in Strasbourg and for making my stay so pleasant.

I would like to thank Dr. Irina Kühne, Dr. Dirk Schray and Sebastian Schmidt, for the great collaborations in clickable coordination clusters and for many fruitful discussions.

I am grateful for having been a member of the Annie K. Powell research group, and I would like to thank all the current and past members that I had the pleasure to meet.

Dr. Florian-Xuan Dang and Dr. Remi Plamont provided the beautiful and amazing styrylpyridinium and styrylpyryllium fluorophores shown in this work. I would like to thank them for brightening my chemistry and for many fruitful discussions and great responsiveness.

Huge thanks goes to Dr. Michael Bruns and Vanessa Trouillet for their great work in XP spectroscopy and for the patience and fruitful discussions. I would also like to thank Dr. Thorsten Scherer for his efforts to try and find the needle of iron in the pegma haystack with EDX. I would also like to thank Dr. Bastian Rapp for giving me permission to use his GenePix scanner and Tobias Nargang for giving me an introduction to the device.

Thanks also to Dr. Fanny Liu, Dr. Nicola Zill, Dr. Timo Augenstein, Dr. Bastian Münster, Dr. Jacob Strifler, Anitha Golla, Barbara Ridder and Daniela Althuon for fruitful and lively discussions in chemistry.

Our secretary, Gertraud Amschlinger always smooths the way such that my path through the past few years has been a pleasant journey. I want to thank her for doing this behind the scenes and want to let her know that this is noticed and appreciated.

I would like to cordially thank Helga Berberich for her great work at the NMR spectrometer, Petra Smie for the mass spectroscopy, Nicole Klaassen for the elemental analysis, , Kalam Munschi for the glass blowing work, Tobias Lampert for his technical assistance, Gabi Leichle for her work in the chemical stores and our lab technician Lena Friedrich for always having a friendly smile.

I am very grateful for having been a member of the Biointerfaces in Technology and Medicine (BIFTM) International Graduate School and having had the opportunity to attend courses in soft skills, specialist skills and transdisciplinary skills. I would also like to thank my Thesis Advisory Committe, Prof. Burkhard Luy and Dr. Alexander Welle, for their great advice and support.